CHARACTERIZATION AND APPLICATION OF CHEMICAL AND MECHANICAL EFFECTS INDUCED BY ULTRASONIC CAVITATION

NGUYEN THANH TAM

Table of Contents

Chapter 1 General Introduction 1
1.1. Ultrasound 2
1.2. Acoustic cavitation 4
1.3. Sonochemistry and its application 7
1.4. Objective of this study 11
References 13
Chapter 2 Theory 15
2. 1. Ultrasound 16
2.1.1. Basic equations 16
2.1.2. Physical Quantities of Sound 18
2.1.3. Relationship between sound pressure and particle velocity 19
2. 2. Ultrasonic cavitation 22
2.2.1. The condition for large expansion of a bubble (Blake threshold) 22
2.2.2. The primary Bjerknes force 27
2.3. Broadband noise 29
References 31
Chapter 3 Sound pressure and cavitation threshold 32
3.1. Introduction 33
3.2. Experiment 36
3.2.1. Apparatus 36
3.2.2. Sound pressure and broadband integrated pressure detection 38
3.2.3. Broadband integrated pressure and sound pressures at fundamental, harmonic, and ultraharmonic frequencies 41
3.2.4. Bubbles observation 42
3.3. Results and discussion 44
3.3.1. Determination of cavitation threshold 44
3.3.2. Sound pressure at the fundamental frequency and broadband integrated pressure 46
3.3.3. Sound pressure at the second harmonic and first ultraharmonic frequencies 54

3.3.4. Cavitation threshold 58
3.3.5. Thresholds of the second harmonic and the first ultraharmonic signals 60
3.4. Conclusion 63
References 65
Chapter 4 Thresholds of chemical and mechanical effects 68
4.1. Introduction 69
4.2. Experiment 70
4.2.1. Materials 70
4.2.2. Apparatus 71
4.2.3. Measurements 72
4.3. Results and discussion 73
4.3.1. Threshold of chemical effect 73
4.3.2. Threshold of mechanical effect 78
4.3.3. Comparisons of cavitation, chemical effect, and mechanical effect thresholds 82
4. 4. Conclusion 84
References 85
Chapter 5 Measurement of distribution of broadband noise and sound pressures in sonochemical reactor 87
5.1. Introduction 88
5.2. Experiments 90
5.3. Results and discussion 93
5.3.1. Distribution at 130 kHz 93
5.3.2. Distribution at 43 kHz 98
5.4. Conclusion 105
References 106
Chapter 6 Application of ultrasonication and silica gel on removal of silicic acid in geothermal water 108
6.1. Introduction 109
6.2. Polymerization of silicic acid 111

6.3. Experiment 113
6.4. Results and discussion 115
6.4.1. Effects of silica gel and samples condition 115
6.4.2. Effect of ultrasonic conditions 123
6. 5. Conclusion 127
References 128
Chapter 7 130
Summary 130
List of publications 135
Acknowledgement 136

Chapter 1

General Introduction

1.1. Ultrasound

Ultrasound is an inaudible sound wave which is greater than the upper hearing limit of human beings, ranges from 20 kHz to 10 MHz. Through a medium, ultrasound propagates and causes the displacement of pressure of high frequency acoustic waves and particle. Ultrasound can propagate through any elastic medium consisting of water, gas-saturated water, and slurry. Generally, in terms of frequency, ultrasound can be categorized into three basic regions as the followings:

- 20 – 100 kHz: low frequency, applied in homogenizing, cleaning, detecting
- 100 kHz – 1 MHz: high frequency, applied in cleaning, detecting
- 1 – 10 MHz: very high frequency, applied in cleaning, atomization, medicine

The frequency ranges of sound are demonstrated in Fig. 1. 1. Ultrasound has been used in a wide range of applications in various fields of chemical, physical, and biological engineering, medical science, and waste treatment. Ultrasound with frequencies in the range of 20 kHz – 1 MHz (high power ultrasound) is applied in industry, nanotechnology, ultrasonic therapy, and sonochemistry. Ultrasound with frequencies in the range of 2 – 10 MHz (low power ultrasound), on the other hand, is applied in medical imaging, nondestructive testing. The energy generated from ultrasound at a relatively high frequency can be focus into very small volumes less than several millimeters in length. Therefore, high frequency ultrasound is usually used for ultrasonic therapy especially for very small treated area [1]. It is known that when ultrasound is irradiated into a liquid medium, chemical and mechanical effects are caused owing to generated cavitation events [2-3].

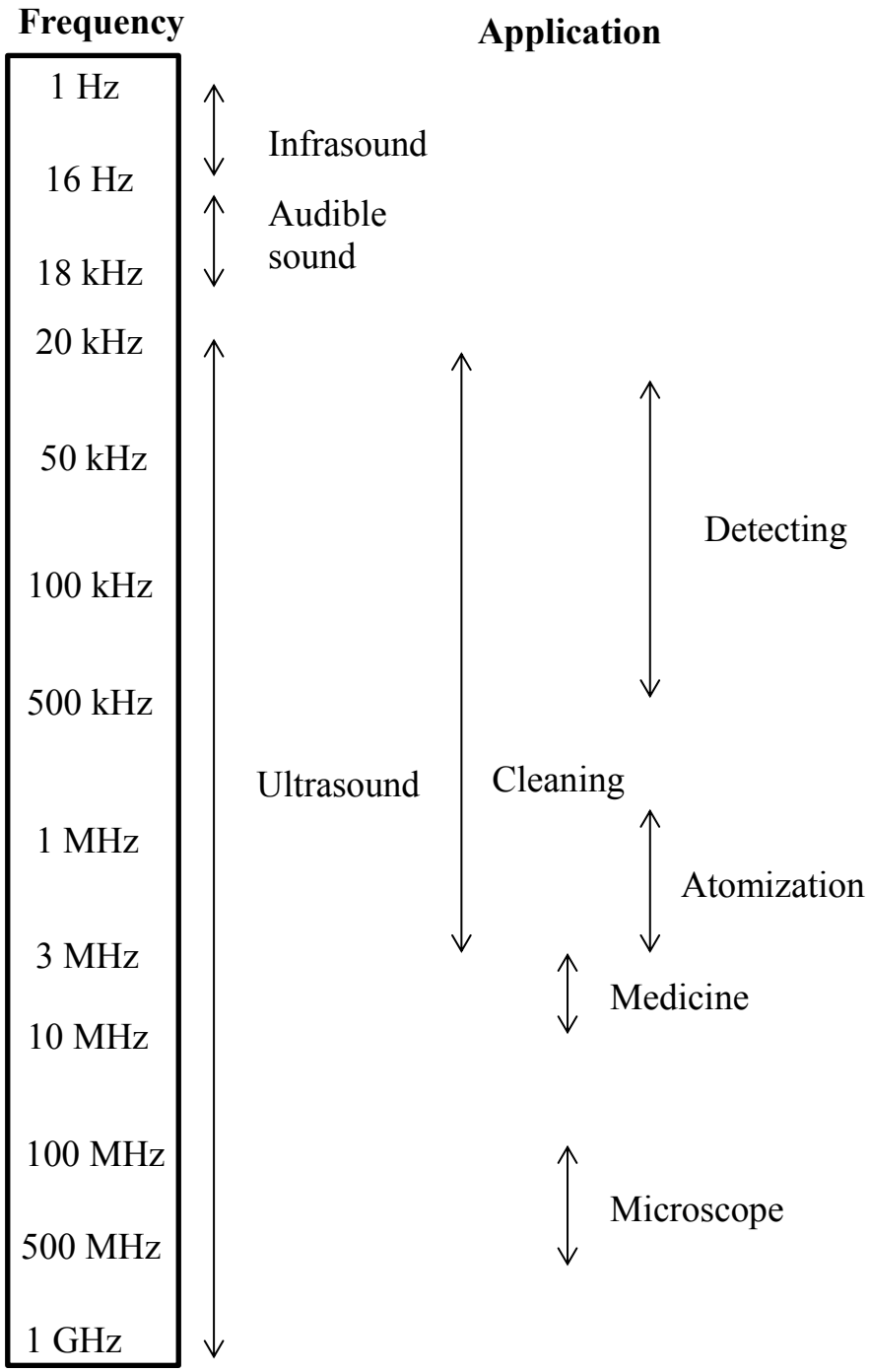

Fig. 1. 1 Frequency range of sound wave and application of ultrasound for different ultrasonic frequency

1.2. Acoustic cavitation

When ultrasound passes through a liquid medium, it causes mechanical vibration and acoustic streaming in the liquid. Under ultrasonic irradiation condition, with the presence of dissolved gas nuclei containing in the liquid, the gas nuclei grow and collapse. The formation and collapse of bubbles due to the decrease in liquid pressure induced by ultrasonic irradiation is defined as acoustic cavitation. The generated bubbles in acoustic cavitation are defined as acoustic cavitation bubbles. These processes of bubbles are illustrated in Fig. 1. 2.

Cavitation is categorized into two forms: transient and stable cavitation [4]. That means there are transient and stable cavitation bubbles. In terms of lifetime or stability of cavitation bubble, transient cavitation bubble is defined as the one which disintegrate into daughter bubbles just in a very short time about one or a few acoustic cycle. Owing to extremely high pressure inside the bubbles, the daughter bubbles dissolve into the liquid, or combine with others to form a larger active bubble. Meanwhile, stable cavitation bubble stays unchanged and oscillates around its equilibrium position over some refraction and compression cycles. In terms of the activity of the bubble, in transient cavitation, the bubbles are highly active in light emission from sonoluminescence or sonochemical reactions, whereas in stable cavitation, the bubbles are inactive. It is known that cavitation bubble size, life, and fate have a tight relationship with ultrasonic frequency, intensity, kinds of solvent, bubbled gas, temperature, and pressure. That relationship is a complicated one.

Physical effects, namely shockwaves, microjets, turbulence, and shear forces are originated from the oscillating and collapsing of cavitation bubble. Applications of physical effect can be listed as emulsification, extraction, and cleaning [5]. Acoustic cavitation produces high local pressure around 1000 atm, temperature to 5000 K, and velocity fields in liquid with very short lifetimes, causing extremely high heating and cooling rates higher than 10^9 K/s. The field which localized with high pressure and temperature is called the hot spot. Under the condition of extreme temperature, highly active radicals are formed, H and OH radicals are generated by the homolysis of water. High energy chemical reactions might occur under ultrasonic irradiation condition and a unique interaction of energy and matter is generated by acoustic cavitation. Taking advantages of these highly active radicals, ultrasonic cavitation is found to be useful in the synthesis of nanomaterials, polymers, and degradation of pollutants [6-8].

.

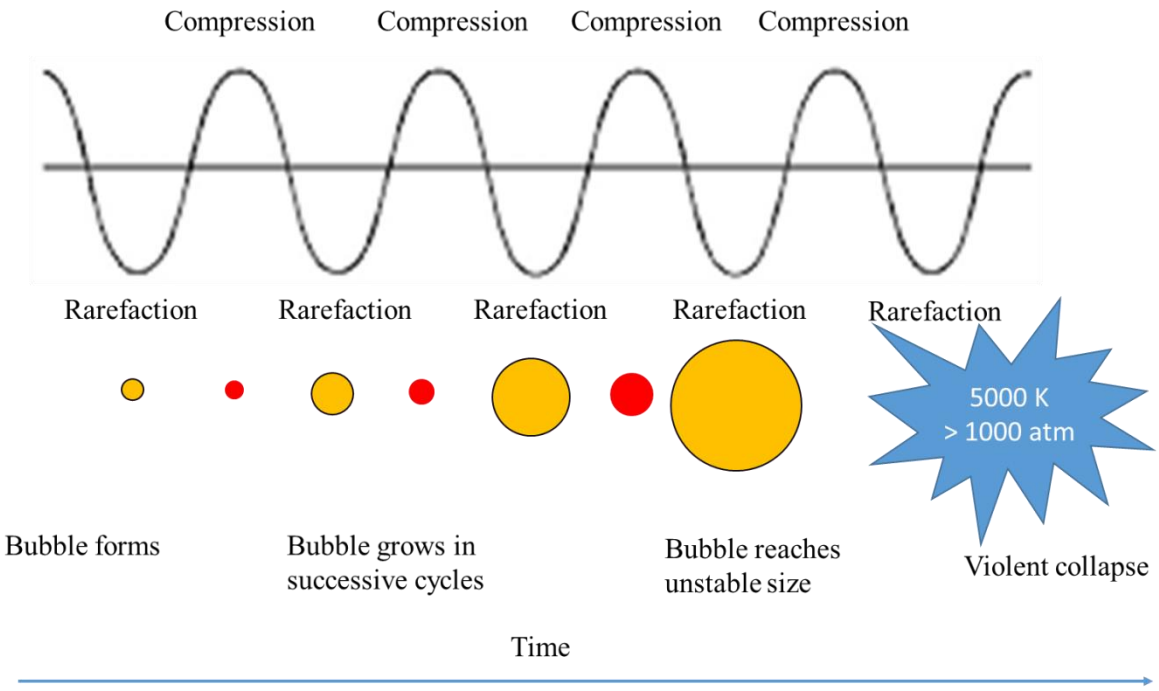

Fig. 1. 2 Growth and collapse of bubble in acoustic cavitation process [9]

1.3. Sonochemistry and its application

Sonochemistry is a scientific field that relates to phenomena and reactions originated from ultrasonic cavitation which is the formation of small cavities in a liquid that undergo highly energetic collapse. The phenomena are induced by shock waves or radicals generation in and around bubbles from the thermal decomposition of molecules in the liquid. In chemical industry, sonochemistry is the application of ultrasound to chemical reactions and processes in which cavitation is produced. The widespread examples of sonochemical equipment can be named as cleaning units, ultrasonic humidifiers, and ultrasonic atomizers.

Sonochemistry was firstly reported by Wood and Loomis [10] who investigated effects of ultrasound on emulsion preparation, atomization, particle aggregation, the acceleration of chemical reactions, crystal segregation and growth, and the dispersion of colloidal soil. In 1929, the chemical reaction effects of ultrasound were studied by Schmitt et al. [11]. Later in 1934, Frenzel and Schultes found out sonoluminescence and sonochemiluminescence phenomena [12]. In 1935, the first study of the effects of ultrasound on electrochemistry was reported by Claus and Hall [13]. They found out that the synthesizing of microparticles of silver and mercury in an electrode reaction by ultrasonic irradiation could make fine particles and high dispersibility. In 1938, first study on the application of ultrasound in organic chemistry was reported by Porter and Young, which showed that ultrasound induces the rearrangement of molecules and accelerate phenyl isocyanate generation from benzamide ($C_6H_5CON_3$) [14].

From 1993, chemical reactions by ultrasonic irradiation has been conducted by many groups of researchers including Moriguchi, Sata, and Kusano [15, 16]. In the late 1930s, polymer ultrasonic degradation which is popularly applied in recent times was investigated by Schmid and Weissler [17]. It is reported that when the sonication time increases, the molecular weight and viscosity of polystyrene decrease. At that time, cavitation threshold was determined as a certain level of ultrasonic intensity needed to generate cavitation by observing the instantaneous decrease of viscosity in toluene solutions containing polystyrene and hydroxyethyl cellulose solution [18].

The first important report about ultrasonic organic synthesis can be seen in the study of Kitazume and Ishikawa synthesizing trifluorotrimethyl carboninols by trifluormethylation of carbonyl compounds with trifluorotrimethyl carboninols [19]. From 1991 sonoluminescence experiments were conducted by Barber and Puttermann, Gaitan et al., Young, Flannigan and Suslick [20-23]. Together with contribution on sonoluminescence, at this time, material and environmental engineering by ultrasonic irradiation also bring much benefit. Nowadays, there are so many applications of sonochemistry available such as chemical engineering, biological engineering, environmental engineering, and medicine.

Compared to other conventional processes, sonochemisty produces highly beneficial effects in chemical industry by the following advantages:

- Useful reactive species are generated
- Reaction time decreases and reaction yield enhances
- Lower reaction temperature is needed

- Induction period is short
- Reaction pathway could be switched
- Less phase transfer catalysts are required
- Reactivity of reagents and catalysts is enhanced
- Metals and solids are strongly activated

The reaction process in sonochemistry is classified into gas – liquid, liquid – liquid, and solid – liquid reactions [10]. Solid – liquid process is applied in ultrasonic cleaning, extraction, separation, aggregation, and dispersion.

- In the industrial applications of ultrasound, ultrasonic cleaners are normally utilized in precision instruments, optical components, and certain semiconductor products. Owing to the object being cleaned and contamination removed, a variety of ultrasonic frequency is used in ultrasonic cleaners. Ultrasound at low frequency in the range of 20 – 100 kHz is used for the disengagement of oil spots attaching firmly on processing machine. However, ultrasound at high frequency above 1 MHz is useful for withdrawal of fine particles from silicon wafers.
- In extraction process, ultrasound promotes the separation of two immiscible phases. Mechanical effect of acoustic cavitation is strongly needed in extraction process, therefore, low frequency less than 100 kHz is usually used for the enhancement of active substance extraction. Ultrasound can be used in the extraction of active substances from plants, bitumen from oil shale, pungent compounds from ginger in supercritical carbon dioxide.
- In separation, when ultrasound is applied in the process, it promotes the permeate

flux of materials propagating through a separation membrane. The mechanism is that ultrasonic cavitation breaks up layers of deposited material and prevents membrane fouling. Furthermore, the micromixing caused by acoustic streaming reduces the solute concentration near the membrane surface. Ultrasonic frequencies less than 100 kHz are usually used for ultrasonic separation.

- The ultrasonic frequency applied in ultrasonic aggregation is normally greater than 100 kHz. Ultrasound is comparatively efficient in aggregation because no aggregation enhancing additives are required, consequently no contamination is caused, and it is easily operated.
- Various kinds of particles including titanium oxide, pigment, silicon, magnetic powder, microbe, and microcapsule have been applied in ultrasonic dispersion. The process is promoted by the localized and high fluid flow caused by ultrasonic cavitation and strong vibration acceleration from the penetrating of the ultrasound through the medium. The suitable ultrasonic frequency for dispersion is less than 100 kHz.

Liquid – liquid process is applied in emulsification. Some emulsified substances have been applied namely oil, fuel, mayonnaise, cosmetics, biodiesel, and lotion. Ultrasonic frequency around 20 kHz is normally used. Using ultrasound, when it is irradiated into an oil – water medium, oil droplets with several μm in diameter are dispersed into the water phase and an emulsion is formed in which no surfactants are used. The main reasons for the formation of emulsion by ultrasound are explained by the breakage of capillary waves at the interface of oil – water medium and the refinement of droplets induced by cavitation.

Gas – liquid process is applied in atomization. Atomization is known as the fountain arises from the liquid surface and fine droplets are generated from that fountain when a high-power ultrasound is irradiated in the liquid. Ultrasound with frequency ranging from 500 kHz to 2.4 MHz is usually used for ultrasonic atomization. The capillary wave at the fountain surface and the cavitation inside the fountain are considered as the mechanism for ultrasonic atomization. A variety of liquid such as water, insecticide, fragrance substance, drug, and fuel has been applied in ultrasonic atomization. The advantage of ultrasonic atomization is its compactness. Additionally, it is easily to obtain the desired droplet size and amount of atomization by adjusting the ultrasonic frequency and intensity, respectively.

1.4. Objective of this study

Ultrasonic cavitation, and its chemical and mechanical effects are powerful tools which have been utilized in a variety of industrial applications at various frequencies. A sufficient understanding of cavitation and its effects on the sound pressures at different frequency components is necessary to effectively to apply ultrasonic cavitation into industry. The outline of this study is divided into 7 chapters.

- Chapter 1, general introduction. In this chapter, ultrasonic cavitation, sonochemistry, and applications of sonochemistry are explained.
- Chapter 2, theory. Theory of ultrasound, ultrasonic cavitation, and broadband noise are explained.

- Chapter 3, sound pressure and cavitation threshold. Cavitation threshold is determined and sound pressures at the second harmonic and the first harmonic frequencies are measured. Dependence of cavitation threshold and sound pressures at those frequency components are reported.
- Chapter 4, chemical and mechanical effects. Chemical and mechanical effect thresholds are measured by KI oxidation and aluminum foil erosion, respectively. The frequency dependence of chemical effect, and mechanical effect thresholds in the wide frequency range from 22 to 4880 kHz is clarified.
- Chapter 5, measurement of distribution of broadband noise and sound pressures in sonochemical reactor. In this chapter, to estimate reaction fields in the sonochemical reactor, the measurement of cross-sectional area distribution of broadband noise is performed. Besides, because it is known that the sound pressure and bubbles largely effect the reaction field, the cross-sectional area distribution of sound pressures at the fundamental and second harmonic frequencies are also measured.
- Chapter 6, application of ultrasonication and silica gel on removal of silicic acid in geothermal water. The experiments are conducted at various experimental conditions to investigate the potential of removal of silicic acid in water by the combination of ultrasonication and silica gel.
- Chapter 7, summary. The thesis is summarized and the future perspective is provided.

References

1. P.P. Lele, "An annular-focus ultrasonic lens for production of uniform hyperthermia in cancer therapy." Ultrasound in Medicine & Biology 7(2) (1981) 191 – 193.
2. K.S. Suslick, Ultrasound: its chemical, physical, and biological effects. VCH Publishers, 1988.
3. A. Henglein, Sonochemistry: historical developments and modern aspects, Ultrasonics 25(1) (1987) 6 – 16.
4. T. Leighton, The acoustic bubble. Academic press, 2012.
5. G. Price (Ed.), Current Trends in Sonochemistry, RSC, Cambridge, UK (1992).
6. M. Ashokkumar, Sonochemical synthesis of inorganic nanoparticles. In Advanced Wet-Chemical Synthetic Approaches to Inorganic Nanostructures (2008) 107 – 318.
7. S. Muthukumaran, S.E. Kentish, M. Ashokkumar, G.W. Stevens, Application of ultrasound in membrane separation processes: a review Rev. Chem. Eng., 22 (2006) 155 – 194.
8. K. Hirai, Y. Nagata, Y. Maeda, Decomposition of chlorofluorocarbons and hydrofluorocarbons in water by ultrasonic irradiation, Ultrason. Sonochem. 3(3) (1996) S205.
9. S. Abbas, K. Hayat, E. Karangwa, M. Bashari, X. Zhang, An overview of ultrasound-assisted food-grade nanoemulsions. *Food Engineering Reviews*, *5*(3) (2013) 139 – 157.
10. R.W. Wood, A.L. Loomis, The physical and biological effects of high-frequency sound-waves of great intensity, Philos. Mag. 4(22) (1927) 417 – 436.
11. F.O. Schmitt, C.H. Jonhnson, A.R. Olson, Oxidations promoted by ultrasonic radiation, J. Amer. Chem. Soc. 51(2) (1929) 370 – 375.
12. H. Frenzel, H. Schultes, Luminescence in ultra-ray layered water. Short announcement, Z. Phys. Chem. B27(1) (1934) 421 – 424.
13. B. Claus, S. Hall, Uber eine neue Method und Einrichtung zur Erzeung Hochdisperser Zustande, Zeitschr. F. Techn. Physik. 3 (1935) 80 – 82.
14. C.W. Porter, L. Young, A molecular rearrangement induced by ultrasonic waves, J. Amer. Chem. Soc. 60(6) (1938) 1497 – 1500.
15. N. Sata, U ¨ber die Bedeutung der Gasphasen fu ¨r die mechanische Synthese disperser Quecksilbersysteme, Kolloid-Zeitschrift 71 (1935) 48 – 55.
16. S. Kusano, Wirkung der ultraakustischen Schallwellen auf Jodkalium undand Wasserstoffsuperoxyd, Tohoku J. Exp. Med. 30 (1936) 175 – 180.
17. G. Schmid, O. Rommmel, ZerreiBen von MakromolecuUlen mit Ultraschall, Z. Physkal. Chem. 185 (1939) 97 – 139.
18. A. Weissler, Depolymerization by ultrasonic irradiation, J. Appl. Phys. 21(2) (1950) 171 – 173.
19. T. Kitazume, N. Ishikawa, Trifluoromethylation of carbonyl compounds with trifluo romethylzinc iodide, Chem. Let. 10(12) (1981) 1679 – 1680.
20. B.P. Barber, S.J. Putterman, Observation of synchronous picosecond sonoluminescence, Nature 352 (1991) 318 – 320.
21. D.F. Gaitan, L.A. Crum, C.C. Church, R.A. Roy, Sonoluminescence and bubble dynamics for a single, stable, cavitation bubble, J. Acoust. Soc. Am. 91(6) (1992) 3166 –

3182.
22. F.R. Young, Sonoluminescence, CRC Press, 2005, pp. 67 – 68.
23. D.J. Flannigan, K.S. Suslick, Plasma formation and temperature measurement during single-bubble cavitation, Nature 434(7029) (2005) 52 – 55.

Chapter 2

Theory

2. 1. Ultrasound

2.1.1. Basic equations

When a sound wave is applied to a continuous and uniform medium, the particles translationally vibrate parallel to the sound wave propagating direction. In an equilibrium state, the pressure and density of the fluid are denoted by P_0 and ρ_0, respectively. Velocity u is different at each position on the propagation path or density. The increment of the density from ρ_0 is denoted by ρ, and then the increment of pressure accompanying ρ is defined as the sound pressure p. The following equation is often used to determine the vibration of a fluid by velocity potential $\emptyset$ instead of u

$$u = -\nabla\emptyset = -(\frac{\partial\emptyset}{\partial x}, \frac{\partial\emptyset}{\partial y}, \frac{\partial\emptyset}{\partial z}) \quad (2.\ 1)$$

The values of u, ρ, and p change with time t. A one-dimensional wave in x direction is used to simplify. The difference of the pressure at two positions of x and x+Δx is $p(x) - p(x + \Delta x) \approx -(\partial p/\partial x)\Delta x$. This force is applied to a mass of $\rho_0\Delta x$. It is known that the acceleration of u can be evaluated as

$$\lim_{\Delta t\to 0}[u(x + u\Delta t, t + \Delta t) - u(x,t)]/\Delta t = \lim_{\Delta t\to 0}[u(x + u\Delta t, t + \Delta t) - u\,(x, t + \Delta t) + u(x, t + \Delta t) - u(x,t)]/\Delta t = u\partial u/\partial x + \partial u/\partial t \quad (2.\ 2)$$

Then the motion for the acceleration d*u*/d*t* is obtained in the next equation

$$\rho_0\left(\frac{\partial u}{\partial t}+u\frac{\partial u}{\partial x}\right)=-\frac{\partial p}{\partial x} \tag{2. 3}$$

When $u \approx 0$, Eq 2.3 is approximated as

$$\rho_0\left(\frac{\partial u}{\partial t}\right)=-\frac{\partial p}{\partial x} \tag{2. 4}$$

While the mass at x is $\rho_0 u$(x)per unit area and unit time, the mass at x+Δx is $\rho_0 u(x+\Delta x)$. The difference $\rho_0[u(x)-u(x+\Delta x)]=-\rho_0(\partial u/\partial x)\Delta x$ is the increase of mass between x and x + Δx per unit area and unit time. Thus, the equation becomes

$$\frac{\partial p}{\partial t}=-\rho_0\frac{\partial u}{\partial x} \tag{2. 5}$$

The change in density, ρ/ρ_0, represents the change in pressure by the following equation

$$p=K\frac{\rho}{\rho_0} \tag{2. 6}$$

where K is the volume elasticity. In a condition of ideal gas, $K = \gamma P_0$, where γ is the specific heat ratio. Thus, the acoustic pressure can be obtained from the velocity potential.

$$p = \rho_0 \frac{\partial \emptyset}{\partial t} \quad (2.\ 7)$$

Finally, Eq 2. 8, which is called the d' Alembert's wave equation in one dimension is obtained

$$\frac{\partial^2 p}{\partial x^2} - \frac{1}{c_0^2}\frac{\partial^2 p}{\partial t^2} = 0 \quad (2.\ 8)$$

Where $$c_0^2 = \frac{K}{\rho_0} \left(= \frac{\partial p}{\partial \rho}\right) \quad (2.\ 9)$$

2.1.2. Physical Quantities of Sound

There are several units of the sound pressure such as N/m^2, Pa, atm, or dB. Under ambient condition, the static pressure in the water is 1 atm. In order to generate ultrasonic cavitation, pressure amplitude above 1 atm is required to overcome the tensile strength of the liquid.

For a harmonic wave radiating from ultrasound at frequency *f*, the local variation of sound pressure at a certain time of 1 s after ultrasonic irradiation is demonstrated along the

propagation pathway c_0 is the distance from the source to the position being monitored after a period of 1 s. In the range c_0, there is f-cycle waves and the length of a single cycle is called wavelength λ, is given by $\lambda = c_0/f$. Since the phase changes by 2π for each single cycle (λ distance), the phase changes by $2\pi/\lambda = 2\pi f/c_0$ per unit distance (1m). $k = 2\pi f/c_0$ is called the wave number. Angular frequency $\omega = 2\pi f$ is the change of the phase of a harmonic frequency f per unit time (1s). A harmonic plane wave with an amplitude P propagating along x direction is expressed as

$$p = Pcos(\omega t - kx) \quad (2.\ 10)$$

2.1.3. Relationship between sound pressure and particle velocity

A particle velocity of a sound wave is assumed as

$$U = U_1 \exp(-jkx) - U_2 \exp(jkx) \quad (2.\ 11)$$

In Eq. 2. 11, the forward wave travelling in the +x direction is denoted by the first term, the backward wave travelling in the -x direction is denoted by the second term. To make certain the particle velocity in the propagating direction of sound wave is always positive, a negative sign is attached to the backward wave. Using Eqs. 2. 5, 2. 6, 2. 9, and 2. 11 is approximated as

$$P = \rho_0 c_0 U_1 \exp(-jkx) + \rho_0 c_0 U_2 \exp(-jkx) \quad (2.\ 12)$$

Comparing Eq. 2. 11 and Eq. 2. 12, it is shown that the difference between sound pressure and particle velocity is a multiplied value of a constant $\rho_0 c_0$. The constant $Z_0 = \rho_0 c_0$ is named as the characteristic impedance of the specific acoustic impedance. Depending on kind of gases and liquids the value of ρ_0, c_0, and Z_0 vary differently. Some examples are listed in Table 2. 1

Table 2. 1 Acoustic properties in some media [1]

Medium	**Density ρ_0 (kg/m^3)**	**Sound speed c_0 (m/s)**	**Characteristic impedance Z_0 (10^6 kg/m^2s)**
Water	1000	1500	1.5
Ice	1000	3980	4.0
Air	1.3	330	0.00043
Methanol	790	1120	0.88
Ethanol	790	1180	0.93
Glycerin	1260	1920	2.42
Olive oil	900	1380	1.24
Rubber	950	1500	1.5
Steel	7700	5850	45
Aluminum	2700	6260	17
Silicon glass	2700	5570	15

In another word, the relation of sound pressure and particle velocity is shown as $u = p/\rho_0 c_0$ or $pu = p^2/\rho_0 c_0$ (instantaneous power per unit area). Thus, the acoustic power of the sound wave is calculated by

$$I = \frac{|P|^2}{2\rho_0 c_0} \text{ (W/m}^2\text{)} \qquad (2.\ 13)$$

2. 2. Ultrasonic cavitation

2.2.1. The condition for large expansion of a bubble (Blake threshold)

The surface tension, σ of the bubble-gas interface is one of the most important factors affect the pressure inside a bubble. Surface tension is the surface energy per unit area. As the bubble radius is R, the surface area is $4\pi R^2$, and the total surface energy of a bubble is $4\pi\sigma R^2$.

When a bubble grows, its radius expands by dR, hence, the surface area increases into $4\pi(R+\mathrm{d}R)^2$. The energy needed to expand the bubble is $8\pi\sigma R\mathrm{d}R$, $(\mathrm{d}R)^2$ term is neglected because dR is sufficiently small. As this energy equals the force multiplied by the distance travelled, the force equals $8\pi\sigma R$. Hence, between inside and outside of the bubble the force balance is demonstrated by$4\pi R^2 p_{in} = 4\pi R^2 p_B + 8\pi\sigma R$, here p_{in} is the pressure inside the bubble and p_{B} is the liquid pressure outside the bubble. Finally, the relationship between force inside and outside of the bubble is obtained as follow:

$$p_{in} = p_B + \frac{2\sigma}{R} \qquad (2.\ 14)$$

The second term on the right side of Eq. 2. 14 is named as the Laplace pressure. It is deduced that Laplace pressure indicates the difference between the bubble internal pressure and the liquid pressure outside the bubble. In another word, the pressure inside the bubble is higher than the pressure outside the bubble by the amount of the Laplace pressure.

Figure 2. 1 shows the relationship between the pressure inside and outside of a

bubble. As seen in the Fig. 2. 1, the internal pressure of the bubble is the sum of the gas pressure and vapor pressure. According to the expansion and collapse of the bubble, the gas pressure dramatically changes, while the vapor pressure is assumed to keep unchanged at the saturated vapor pressure, even during the pulsation period of the bubble.

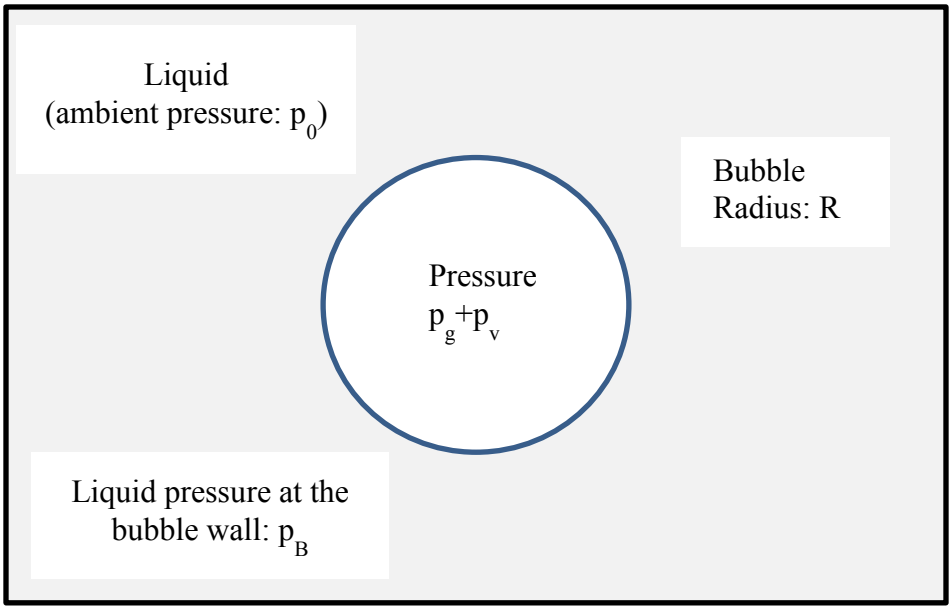

Fig. 2. 1 The relationship between the internal pressure of a bubble and the surrounding liquid pressure

The gas pressure inside the bubble is approximately expressed by Eq. 2. 15

$$p_g V^k = const \qquad (2.\ 15)$$

where V is the volume of bubble and k is a constant. When the heat transfer between inside

and outside of a bubble is negligible, the pulsation process of bubble becomes adiabatic, hence, $k = \gamma = C_p/C_v$, here γ is called the specific-heat ration, C_p is the specific at constant pressure, and C_v is specific heat at constant volume. In the case bubble pulsation is mild, bubble pulsation becomes an isothermal process, hence, k = 1. In reality, the bubble pulsation could not be adiabatic or isothermal, therefore, k varies between 1 and γ.

When there is no ultrasonic irradiation in a liquid, a bubble is considered static, and the gas pressure inside a static bubble is expressed by Eq. 2. 16 using Eq. 2. 14 with both of p_B and p_0 are the static ambient pressure. Usually the static ambient pressure is equivalent to 1 atm.

$$p_{g,s} = p_0 + \frac{2\sigma}{R_0} - p_v \qquad (2.\ 16)$$

where g and s indicate gas and static bubble, R_0 is the ambient bubble radius (bubble in the condition of without ultrasound), and the relationship $p_{in} = p_{g,s} + p_v$ is used.

When the liquid is irradiated by ultrasound, the bubble radius temporally changes. When the instantaneous bubble radius is R, the gas pressure inside the bubble p_g is calculated by

$$p_g = p_{g,s}(\frac{R_0}{R})^{3k} = (p_0 + \frac{2\sigma}{R_0} - p_v)(\frac{R_0}{R})^{3k} \qquad (2.17)$$

using $V = 4\pi R^3/3$, then, the liquid pressure at the bubble wall (p_B) is expressed by Eq.

2.18.

$$p_B = \left(p_0 + \frac{2\sigma}{R_0} - p_v\right)\left(\frac{R_0}{R}\right)^{3k} + p_v - \frac{2\sigma}{R} \qquad (2.\ 18)$$

To determine the acoustic pressure required for a large expansion of bubble, a minimum value of p_B is calculated. p_B in Eq. 2. 18 is differentiated with respect to R

$$\frac{\partial p_B}{\partial R} = -3k\left(p_0 + \frac{2\sigma}{R_0} - p_v\right)R_0^{3k}R^{-(3k+1)} + \frac{2\sigma}{R^2} \qquad (2.\ 19)$$

When p_B is at minimum value, $\partial p_B/\partial R$ =0. In this case, R is expressed by R_{crit}, Eq. 2. 19 becomes

$$(R_{crit})^{3k-1} = \frac{3k}{2\sigma}\left(p_0 + \frac{2\sigma}{R_0} - p_v\right)R_0^{3k} \qquad (2.\ 20)$$

Under ultrasonic irradiation, the expansion of a bubble is relatively slow due to the affect of the compression of surrounding liquid. Therefore, bubble expansion in most cases is nearly isothermal, that is the temperature of internal bubble and the liquid surrounding the bubble approximately equal. In this condition, k = 1

$$R_{crit} = \sqrt{\frac{3R_0^3}{2\sigma}\left(p_0 + \frac{2\sigma}{R_0} - p_v\right)} \quad (2.\ 21)$$

Inserting Eq. 2. 21 into Eq. 2. 18, the minimum value of p_B is obtained as below

$$p_{B,min} = p_v - \frac{4\sigma}{3}\sqrt{\frac{2\sigma}{3R_0^3\left(p_0 + \frac{2\sigma}{R_0} - p_v\right)}} \quad (2.\ 22)$$

Under ultrasonic irradiation condition, the liquid pressure far from a bubble is expressed by $p_0 + p_s(t)$, here p_0 is the static ambient pressure and $p_s(t)$ is the sound pressure at time *t*. The bubble will expand when this pressure is smaller than the liquid pressure at the bubble wall (p_B). If this pressure is even smaller than the minimum value of p_B given by Eq. 2. 22, the bubble will continuously expand. As the pressure amplitude of ultrasound is *A* and its angular frequency is ω, hence $p_s(t) = Asin\omega t$ and the minimum value of $p_s(t)$ is *–A*. The bubble will dramatically expand when $p_0 - A$ is smaller than the minimum value of p_B from Eq. 2. 27. The condition for bubble dramatically expanding is that the threshold condition is adapted, $A \geq A_{Blake}$. A_{Blake} is called Blaked threshold and expressed by Eq. 2. 23

$$A_{Blake} = p_0 - p_{B,min} = p_0 - p_v + \frac{4\sigma}{3}\sqrt{\frac{2\sigma}{3R_0^3\left(p_0 + \frac{2\sigma}{R_0} - p_v\right)}} \quad (2.\ 23)$$

Because a bubble often violently collapses after a large radical expansion, the Brake threshold is referred to as the cavitation threshold.

2.2.2. The primary Bjerknes force

The Eq. 2. 24 expresses the ultrasonic radiation force on a pulsating bubble in a standing wave field of ultrasound which is called the primary Bjerknes force.

$$\vec{F}_B = -\langle \vec{F}_p \rangle = -\langle V \nabla p \rangle \quad (2.\ 24)$$

where $\vec{F}_p$, $\langle \vec{F}_p \rangle$, and V are the instantaneous radiation force on a bubble, the time-averaged value, and the bubble volume, respectively. In a standing wave field, the acoustic pressure p is expressed by the next equation

$$p(z,t) = -Acos(kz)\sin(\omega t) \quad (2.\ 25)$$

where A is the pressure – amplitude of ultrasound, $k = 2\pi/\lambda$ is wave number, $\omega = 2\pi f$ is

the angular frequency, and f is the ultrasonic frequency. When ultrasound is irradiated from the transducer attached to the bottom of a liquid reactor, a standing wave is formed at the positions of $z = (2n + 1)\pi/2k$. It is should be noted that z-axis is in the vertical direction of the reactor and n is a natural number. Thus, the primary Bjerknes force is expressed by

$$\vec{F}_p = \left(-\frac{4\pi}{3}\right) R^3 kAsin(kz)\sin(\omega t)\vec{e}_z \qquad (2.\ 36)$$

where R is the instantaneous radius of bubble and $\vec{e}_z$ is a unit vector in z direction.

During the rarefaction phase of an ultrasonic wave at the initial half-wave period, a bubble expands, whereas during the compression phase of ultrasonic wave at the latter half-wave period, a bubble collapses and continuously repeats small pulsations. In the former case, at the pressure antinode the smallest acoustic pressure is obtained, and the instantaneous radiation force is directed toward the pressure antinode. On the other hand, in the latter case, at the pressure antinode the highest acoustic pressure is obtained, and the instantaneous radiation force is directed away from the pressure antinode. From Eq. 2. 24, it can be seen that the instantaneous radiation force is proportional to the volume of a bubble, comparing the force during bubble expansion and bubble collapse, the force in the former phase is stronger. Consequently, the time-averaged value in Eq. 2. 24 is directed toward the pressure antinode. Nevertheless, if the force is over a critical value, the bubble continuously expands at the beginning of the second phase of the ultrasound wave, that is, the compression phase. As a result, the repulsion force from the pressure antinode in the

compression phase is stronger than the attractive force generated in the rarefaction phase. Then, a bubble is moved away from the pressure antinode. Bubbles will gather at the positions between pressure node and antinode in the liquid. At those regions, a jellyfish or double-layer structure of bubbles is formed.

Large bubbles whose ambient radius are larger than the resonance radius, bubble pulsation is an antiphase mode of the ultrasound wave. Instead of collapsing, bubble expands during the compression phase, and the time-averaged radiation force is directed away from the pressure antinode of the standing wave. Consequently, those large bubbles are trapped at the pressure nodes in the liquid.

2.3. Broadband noise

Under acoustic cavitation condition, pulsating of bubbles leads to the emitting of acoustic wave which is called acoustic cavitation noise. The frequency spectra of acoustic cavitation noise contain various components consisting of the driving frequency, harmonics, ultraharmonics, subharmonics and broadband noise. Broadband noise is defined as a continuum part of the frequency spectrum [2]. The intensity of the broadband noise has been used as an indicator for the intensity of the acoustic cavitation [3]. There are several hypotheses of the origin of the broadband noise. Non-periodic pulsation of bubbles which is called chaotics pulsations is one of the reasons [4]. An acoustic wave radiated from the chaotics pulsation which is temporally non-periodic results in the broadband noise. The second hypothesis is that broadband noise originates from shock waves emitted

from bubble collapse [5, 6]. At the end of bubble collapse, shock wave is emitted and hits a hydrophone as a strong pulse. Broadband noise is originated from a single strong pulse which is likely a delta function pulse. Lately, Yasui et al. confirmed that shock waves emitted from stable bubbles do not generate broadband noise [7]. The explanation is that the frequency spectrum from collapse of stable bubble only contains fundamental frequency and its harmonics. It is reported that the temporal fluctuation in the number of bubbles leads to the formation of broadband noise. The result from numerical simulations showed that in the case of no temporal fluctuation in the number of bubbles, the pressure of acoustic waves radiated from bubbles is a periodic function of time with acoustic period. As a result, the hydrophone signal is also a periodic function of time and its frequency spectrum consists of peaks at driving frequency and harmonics due to the nature of any periodic function. Therefore, there is no broadband noise in the frequency spectrum in the case of temporally periodic bubble pulsation and constant bubble number. On the other hand, if bubbles could disintegrate into daughter bubbles, then the number of bubbles change, that is, there is a temporal fluctuation in the number of bubbles. It leads to the random variation of pressure of shock waves with time. As a result, beside of peaks at driving frequency and its harmonics, the frequency spectrum of the hydrophone signal also contains the broadband noise. Therefore, it is concluded that the temporal fluctuation in the number of transient bubbles results in the broadband noise. Broadband noise is directly attributed to bubble collapse, hence, it is used to measure cavitation intensity.

References

1. P.P. Lele, "An annular-focus ultrasonic lens for production of uniform hyperthermia in cancer therapy." Ultrasound in Medicine & Biology 7(2) (1981) 191 – 193.
2. S. Koda, K. Yasuda, Sonochemical engineering process. In: F. Grieser, P. Choi, N. Enomoto, H. Harada, K. Okitsu, K. Yasui, Sonochemistry and the acoustic bubble, Elsevier, Amsterdam, 2015, 151 – 169.
3. E.A. Neppiras, Acoustic cavitation, Phys. Rep. 61(3) (1980) 159 – 251.
4. J. Frohly, S. Labouret, C. Bruneel, I. Looten-Baquet, R. Torguet, Ultrasonic cavitation monitoring by acoustic noise power measurement, J. Acoust. Soc. Am. 108(5) (2000) 2012 – 2020.
5. V.I. Ilyichev, V. L. Koretz, N.P. Melnikov, Spectral characteristics of acoustic cavitation, Ultrasonics 27(6) (1989) 357 – 361.
6. E.A. Nepprias, Subharmonic and other low-frequency emission from bubbles in sound-irradiated liquids, J. Acoust. Soc. Am. 46(3B) (1969) 587 – 601.
7. A.J. Coleman, M.J. Choi, J.E. Saunders, T.G. Leighton, Acoustic emission and sonoluminescence due to cavitation at the beam focus of an electrohydraulic shock wave lithotripter, Ultrasound Med. Biol. 18(3) (1992) 267 – 281.
8. K. Yasui, T. Tuziuti, J. Lee, T. Kozuwa, A.Towata, Y. Iida, Numerical simulations of acoustic cavitation noise with the temporal fluctuation in the number of bubbles, Ultrason. Sonochem. 17(2) (2010) 460 – 472.

Chapter 3

Sound pressure and cavitation threshold

3.1. Introduction

High-intensity ultrasound in liquid has practical applications such as ultrasonic cleaning, homogenization [1], and atomization [2, 3], and has potential applications in extraction [4], emulsification [5], crystallization [6], sonochemical reactions [7-9], droplet coalescence [10], pharmaceutical processing [11], and therapy [12-15]. The evaluation of sound intensity in liquid is important for the development of ultrasonic devices. Sound intensity was evaluated by, for example, sound pressure measurement [16], radiation force measurement [17], and calorimetry [18].

Among these techniques, sound pressure measurement has been proposed as a particularly effective method to obtain the spatial distribution of sound pressure [19]. For example, the measurement of sound pressure distribution in a cleaner is important to analyze the nonuniform sound field when continuous ultrasound is irradiated and a standing wave is formed [20]. In sound pressure measurement, a hydrophone is normally used. Acoustic cavitation is a phenomenon when tiny bubbles are created through the irradiation of ultrasound into a liquid, and then these tiny bubbles oscillate and collapse. It is known that acoustic cavitation makes high local pressure, temperature, and velocity fields in a liquid. Since a hydrophone easily breaks owing to acoustic cavitation, the sound pressure measurement using a continuous wave at a high sound intensity has not been sufficiently conducted in a wide range of driving ultrasonic frequencies. A tough needle-type hydrophone has been fabricated by a hydrothermal synthesis method. This hydrophone can measure high sound pressures in a wide range of ultrasonic frequencies within which a

high-intensity continuous ultrasound is irradiated and many cavitation bubbles occur [21, 22].

Cavitation threshold refers to the minimum acoustic pressure amplitude required to initiate acoustic cavitation. Study on cavitation threshold is necessary to prevent cavitation damage to objects and medium during irradiation in its applications. It is considerably important to know the cavitation threshold to effectively avoid cavitation damage. Many methods including broadband noise [23, 24], acoustic emission [25-27], bubble observation [28], sonochemical luminescence [29], sonoluminescence [30], and aluminum foil erosion [31] have been used to measure the cavitation threshold. Under ultrasonic irradiation, the acoustic emission from bubbles is composed of harmonics (integer multiples of fundamental), subharmonics (fundamental frequency divided by integer), ultraharmonics (integer multiples of subharmonics excepting the fundamental and harmonics), and broadband noise components. A hydrophone is used to detect these frequency spectra. In recent times, in order to measure cavitation threshold, broadband noise is used because it is directly attributed to cavity collapse. The broadband integrated voltage (BIV) which is an integration value of broadband noise is used to quantify the broadband noise. Specifically, Hodnett and Zeqiri irradiated ultrasound at 25 kHz and measured broadband noise in the frequency range of 1.5 - 8 MHz [24]. Uchida et al. used much higher driving frequency at 150 kHz and measured broadband noise in the narrower region from 1 to 5 MHz [32, 33]. Shiiba et al. investigated spatial distribution of cavitation in the same level of ultrasound at 150 kHz sonoreactor and calculated BIV in the much wider frequency range from 1 to 10 MHz [34]. However, in order to measure broadband noise accurately, it is necessary to

completely eliminate a fundamental, all harmonic, all subharmonic, and all ultraharmonic components in the frequency spectra.

The sound intensity in the liquid from low to high electric power is evaluated, especially near the vicinity of cavitation threshold to know the effect of ultrasonic cavitation on the sound intensity measurement. Theoretically, the sound intensity is proportional to the effective electric input power applied to a transducer [35]. Thus the sound pressure is proportional to the square root of the electric input power. However, Neppiras reported that received sound pressure from a microphone decreased rapidly in the vicinity of applied sound pressure of cavitation threshold. He detected the cavitation threshold by the appearance of the broadband noise. He also measured the subharmonic (fundamental frequency divided by integer) component and reported that the subharmonic signal drastically arose in the vicinity of applied sound pressure of cavitation inception and visible bubbles were observed. The broadband noise has been utilized by several researchers to detect cavitation generation. Additionally, the harmonic (integer multiplies of fundamental) component has been used as an indicator for bubble generation. The effect of driving frequency on the relationship between the broadband noise and the sound pressures of the fundamental, harmonics, and subharmonics was little investigated.

For the evaluation of ultrasonic apparatus, it is important to measure sound pressures of some components in the presence of cavitation bubbles. Therefore, a broadband integrated pressure (BIP) and sound pressures at the fundamental (f_1), first harmonic (f_2), and first ultraharmonic (1.5 multiplies of fundamental, $f_{1.5}$) frequencies were measured by the needle type tough hydrophone with increasing effective input power applied to a

transducer. The driving frequencies of transducer were chosen specifically from low to high frequency at 22, 43, 98, 304, and 488 kHz. In order to visualize bubbles in the presence of cavitation, an ultrasonic diagnostic equipment was used.

Ultrasonic applications are utilized at various frequencies. However, until now the measurement of cavitation threshold has been mainly conducted below frequency of 100 kHz used for the cleaner and homogenizer. Threshold data in the frequency range from 100 kHz to 1 MHz are important for sonochemical reactor because the performance of sonochemical reaction is high [36]. Cavitation threshold for this frequency range are few reported. In this chapter, cavitation threshold will be reported at wide range of frequency from 22 to 4880 kHz and the dependence of cavitation threshold on frequency will be clarified. In addition, the sound pressures at the second harmonic and the first ultraharmonic frequencies in the spectra were measured for an indicator of bubble occurrence in water [37]. The minimum sound pressure amplitude required to emit the second harmonic and the first ultraharmonic components, that is, thresholds of the second harmonic and the first ultraharmonic signals were estimated.

3.2. Experiment

3.2.1. Apparatus

This study was carried out with various frequencies of acoustic wave at 22, 43, 98, 304, 488, 1000, 2000, and 4880 kHz using a directly sonochemical reactor. A stainless steel reactor with inner diameter of 56.8 mm was used for all experiments. The stainless steel

reactor was connected to a cooling system with the aim of giving the constant temperature of solution inside the reactor at 298 K during entirely experimental period. Corresponding to frequency needed to be generated, Langevin and disc transducers were used at low and high frequencies, respectively. A Langevin transducer 45 mm in diameter with multiple frequencies (HEC45242M, Honda Electronics) was used for 22, 43, and 98 kHz. Disc transducers 50 mm in diameter were used for 304, 488, 1000 and 2000 kHz. A disc transducer 20 mm in diameter was used for 5000 kHz. Details of transducers at all frequencies utilized in the experiments are summarized in Table 3. 1.

Table 3. 1 Details of transducers

Frequency (kHz)	**Type of transducer**	**Diameter of transducer (mm)**
22	Langevin	45
43	Langevin	50
98	Langevin	50
304	Disc	50
488	Disc	50
1000	Disc	50
2000	Disc	50
4880	Disc	20

3.2.2. Sound pressure and broadband integrated pressure detection

Figure 3. 1 schematically illustrates the experimental system for measurement the sound pressures and broadband noise. To measure generated sound pressure and BIP in a wide range of frequency, the tough needle-type hydrophone (HUS-200S, Honda Electronics) was submerged into the irradiation vessel at the position of highest sound pressure. An XYZ-axis stage and a stage controller (SHOT-204, Sigmakoki) were used to precisely adjust the hydrophone position. The needle-type hydrophone was calibrated the sound pressure in the frequency range from 20 kHz to 20 MHz. The hydrophone was connected to a spectrum analyzer (8595E, HP) through a preamplifier (HUS-200A, Honda Electronics) which converted impedance. The electric power applied to the transducer was calculated from the voltage of both ends of the transducer measured by an oscilloscope (TDS3014B, Tektronix) and current through the transducer measured by a current probe (TCP202, Tektronix). Electric noise from experimental apparatus and surrounding environment was minimized by averagely recording as 16 sweeps in the oscilloscope. The effective electric power was transferred to PC via general purpose interface bus (GPIB). A continuous sinusoidal wave signal was generated by a signal generator (WF1974, NF) and amplified by a power amplifier (1040L, E&I). The output waveform amplitude of signal generator was set by PC via GPIB. At 22 kHz, an impedance matching circuit was connected between the amplifier and the transducer. To keep the electric power applied to the transducer constant, the amplitude of signal was controlled by a program (Honda Electronics) and PC.

It was reported that a hysteresis effect was observed in sound pressures at the harmonic frequency, subharmonic frequency, and broadband noise when the sound intensity changed [37]. This effect could be impeded through a procedure of sound pressure measurement which was carried out by increasing the electric power applied to the transducer. The sample of distilled water with 100 mL in volume was air-saturated and put into the resonance condition beforehand by adjusting driving frequency.

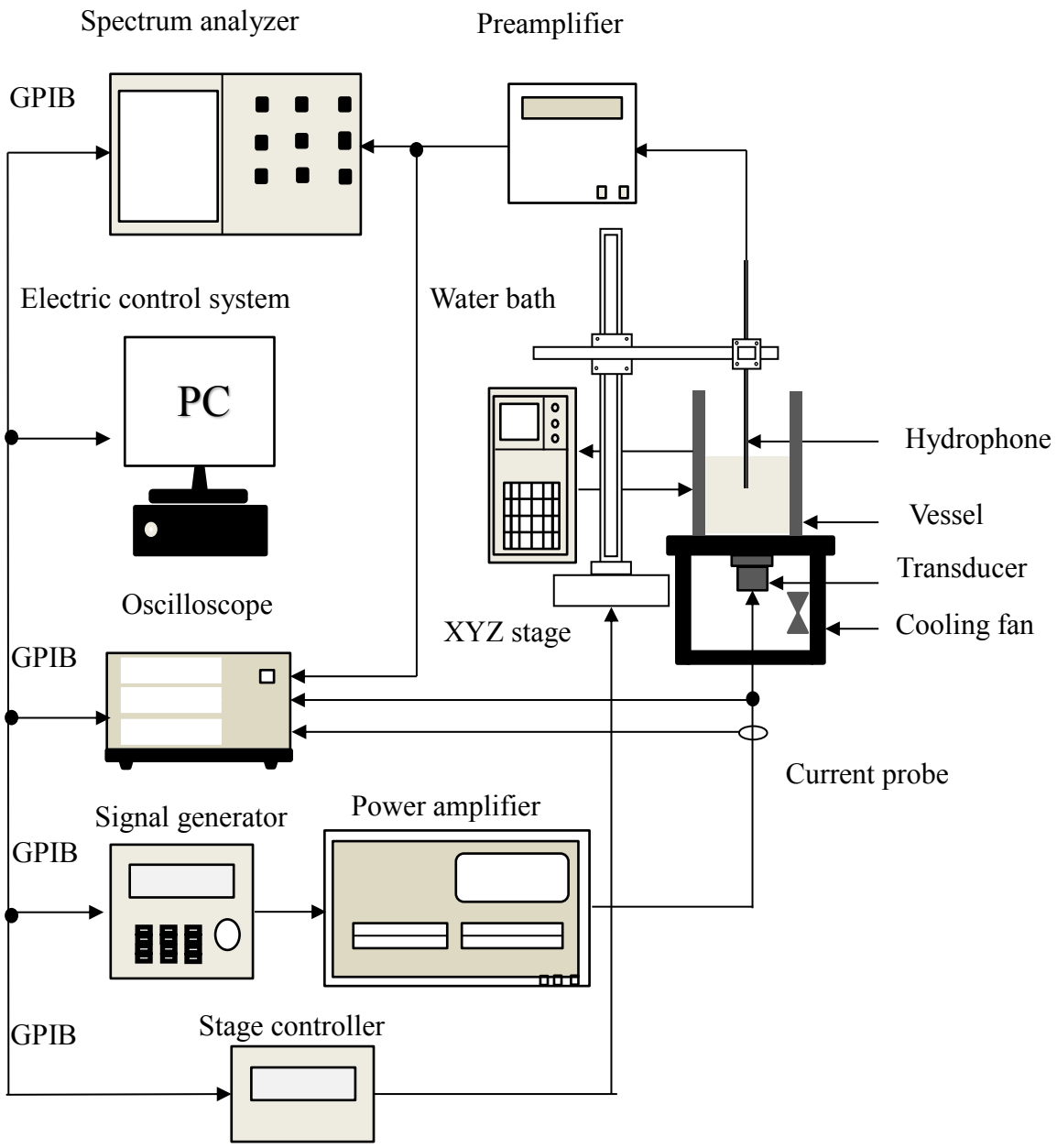

Fig 3. 1. Setup of experimental apparatus

3.2.3. Broadband integrated pressure and sound pressures at fundamental, harmonic, and ultraharmonic frequencies

In this study, the BIP was utilized as the broadband noise to estimate the ultrasonic cavitation generated in water. An example of a sound pressure spectrum at a driving frequency of 304 kHz was illustrated in Fig. 3. 2 in which the sound pressure spectrum was measured by the tough needle-type hydrophone. In this case, the effective electric input power applied to the transducer is 4 W. This hydrophone was calibrated sound pressure in the frequency range from 20 kHz to 20 MHz. The value of BIP was figured out by the following equation:

$$\mathrm{BIP} = \int_{f_s}^{f_e} [P_S(f) - P_N(f)]\, df \qquad (3.\ 1)$$

where $P_S(f)$ represents broadband sound pressures excluding the fundamental, harmonic, subharmonic, and ultraharmonic components and $P_N(f)$ represents sound pressures of the background noise. The start frequency of the integration region, f_s, was decided as 20 kHz and the end frequency, f_e, was 20 MHz for all driving frequencies. The broadband sound pressure represented in decibels (dB) and was employed to calculate the BIP identified as the shaded area in Fig. 3. 2.

Acoustic signals at the fundamental, second harmonic and first ultraharmonic frequencies were obtained by the needle type tough hydrophone, the preamplifier, and the

spectrum analyzer. The signals were converted to sound pressure.

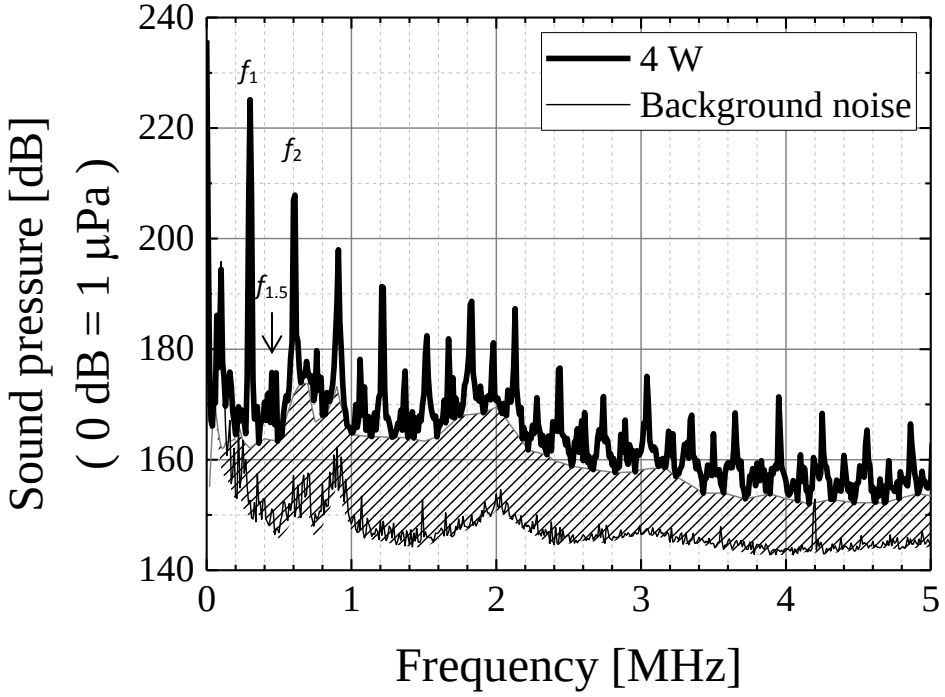

Fig 3. 2. Example of sound pressure spectrum at a driving frequency of 304 kHz and an electric power of 4 W

3.2.4. Bubbles observation

In order to visualize bubbles in water under ultrasonic irradiation, an ultrasonic diagnostic equipment (Honda Electronics HS–2100) with a 10 MHz probe (Honda Electronics HLS–513M) was used. Figure 3. 3 shows an experimental setting for the bubble observation. The ultrasound irradiation system was the same as that for the measurement of sound pressures. Ultrasound was irradiated horizontally by an immersed transducer. To

reflect ultrasound in the same proportion at the water surface, a polystyrene foam reflector was used. The experimental setting of bubbles observation is illustrated in Fig. 3. 3.

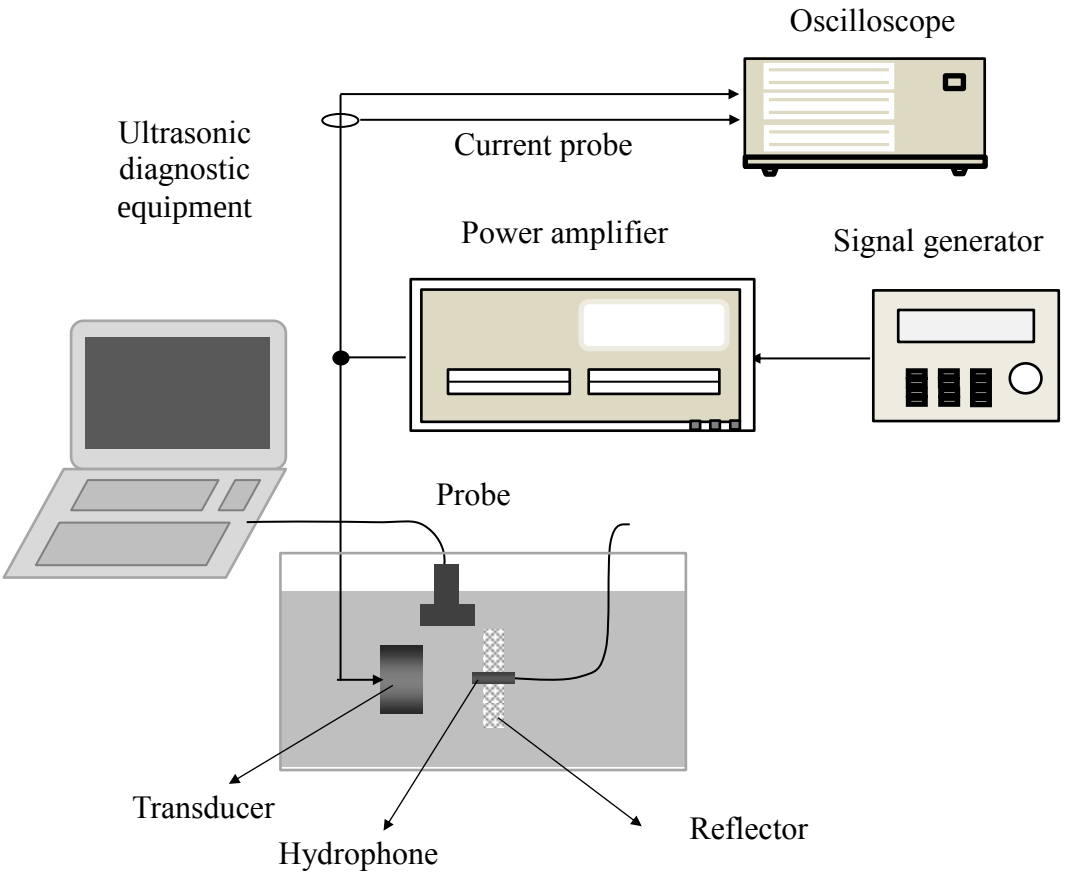

Fig 3. 3. Experimental setting for the bubble observation

3.3. Results and discussion

3.3.1. Determination of cavitation threshold

The ultrasonic frequency was adjusted to a minimum impedance of the transducer in order to obtain resonance condition of water. The vertical distribution of hydrophone output voltage at fundamental frequency on the axis of the transducer center is described on Fig. 3. 4. The abscissa indicates the distance between the hydrophone and the transducer. The driving frequency and effective electrical power applied to the transducer are 43 kHz and 0.01 W, respectively. A standing wave can be seen and the output voltage achieves its highest value when the hydrophone position is at 33 mm. The cavitation threshold was determined by experiments in which the hydrophone position was adjusted to its highest sound pressure for each driving frequency.

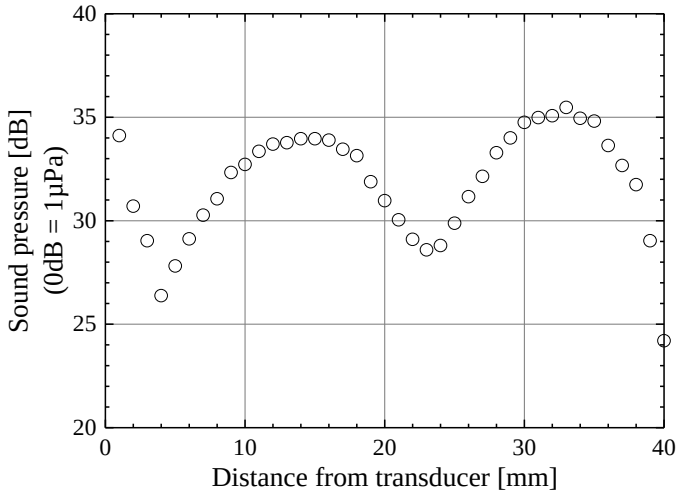

Fig 3. 4. Vertical distribution of sound pressure at fundamental frequency on the axis of transducer center at 43 kHz and 0.01 W

The sound pressure at the fundamental frequency and BIP against the square root of electric power at 1000, 2000, and 4880 kHz are demonstrated on Figs. 3. 5 (a, b, c). The sound pressure is zero-to-peak amplitude. As seen in Fig. 3. 5 (a), the sound pressure increases linearly with increase square root of electric power at low electric power and BIP is almost zero. However, above the square root of electric power of 1.3 $W^{1/2}$, an increasing tendency can be found for BIP meanwhile an unstable trend for sound pressure. This result proves that acoustic cavitation begins to generate at 1.3 $W^{1/2}$. In order to obtain the cavitation threshold, the sound pressure is assumed to be proportional to the square root of electric power at high electric power. The sound pressure at 1.3 $W^{1/2}$ is regarded as the cavitation threshold (dotted lines). The average value of cavitation threshold measured at three times at the same experimental condition at 1000 kHz is 169 kPa. The similar trend is also observed at 2000 and 4880 kHz as shown in Figs. 3. 5 (b, c). The cavitation threshold at 2000 kHz is 412 kPa. The cavitation threshold at 4880 kHz is 621 kPa.

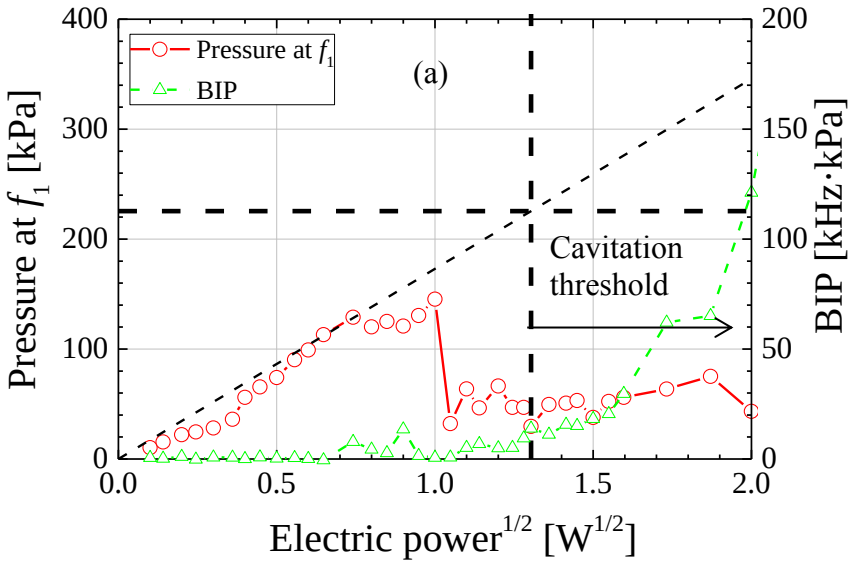

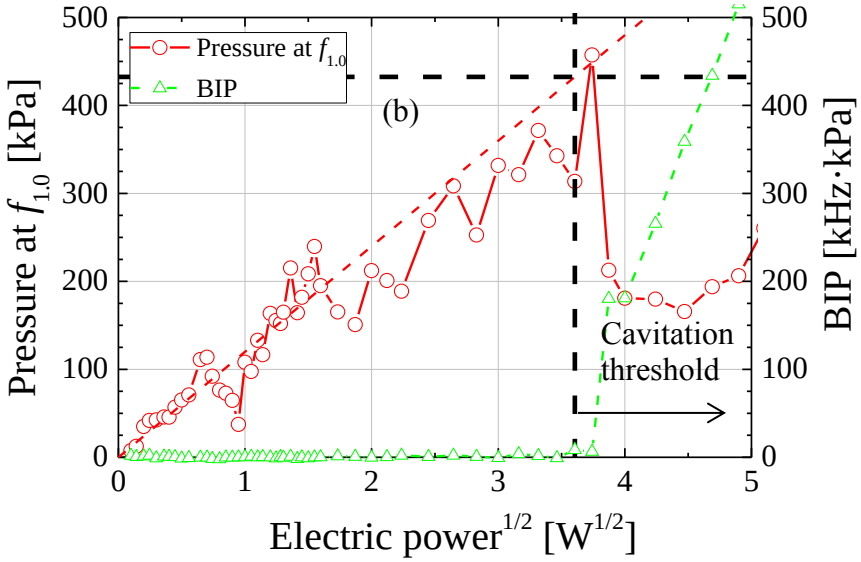

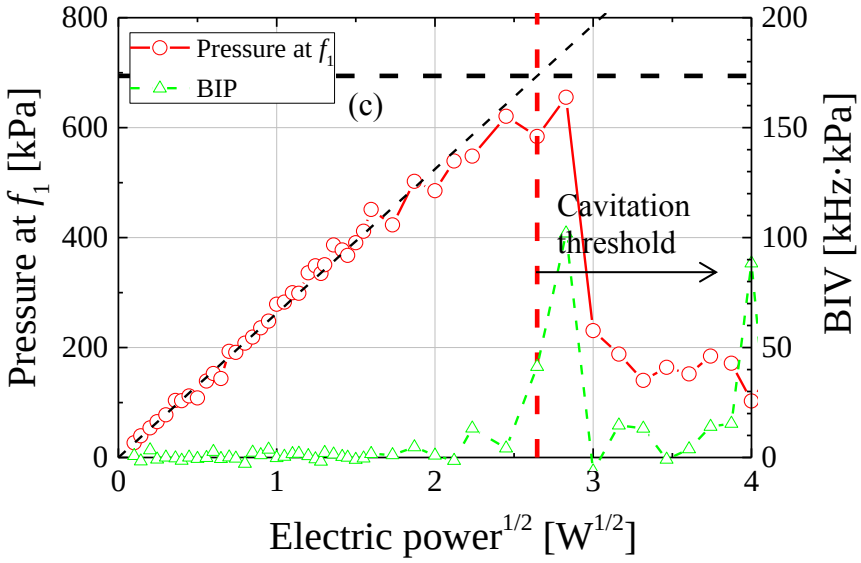

Fig 3. 5. Determination of cavitation threshold at (a) 1000 kHz, (b) 2000 kHz, (c) 4880 kHz

3.3.2. Sound pressure at the fundamental frequency and broadband integrated pressure

In this session, effect of ultrasonic cavitation on the sound pressure at the fundamental frequency and broadband integrated pressure will be discussed. The sound pressure at the fundamental frequency and the BIP are plotted as functions of the square root of the effective electric power applied to the transducer in Figs. 3. 6 (a – e). The driving frequencies are 22, 43, 98, 304, and 488 kHz, respectively. At each frequency, Fig (a – 1) – (a – 2) at the left side shows the sound pressure and BIP in the low-electric-power range, Fig (2) at the right side shows the sound pressure and BIP in the high-electric-power range. The broadband noise has been used as an indicator for ultrasonic cavitation. The main mechanism behind the generation of the broadband noise is the sound signals due to shockwaves emitted from cavitation bubbles. The shock-waves are detected by a hydrophone as vibrations which result in the broadband component of the frequency spectrum. The broadband noise is generated by the temporal fluctuation in the number of bubbles due to the fragmentation of cavitation bubbles at a variety of bubble sizes.

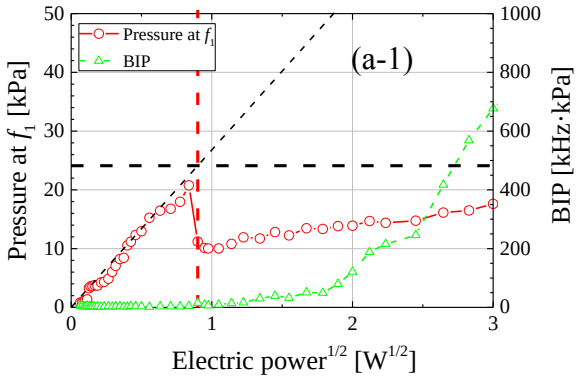
Pressure at f_1
BIP
(a-1)
Pressure at f_1 [kPa]
BIP [kHz·kPa]
Electric power$^{1/2}$ [W$^{1/2}$]

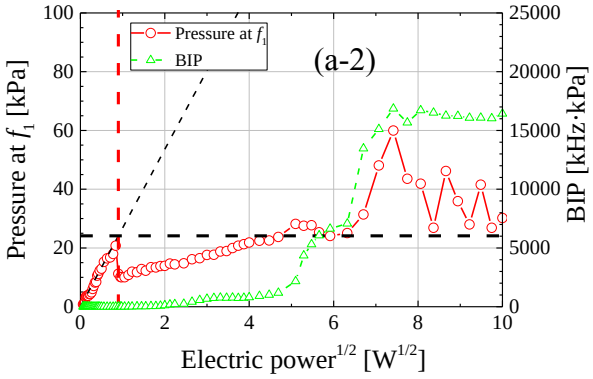
Pressure at f_1
BIP
(a-2)
Pressure at f_1 [kPa]
BIP [kHz·kPa]
Electric power$^{1/2}$ [W$^{1/2}$]

(a)

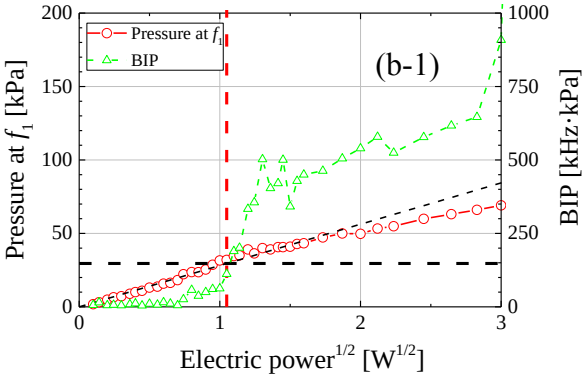
Pressure at f_1
BIP
(b-1)
Pressure at f_1 [kPa]
BIP [kHz·kPa]
Electric power$^{1/2}$ [W$^{1/2}$]

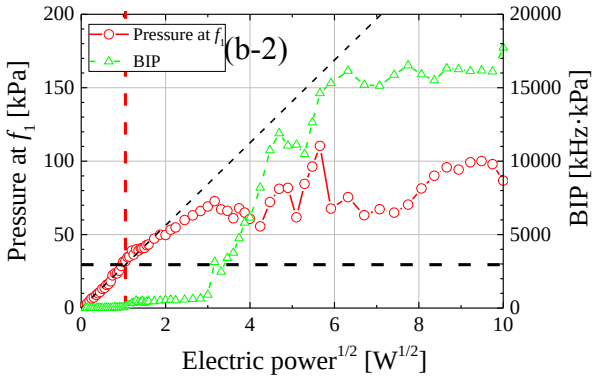
Pressure at f_1
BIP
(b-2)
Pressure at f_1 [kPa]
BIP [kHz·kPa]
Electric power$^{1/2}$ [W$^{1/2}$]

(b)

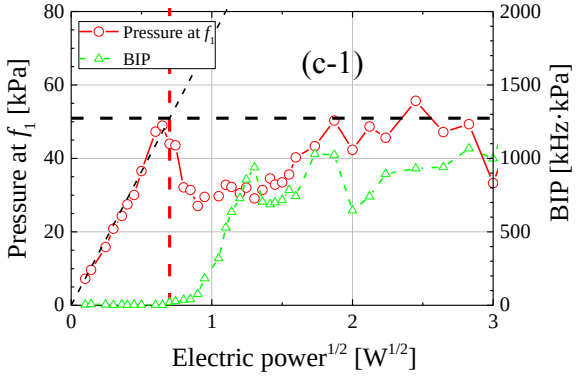
Pressure at f_1
BIP
(c-1)
Pressure at f_1 [kPa]
BIP [kHz·kPa]
Electric power$^{1/2}$ [W$^{1/2}$]

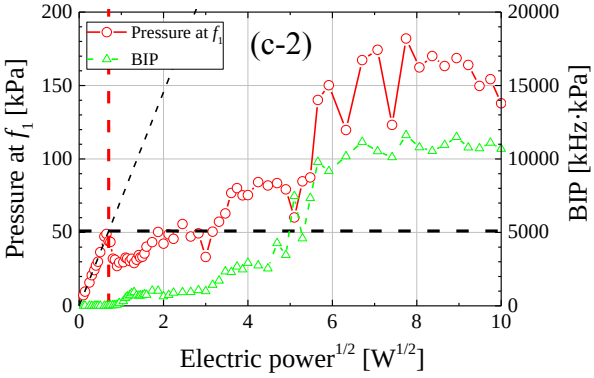
Pressure at f_1
BIP
(c-2)
Pressure at f_1 [kPa]
BIP [kHz·kPa]
Electric power$^{1/2}$ [W$^{1/2}$]

(c)

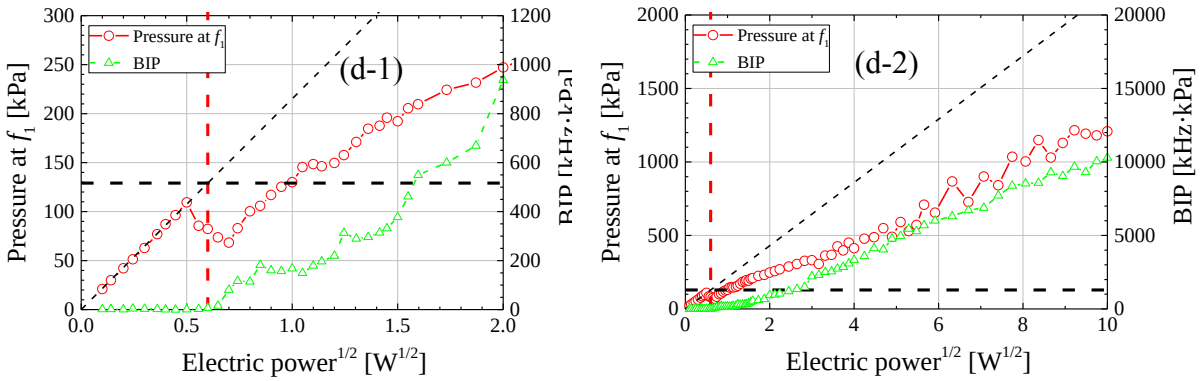

(d)

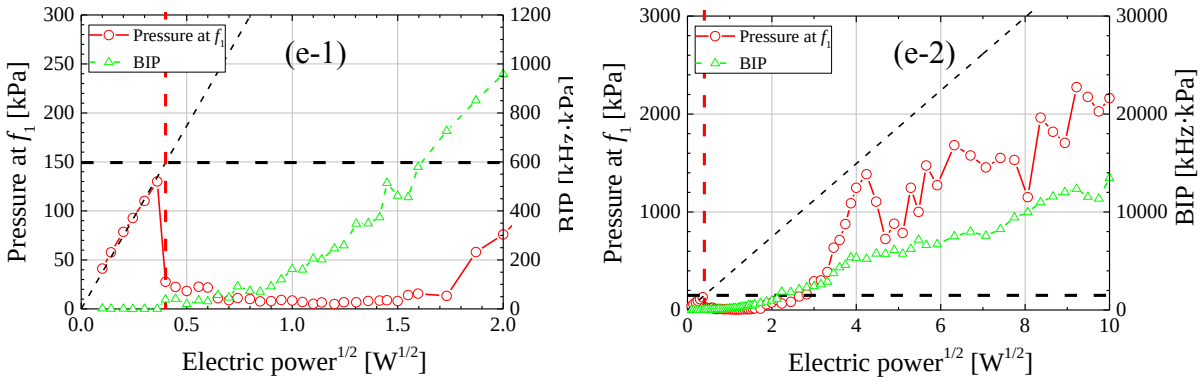

(e)

Fig 3. 6. Sound pressure at the fundamental frequency and BIP as functions of the square root of the effective electric power applied to the transducer at a driving frequency of (a) 22 kHz, (b) 43 kHz, (c) 98 kHz, (d) 304 kHz, and (e) 488 kHz.
Figure (1) at left side shows low-electric-power range and figure (2) at right side shows high-electric-power range

At 22 kHz, to easily observe the tendency of the sound pressure near the cavitation threshold, the electric power is changed from 0 to 9 W in Fig. 3. 6 (a-1). As the square root of the electric power increases, the sound pressure at the fundamental frequency is proportional to the square root of the electric input power. This linear increment agrees to theory earlier reported by Hamonic et al. [35]. As explained in the last part (3.2.2), the electric power which the BIP starts to appear is defined as the electric power of cavitation threshold. In other words, cavitation threshold is defined at the sound pressure at which BIP starts to occur. In the vicinity of the square root of the electric power of cavitation threshold, the sound pressure at the fundamental frequency, however, instantaneously decreases. This unstable change of sound pressure was similarly reported by Neppiras which the microphone output at the fundamental frequency in bars was plotted against the applied acoustic pressure at 40 kHz, a rapid decrease in signal was obtained near the cavitation threshold. The sound pressure decreased notably around cavitation threshold. This drop of sound pressure at the fundamental frequency can be explained by the attenuation in the solution by cavitation bubbles. The BIP increases with electric power above the electric power of cavitation inception.

In the whole range of electric power from 0 to 100 W, as square root of electric power increases, the sound pressure at the fundamental frequency linearly increases initially, decreases around cavitation threshold and then increases again, as can be seen in Fig. 3. 6 (a-2). Nevertheless, the sound pressure no longer increases and becomes unstable when it comes to very high electric power of 50 W. In the similar way, the BIP accelerates up to above of cavitation threshold then does not increase as well when it comes to the

same high value of electric power.

In this study, the effective measurement range of the hydrophone was investigated with the degassed water. The sound pressure at the fundamental frequency increased linearly in relation to the increment of the square root of the electric power applied to the transducer as far as the sound pressure reached roughly 8 MPa [22]. According to this result, it is obvious that the sound pressure in Fig. 3. 6 (a-2) is within the effective measurement range. In terms of the conversion efficiency of the transducer which transforms the electric power to ultrasonic power above cavitation threshold, a calorimetry was adopted for ultrasonic power measurement. This result indicates that the ultrasonic power was proportional to the effective electric power applied to the transducer at high electric powers, which means that the conversion is properly under these experimental conditions.

In respect of the cavitation bubbles' size, the performance at low driving frequencies produces larger ones than those at high driving frequencies. Those large bubbles exist in water and on the hydrophone surface could explain for the instability of sound pressure at a high electric power. Therefore, they enhance the scattering and absorbance of ultrasound in water.

In the cases of 43 and 98 kHz, the similar bents in sound pressure at the fundamental frequency and the BIP are observed in Fig. 3. 6 (b) and (c) not only at low electric power near cavitation threshold but also at the whole range of electric power up to 100 W. That is, in the low range of ultrasonic frequency from 22 to 98 kHz, as the square root of the electric power increases, the sound pressure at the fundamental frequency is

proportional to the square root of the electric power at first, thereafter instantaneously decreases near the vicinity of cavitation threshold, and then increases again. However, at very high electric power, the sound pressure at the fundamental frequency becomes unstable instead of continuously increases.

At 304 kHz, at the low range of electric power, a similar trend of changes in sound pressure at the fundamental frequency and the BIP as those at low frequencies is reported in Fig. 3. 6 (d-1). Meanwhile, at the whole range of electric power up to 100 W, both the sound pressure at the fundamental frequency and the BIP increase with electric power above the cavitation threshold. There is no unstable phase of the sound pressure at the fundamental frequency and the BIP at very high electric power as seen at low frequencies. At a high electric power, there is a fact that the sound pressure in the reflected wave is significantly lower than that in the incident wave owing to ultrasonic attenuation by a great amount of cavitation bubbles and water. This phenomenon enhances an acoustic radiation force. The ultrasonic attenuation is enhanced with increasing driving frequency. As a consequence, the trapped bubbles on the hydrophone surface and in standing waves mostly removed by the acoustic radiation force. It leads to the increase of sound pressure again when a high electric power is used.

At 488 kHz, at the low range of electric power, the sound pressure at the fundamental frequency drops drastically towards nearly the zero value in the vicinity of cavitation threshold, as can be clearly seen in Fig. 3. 6 (e-1). It is considered that numerous cavitation bubbles were generated in water. In order to clarify the existence of bubbles in water under ultrasonic irradiation, visualization was achieved by the ultrasonic diagnostic

equipment with the probe located between the hydrophone and the transducer as shown in Fig. 3. 3. The images from the diagnostic equipment in water without and with ultrasonic irradiation when the driving frequency is 488 kHz and the effective electric power applied to the transducer is 1 W as can be seen in Fig 3. 7 (a) and (b), respectively. In the absence of ultrasonic irradiation in Fig. 3. 7 (a), the image is black as a whole, which implies that no bubbles exist in the water. On the contrary, in the presence of ultrasound irradiation in Fig. 3. 7 (b), many white dots indicating bubbles in water are observed, and horizontal interval of dots corresponds to one half of ultrasonic wavelength in water. This result indicates the presence of many bubbles trapped in standing waves of ultrasound. Since the ultrasound at high frequency has a short wavelength which emits a high level of energy, hence, the number density of bubbles is high in water. In additional, bubbles might be attached on the hydrophone surface and causes largely obstruct for the detection of sound pressure. This could be the reason for the drastic drop of the sound pressure at the fundamental frequency of 488 kHz above the electric power of cavitation threshold. For the whole range of electric power as illustrated in Fig (a – 2) – (e – 2), the sound pressure at the fundamental frequency and the BIP show the same behavior as that at 304 kHz, that is, they increase when the electric power increases until 100 W.

Even so, at a high electric power, for the whole range of ultrasonic frequency from 22 to 488 kHz, all plots in Figs 3. 6 (a-e) show that the sound pressures are lower than the values extrapolated from the linear relationship between the sound pressure at the fundamental frequency and the square root of the electric power of cavitation threshold. This can be explained by the absorption and scattering caused by bubbles in water.

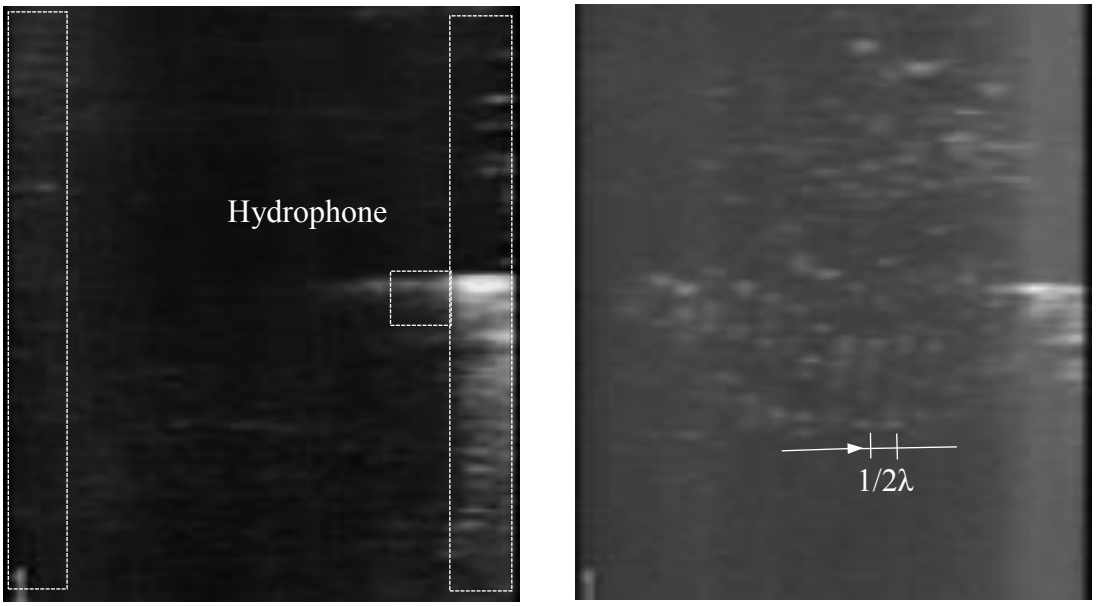

(a) (b)

Fig 3. 7. Images obtained using ultrasonic diagnostic equipment in water (a) without and (b) with ultrasonic irradiation at a driving frequency of 488 kHz and an electric power of 1 W

3.3.3. Sound pressure at the second harmonic and first ultraharmonic frequencies

In this part, the effect of ultrasonic cavitation at different driving frequencies on the sound pressures at the second harmonic (f_2) and first ultraharmonic ($f_{1.5}$) will be explained. Figures 3. 8 (a – e) show the sound pressures at the second harmonic and first ultraharmonic frequencies as functions of the square root of the effective electric power applied to the transducer at 22, 43, 98, 304, 498 kHz, respectively. In the circumstance of 22 kHz in Fig. 3. 8 (a) as the square root of the electric power accelerates, the sound pressure at the second harmonic frequency is initially zero then increases. The square root

of the electric power of threshold of the second harmonic is slightly lower than that of the cavitation threshold. It was stated from Neppiras that the harmonic signals are derived from nonlinear oscillations of stable bubbles in water [23]. It should be noted that when the driving frequency is above 1 MHz, the nonlinear propagation of ultrasound affects the harmonic signals [38]. In this study, the effect of nonlinear propagation of ultrasound is small. The bubbles occur at first when the electric power applied to the transducer increases, then they oscillate with ultrasound and finally collapse at a high electric power, that is, ultrasonic cavitation is generated. This can be the commentary for the occurrence of the second harmonic component of sound pressure below the electric power of cavitation threshold.

Concerning with the mechanism of the generation of half-order subharmonics, Yasui undertook the study using numerical simulations and found that the generation of half-order subharmonics is mainly attributed to the sound waves from relatively large bubbles, which oscillate with a doubled period of driving frequency [38]. From a Fourier series, the spectrum of any arbitrary periodic function with doubled period of driving frequency consists of the half-order subharmonics and ultraharmonics (integer multiples of subharmonics excluding the fundamental and harmonics) such as the first ultraharmonic, $f_{1.5}$. At first, the sound pressure at the first ultraharmonic frequency is zero, and then with increasing electric power, it increases at a relatively high electric power. Besides that, the square root of the electric power of threshold of the first ultraharmonic is higher than that of cavitation inception. Accordingly, it is thought that there are few relatively large bubbles oscillating with a doubled period in the vicinity of the electric

power of cavitation threshold, whereas they would be large bubbles formed by coalescence of bubbles at a high electric power.

When it comes to the cases of the driving frequencies of 43 and 98 kHz, thresholds of the second harmonic and first harmonic appear at the same behavior at that of 22 kHz. As can be seen in Figs. 3. 8 (b) and (c), the electric power of threshold of the second harmonic is lower than that of cavitation threshold. The electric power of threshold of the first ultraharmonic is far beyond from that of cavitation threshold.

When the driving frequencies are 304 and 488 kHz, as shown in Figs. 3. 8 (d) and (e), respectively, the electric power of threshold of the second harmonic is also lower than that of cavitation threshold which is the same manner at frequencies below 98 kHz. However, the square root of the electric power of threshold of the first ultraharmonic at 304 kHz is slightly higher than that of cavitation threshold, and the square root of the electric power of threshold of the first ultraharmonic at 488 kHz is mostly similar with that of cavitation threshold. It can be extracted from this result that a higher driving frequency favors for the formation of large bubbles at the electric power of cavitation threshold. Particularly, at 488 kHz, the sound pressures at the second harmonic and first ultraharmonic frequencies are small when the square root of electric power spans from 0.5 to 1.5 $W^{0.5}$. This result is due to the fact that the number density of bubbles is high and many cavitation bubbles are trapped at the standing waves, as shown in Fig. 3. 7 (b).

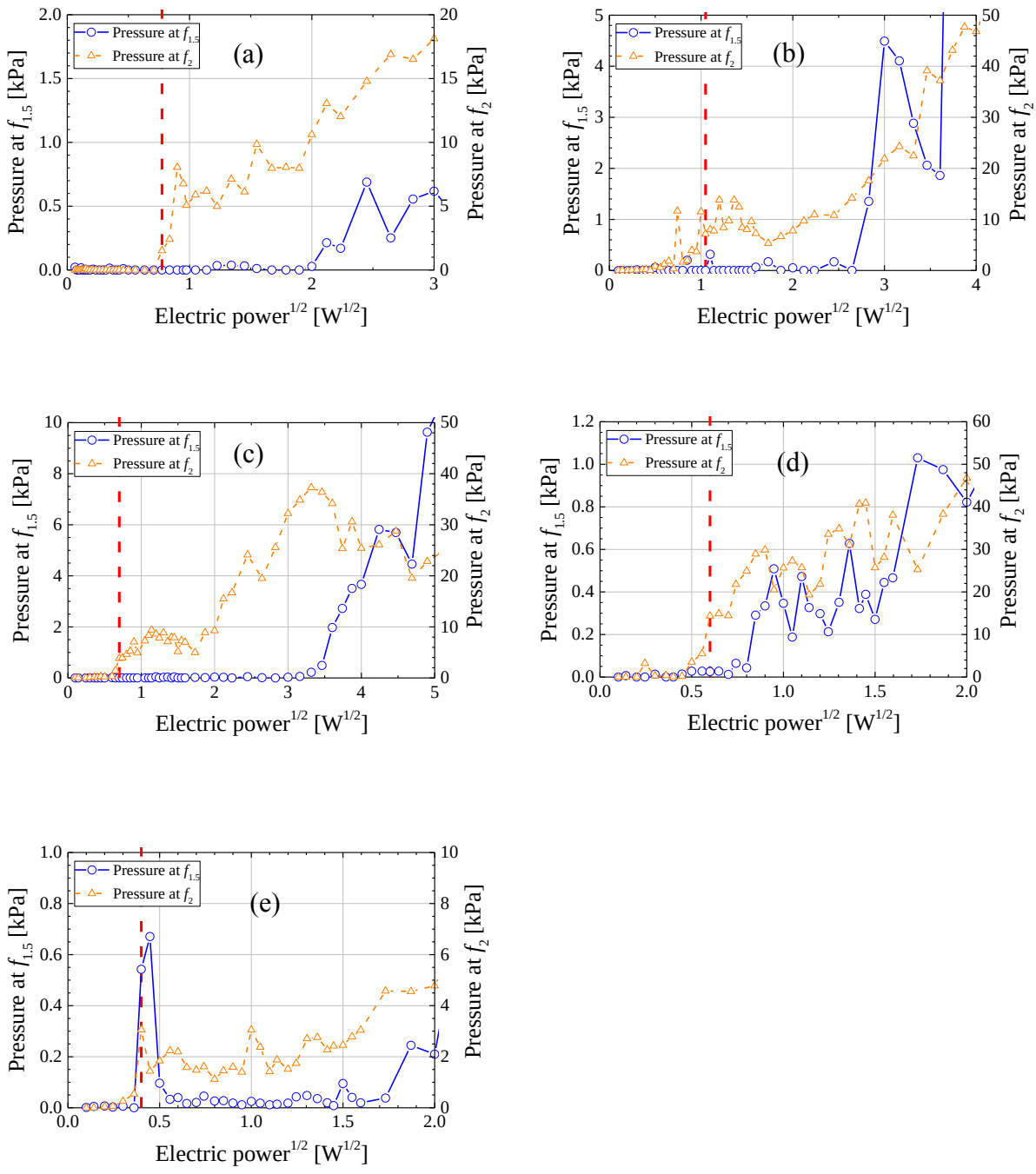

Fig 3. 8. Sound pressures at the second harmonic and first ultraharmonic frequencies as functions of the square root of effective electric power applied to the transducer at (a) 22 kHz, (b) 43 kHz, (c) 98 kHz, (d) 304 kHz, and (e) 488 kHz

3.3.4. Cavitation threshold

As being calculated as shown in section 3.3.1, the average values of cavitation threshold at 22, 43, 98, 304, 488, 1000, 2000, and 4880 kHz are summarized in Table 3. 2.

Table 3. 2. Cavitation threshold

Frequency [kHz]	22	43	98	304	488	1000	2000	4880
Cavitation [kPa]	22.4	27.9	63.7	113	152	169	412	621

The dependence of cavitation threshold on the ultrasonic frequency is demonstrated on Fig. 3. 9. When we increase the ultrasonic frequency, the cavitation threshold also increases. As the ultrasonic frequency increases, the duration of the rarefaction phase decreases because the pressure oscillation period decreases [39, 40]. As a result, the occurrence of cavitation bubbles becomes more difficult. Therefore, in order to generate acoustic cavitation at high frequency, it is necessary to supply a high sound pressure.

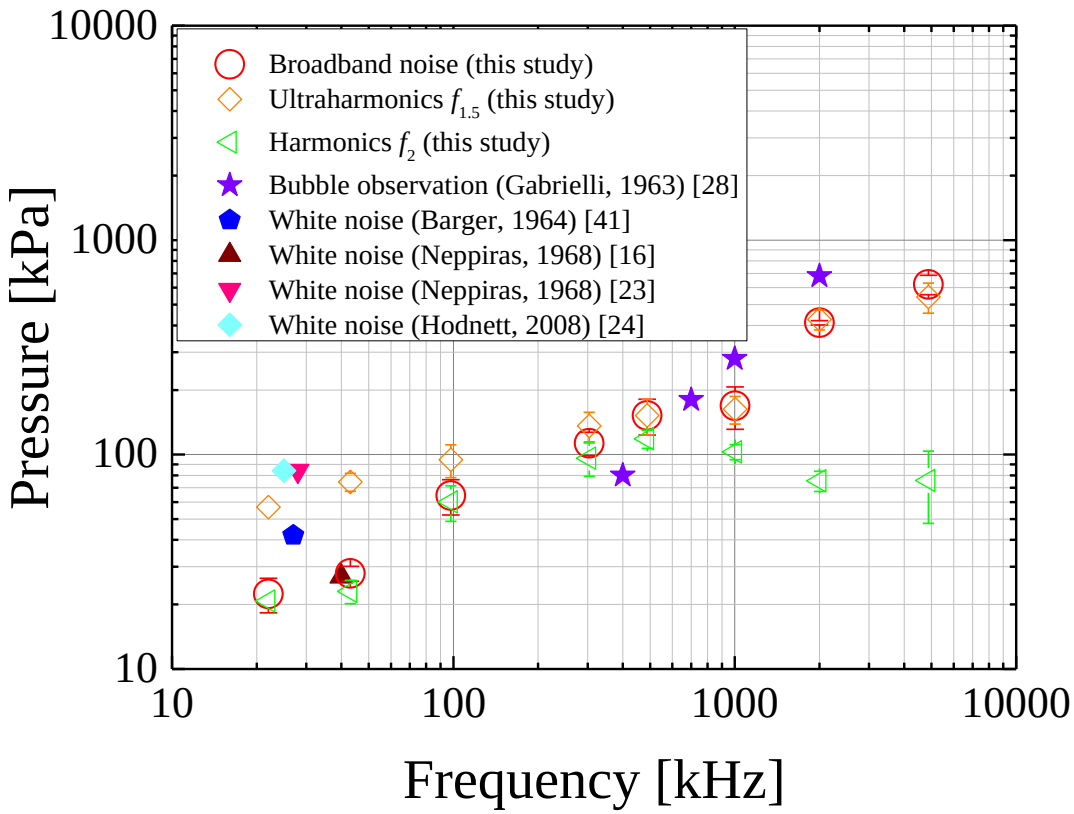

Fig 3. 9. Dependence of thresholds of cavitation, the second harmonic and first ultraharmonic on ultrasonic frequency

Figure 3. 9 also includes the values of the cavitation thresholds using broadband noise and bubble observation reported in previous studies. For instance, Neppiras researched on broadband noise measurement and confirmed that cavitation threshold at 40 kHz was 27 kPa [16]. This result is close to the finding of this research. Moreover, he also pointed out that the cavitation threshold at 28 kHz was 84 kPa [23]. This data is very much different with that of Barger. Barger revealed that the cavitation threshold at 27 kHz was 42 kPa [41]. Hodnett and Zeqiri disclosed that the cavitation threshold at 25 kHz was given as 82 kPa [24]. The existence of bubble nucleus originated from fine bubbles and roughness on surface of transducer and reactor might be a reason for the differences of cavitation thresholds. Using numerical analysis to estimate cavitation threshold, Gaete-Garreton et al. stated that cavitation threshold at 20 kHz was 30 kPa in the case of diameter of collapsing bubbles at 0.12 mm [31]. In the ultrasonic frequency range from 400 to 2000 kHz, Gabrielli and Iernetti carried out bubble observation by using a lateral light source [28]. The cavitation thresholds increased as the frequency became higher and their data almost coincide with that of this study.

3.3.5. Thresholds of the second harmonic and the first ultraharmonic signals

In Fig 3. 2, the signals of the second harmonic and first ultraharmonic frequency in the spectrum are clearly demonstrated. As the sound pressure at the fundamental frequency increased in water, the sound signal at the second harmonic frequency (f_2) was not observed at first and it appeared above a certain threshold. The nonlinear oscillations of stable

bubbles in water are the main source of the harmonic signals [16]. However, the harmonic signal in megahertz range of ultrasound can be influenced by the nonlinear propagation of sound. The minimum sound pressure required to emit sound signal at the second harmonic frequency is defined as the threshold of the second harmonic signal.

The sound signal at the first ultraharmonic ($f_{1.5}$) frequency also appeared above a certain sound pressure. The half-order subharmonic signals are mainly attributed to the sound waves from relatively large bubbles which oscillate with a doubled period of driving frequency [38]. From Fourier series of subharmonic components, the spectrum of any arbitrary periodic function is composed of the subharmonics and ultraharmonics for example the first ultraharmonic. The threshold of the first ultraharmonic signal was defined in the same way as threshold of the second harmonic. Thresholds of the second harmonic and the first ultraharmonic signals are shown in Table 3. 3 and plotted against ultrasonic frequency in Fig. 3. 9. The threshold of the second harmonic signal increases with increasing ultrasonic frequency in the frequency ranges of 22 - 488 kHz. This is because the low pressure period of ultrasound decreases at high frequency and it is difficult to generate stable bubbles. The threshold of the second harmonic signal approximates to the cavitation threshold below 1000 kHz. Above 1000 kHz, the threshold of the second harmonic signal declines as the frequency increases because of the nonlinear propagation of sound.

There is a parallel between the threshold of the first ultraharmonic signal and the ultrasonic frequency. When the latter increases, the former also gets higher. Above 98 kHz, the threshold of the first ultraharmonic signal is close to the cavitation threshold. However, below 98 kHz, the threshold of the first ultraharmonic signal is higher than the cavitation

threshold. At low ultrasonic frequency and low sound pressure, large bubbles were found to be difficult to be trapped at standing waves because of large buoyant force. At high sound pressure, large bubbles which oscillate with a doubled period of driving frequency are easily trapped at standing waves because primary Bjerknes force exceeds buoyant force. Therefore, the threshold of the first ultraharmonic signal is higher than the cavitation threshold at low ultrasonic frequency.

Table 3. 3: Thresholds of the second harmonic and first ultraharmonic

Frequency [kHz]	22	43	98	304	488	1000	2000	4880
Second harmonic [kPa]	20.8	23.0	60.1	96.2	118	103	75.5	75.8
First ulharmonic [kPa]	56.9	74.5	94.6	136	152	163	426	543

3.4. Conclusion

In chapter 3, the cavitation threshold was examined in a wide range frequency from 22 kHz to 4880 kHz by broadband noise using the tough needle-type hydrophone. The broadband noise in the integration region from 20 kHz and 20 MHz for all frequencies was used to determine the BIP. In order to increase its credibility, all fundamental, harmonic and subharmonic components were totally abolished from signal spectrum before being calculated. The results showed a tendency of increasing cavitation threshold as ultrasonic frequency increased.

This chapter also considered the possible effect of bubble occurrence in a liquid. Therefore, the thresholds of the second harmonic and the first ultraharmonic components were measured to detect the occurrence of bubbles in the liquid. At the frequencies of below 1000 kHz, the threshold of the second harmonic and cavitation threshold were similar to each other. On the other hand, the threshold of the first ultraharmonic was higher than the cavitation threshold below 98 kHz and near to the cavitation threshold at high frequency.

Besides that, we investigated how the ultrasonic cavitation affects the sound pressures at the fundamental, second harmonic, and first ultraharmonic frequencies, and BIP at 22, 43, 98, 304, and 488 kHz. For the fundamental frequency, sound pressure increased linearly with increasing square root of the effective electric power when there were no cavitation bubbles in water. On the other hand, sound pressure drastically decreased at around the electric power of cavitation threshold because of ultrasonic attenuation, caused by

numerous bubbles trapped in standing waves and on the hydrophone surface. Above the electric power of cavitation threshold, sound pressure increased again. The possible reason is that trapped bubbles were mostly removed by the acoustic radiation force. However, at a high electric power, the sound pressure was lower than the value extrapolated from the linear relationship between the sound pressure at the fundamental frequency and the square root of electric power below the electric power of cavitation threshold.

For the second harmonic signal, the electric power of threshold was relatively lower than that of cavitation threshold. This means that stable bubbles are generated at a lower electric power than cavitation bubbles. The first ultraharmonic component was detected near the electric power of cavitation threshold at 304 and 488 kHz, and above that at 22, 43, and 98 kHz. It is considered that at low driving frequencies, relatively large bubbles that oscillate with a doubled period were few at the electric power of cavitation inception and large bubbles were formed by coalescence of bubbles at a high electric power.

References

1. F. Martinez, A. Davidson, J. Anderson, S. Nakai, I. Desai, A. Radcliffe, Effects of ultrasonic homogenization of human milk on lipolysis, IgA, IgG, lactoferrin and bacterial content , Nutr. Res. 12(4-5) (1992) 561 – 568.
2. K. Yasuda, H. Honma, Z. Xu, Y. Asakura, S. Koda, Ultrasonic atomization amount for different frequencies, Jpn. J. Appl. Phys. 50(7S) (2011) 07HE23.
3. A. Endo, M. Yanagimoto, T. Asami, H. Miura, Noncontact atomization of droplets using an aerial ultrasonic source with two vibrating plates , Jpn. J. Appl. Phys. 54(7S1) (2015) 07HE13.
4. M. Vinatoru, An overview of the ultrasonically assisted extraction of bioactive principles from herbs, Ultrason. Sonochem. 8(3) (2001) 303 – 313.
5. G. Cravotto, L. Boffa, S. Mantegna, P. Perego, M. Avogadro, P. Cintas, Improved extraction of vegetable oils under high-intensity ultrasound and/or microwaves, Ultrason. Sonochem. 15(5) (2008) 898 – 902.
6. T.S.H. Leong, T.J. Wooster, S.E. Kentish, M. Ashokkumar, Minimising oil droplet size using ultrasonic emulsification, Ultrason. Sonochem. 16(6) (2009) 721 – 727.
7. M. Luque de Castro, F. Priego-Capote, Ultrasound-assisted crystallization (sonocrystallization), Ultrason. Sonochem. 14(6) (2007) 717 – 724.
8. Z. Xu, K. Yasuda, Enhancement of sonochemical reaction by dual-pulse ultrasound, Jpn. J. Appl. Phys. 50(7S) (2011) 07HE07.
9. T. Yotsumoto, T. Morita, Y. Noiri, Y. Kojima, Y. Asakura, S. Koda, Influence of pressure and temperature on sonochemical reaction in a flow-type reactor equipped with a PZT transducer, *Jpn. J. Appl. Phys.* 53(7S) (2014) 07KE09.
10. K. Yasuda, T.T Nguyen, R. Okura, S. Nakayama, Y. Asakura, J. Jin, Dispersion and coalescence of oil droplets by ultrasound and application for solvent extraction of gallium, *Jpn. J. Appl. Phys.* 54(7S1) (2015) 07HE03.
11. M. Sivakumar, S.Y Tang, K.W Tan, Cavitation technology–a greener processing technique for the generation of pharmaceutical nanoemulsions, Ultrason. Sonochem. 21(6) (2014) 2069 – 2083.
12. C.D. Arvanitis, M. Bazan-Peregrino, B. Rifai, L.W. Seymour, C.-C. Coussios, Cavitation-enhanced extravasation for drug delivery, Ultrasound Med. Biol. 37(11) (2011) 1838 – 1852.
13. Y. Uemura, K. Sasaki, K. Minami, T. Sato, P.K. Choi, S. Takeuchi, Observation of cavitation bubbles and acoustic streaming in high intensity ultrasound fields, Jpn. J. Appl. Phys. 54(7S1) (2015) 07HB05.
14. J. Yasuda, T. Miyashita, K. Taguchi, S. Yoshizawa, S.I. Umemura, Quantitative assessment of reactive oxygen sonochemically generated by cavitation bubbles, Jpn. J. Appl. Phys. 54(7S1) (2015) 07HF21.
15. X. Qu, T. Azuma, R. Sugiyama, K. Kanazawa, M. Seki, A. Sasaki, S. Takagi, Improved highly accurate localized motion imaging for monitoring high-intensity focused ultrasound therapy, Jpn. J. Appl. Phys. 55(7S1) (2016) 07KF04.
16. E.A. Neppiras, Measurement of acoustic cavitation, IEEE Trans. Sonics Ultrason.

15(2) (1968) 81 – 88.
17. T. Kikuchi, S. Sato, Ultrasonic Power Measurements by Radiation Force Balance Method–Characteristics of a Conical Absorbing Target, Jpn. J. Appl. Phys. 39(5S) (2000) 3158.
18. T. Uchida, T. Kikuchi, Effect of heat generation of ultrasound transducer on ultrasonic power measured by calorimetric method, Jpn. J. Appl. Phys. 52(7S) (2013) 07HC01.
19. Y. Asakura, Experimental methods in sonochemistry. In: F. Grieser, P. Choi, N. Enomoto, H. Harada, K. Okitsu, K. Yasui, Sonochemistry and the acoustic bubble, Elsevier, Amsterdam, 2015, 119 – 150.
20. S. Nomura, S. Mukasa, M. Kuroiwa, Y. Okada, K. Murakami, Cavitation bubble streaming in ultrasonic-standing-wave field, Jpn. J. Appl. Phys. 44(5R) (2005) 3161.
21. M. Shiiba, N. Okada, T. Uchida, T. Kikuchi, M. Kurosawa, S. Takeuchi, Frequency characteristics of receiving sensitivity and waveform of an anti-acoustic cavitation hydrophone, Jpn. J. Appl. Phys. 53(7S) (2014) 07KE06.
22. M. Shiiba, N. Okada, M. Kurosawa, S. Takeuchi, Development of anticavitation hydrophone using a titanium front plate: Effect of the titanium front plate in high-intensity acoustic field with generation of acoustic cavitation, Jpn. J. Appl. Phys. 55(7S1) (2016) 07KE16.
23. E.A. Neppiras, Subharmonic and other low-frequency emission from bubbles in sound-irradiated liquids, J. Acoust. Soc. Am. 46(3B) (1969) 587 – 601.
24. M. Hodnett, B. Zeqiri, Toward a reference ultrasonic cavitation vessel: Part 2 - Investigating the spatial variation and acoustic pressure threshold of inertial cavitation in a 25 kHz ultrasound field, IEEE Trans. Ultrason. Ferroelectr. Freq. 55(8) (2008) 1809 – 1822.
25. H.B. Briggs, J.B. Johnson, W.P. Mason, Properties of liquids at high sound pressure, J. Acoust. Soc. Am. 19(4) (1947) 664 – 677.
26. M.B. Moffett, Cavitation thresholds of a polyalkylene glycol and of castor oil, J. Acoust. Soc. Am. 68(3) (1980) 966 – 969.
27. E. Meyer, Some new measurements on sonically induced cavitation, J. Acoust. Soc. Am. 29(1) (1957) 4 – 8.
28. I. Gabrielli, G. Iernetti, Cavitation and chemical effects in ultrasonic stationary fields, Acoustica. 13(3) (1963) 165 – 174.
29. H. Yanagida, Y. Masubuchi, K. Minagawa, J.I. Takimoto, K. Koyama, Effect of ultrasound frequency on sonochemical luminescence under well-determined sound pressure, Jpn. J. Appl. Phys. 38(5S) (1999) 3103 – 3104.
30. M.J.W. Pickworth, P.P. Dend, T.G. Leighton, A.J. Walton, Studies of the cavitational effects of clinical ultrasound by sonoluminescence: 2. Thresholds for sonoluminescence from a therapeutic ultrasound beam and the effect of temperature and duty cycle, Phys. Med. Biol. 33(11) (1988) 1249 – 1260.
31. L. Gaete-Garretón, Y. Vargas-Hernández, R. Vargas-Herrera, J.A. Gallego-Juárez, F. Montoya-Vitini, On the onset of transient cavitation in gassy liquids, J. Acoust. Soc. Am. 101(5) (1997) 2536 – 2540.
32. T. Uchida, H. Sato, S. Takeuchi, T. Kikuchi, Investigation of output signal from cavitation sensor by dissolved oxygen level and sonochemical luminescence, Jpn. J. Appl.

Phys. 49(7S) (2010) 07HE03.
33. T. Uchida, S. Takeuchi, T. Kikuchi, Measurement of amount of generated acoustic cavitation: investigation of spatial distribution of acoustic cavitation generation using broadband integrated voltage, Jpn. J. Appl. Phys. 50(7S) (2011) 07HE01.
34. M. Shiiba, N. Kawashima, T. Uchida, T. Kikuchi, M. Kurosawa, S. Takeuchi, Estimation of cavitation sensor with hydrothermally synthesized lead zirconate titanate film on titanium cylindrical pipe: spatial distribution of acoustic cavitation field and basic characteristics of cavitation sensor, Jpn. J. Appl. Phys. 50(7S) (2011) 07HE02.
35. B. Hamonic, J.N. Decarpigny, Power Sonic and Ultrasonic Transducers Design, Springer, 1988.
36. S. Koda, T. Kimura, T. Kondo, H. Mitome, A standard method to calibrate sonochemical efficiency of an individual reaction system, Ultrason. Sonochem. 10(3) (2003) 149 – 156.
37. J. Frohly, S. Labouret, C. Bruneel, I. Looten-Baquet, R. Torguet, Ultrasonic cavitation monitoring by acoustic noise power measurement, J. Acoust. Soc. Am. 108(5) (2000) 2012 – 2020.
38. K. Yasui, T. Tuziuti, J. Lee, T. Kozuka, A. Towata, Y. Iida, Numerical simulations of acoustic cavitation noise with the temporal fluctuation in the number of bubbles, *Ultrasonics sonochemistry* 17(2) (2010): 460 – 472.
39. K. Yasui, Dynamics of acoustic bubbles. In: F. Grieser, P. Choi, N. Enomoto, H. Harada, K. Okitsu, K. Yasui, Sonochemistry and the acoustic bubble, Elsevier, Amsterdam, 2015, 41 – 83.
40. C. Pétrier, A. Francony, Ultrasonic waste-water treatment: incidence of ultrasonic frequency on the rate of phenol and carbon tetrachloride degradation, Ultrason. Sonochem. 4(4) (1997) 295 – 300.
41. J. Barger, Acoust. Res. Lab., Harvard Univ., Tech. Mem. No. 57 (April 1964).

Chapter 4

Thresholds of chemical and mechanical effects

4.1. Introduction

There are chemical and mechanical effects resulted from acoustic cavitation in a liquid. These effects can be seen as powerful tools for industrial applications of ultrasound. Chemical effect is produced during the process of free radical production and pyrolysis owing to local high temperature and pressure [1-4]. Meanwhile mechanical effect is mainly generated by shockwaves and microjets with high velocity. With such different generation mechanisms, the thresholds of chemical and mechanical effects should be separately examined as well as distinguished with cavitation threshold.

Various methods such as Frickle [5], Weissler [6, 7], hydrogen peroxide [8, 9], sonochemical luminescence [10], phenolphtalein [11], porphyrin [12], rhodamin B [13], and potassium iodide (KI) [14, 15] have been used to quantify chemical effect. Carbon tetrachloride and strong acid are respectively used in Frickle and Weissler methods. However, both carbon tetrachloride and strong acid show high toxicity, the concentration measurement of hydrogen peroxide in the solution is not simple. A transparent reactor is used to detect sonochemical luminescence with high sensitivity. Also, luminescence is gathered from the whole reactor into a photodetector in a dark room. The reaction mechanism of phenolphtalein, porphyrin, and rhodamin B are complex. A safer and easier method is KI solution. The KI solution is considered as a popular chemical dosimetry and standard method for the estimation of sonochemical efficiency [15]. In the KI method, it is safer to handle the solution. The concentration measurement is also easier.

There are few detection methods of mechanical effect. Polymer degradation has been utilized to determine mechanical effect. However it is known the degradation of polymer under ultrasonic sonication is caused by both chemical and mechanical effects. Chemical materials such as radical trap agent and tert butanol were used to quench the generation of radicals, therefore, mechanical effect can be determined by extracting the chemical effect. Under ultrasonic irradiation, an aluminum foil is pitted in the solution by shock waves and micro-jet generated from the collapse of bubbles. Observing the erosion on the surface of aluminum foil under ultrasonic irradiation, the mechanical effect threshold can be specified [16]. Aluminum foil erosion is an easy and simple method to investigate mechanical effect.

Until now, thresholds of chemical effect and mechanical effect have been still insufficiently investigated. Its available data are much lesser than those of cavitation threshold. This study focuses on examining the frequency dependence of chemical effect, and mechanical effect thresholds in the wide frequency range from 22 to 4880 kHz and comparing with those of cavitation threshold. KI oxidation, and aluminum foil erosion are respectively used to measure the chemical effect, and mechanical effect thresholds.

4.2. Experiment

4.2.1. Materials

Air-saturated distilled water was used in all experiments. KI solution was prepared as a concentration of 0.1 $mol \cdot dm^{-3}$ to study chemical effect threshold. For mechanical effect threshold, aluminum foil was used as 12 μm. Sample volumes were 0.100 dm^3. All

experiments were carried out at 298 ±1 K. Before ultrasonic irradiation, all the samples were put at rest in the reactor for 30 minutes. In order to ensure its credibility, in each experiment, the fresh solution was used to replace the used one. Also, each threshold value was measured three times.

4.2.2. Apparatus

The experimental apparatus setup can be seen in Chapter 3. The range of driving ultrasonic frequencies was 22, 43, 98, 304, 488, 1000, 2000, and 4880 kHz, respectively. A stainless steel reactor was used for all experiments. Its inner diameter was 56.8 mm. A Langevin type transducer with multiple frequencies (HEC45242M, Honda Electronics) in which its diameter was 45 m, was used from 22 to 98 kHz. For 304, 488, 1000, and 2000 kHz, the disc type transducers (Honda Electronics) with 50 mm in its diameter were utilized. For 4880 kHz, the usage of a disc type transducer with 20 mm in diameter was applied. The transducer was installed at the bottom of the reactor. In order to avoid heating the transducer, a cooling fan was also attached. To maintain the sample temperature at 298 ± 1 K, a circulating water bath was connected to the annular section of the reactor.

In order to produce a continuous sinusoidal wave signal, a signal generator (WF1974, NF) was put in use. A power amplifier (1040L, E&I) was installed to amplify the signal. To match the impedance of transducer at 22, 43, 98, 1000, 2000, and 4880 kHz, an impedance matching circuit (Honda Electronics) was connected between the power amplifier and the transducer. In order to measure the voltage at the both end of transducer

and the current through the transducer, an oscilloscope (TDS3014B, Tektronix) and a current probe (TCP202, Tektronix) were respectively used. The effective electric power applied to the transducer was calculated from these voltage and current. Using PC via a general purpose interface bus (GPIB), the output waveform amplitude of signal generator was chosen. To set a constant electric power applied to the transducer, an electric control system (Honda Electronics) was utilized.

4.2.3. Measurements

4.2.3.1. Threshold of chemical effect

KI oxidation method was used to identify the chemical effect threshold. The ultrasound is irradiated to KI aqueous solution at a concentration of 0.1 $mol \cdot dm^{-3}$. As a result, I^- ions are oxidized by OH radical, and I_2 is produced. Then, I_2 reacts with the excess I^- in the solution to form I_3^- ion by the next reaction [15],

$$I_2 + I^- \leftrightarrows I_3^- \qquad (4.1)$$

The concentration of I_3^- ions was measured by an ultraviolet spectrometer (UV-1600, Shimadzu) at 355 nm using quartz cuvettes with 5 cm in length. The reaction rate of KI oxidation was calculated by the following equation,

$$k = \frac{AW}{\varepsilon l t} \quad (4.\ 2)$$

In which k is reaction rate ($mol \cdot s^{-1}$), ε is the molar extinction coefficient of I_3^- (ε = 26,303 $dm^3\ mol^{-1}\ cm^{-1}$), A is absorbance, l is the cuvette length (cm), W is the solution volume (dm^3), and t is sonication time (s). The total irradiation time of ultrasound was 120 minutes.

4.2.3.2. Threshold of mechanical effect

The aluminum foil pitted by ultrasonic irradiation in air-saturated water was used to determine mechanical effect threshold. The thickness, length, and width of an aluminum foil were 12 μm, 200 mm, and 50 mm, respectively. The surface of aluminum foil was placed perpendicular to the transducer surface and its center was located on the axis of the transducer center. The irradiation duration of ultrasound was within 180 minutes.

4.3. Results and discussion

4.3.1. Threshold of chemical effect

The generation of cavitation causes the present of OH radicals which are initial for a great deal of chemical effect in the solution due to water pyrolysis. The OH radicals oxidize KI to I_2. They combine with the excess of I^- to form I_3^- ion via reaction (4. 1) [17]. Therefore, the generating rate of I_3^- has a relationship with chemical effect in the solution. Figs. 4. 1 and 4. 2 display the effect of electric power applied to the transducer on the reaction rate of I_3^- ion formation at 43 and 2000 kHz. The reaction rate is zero when the

electric input power of below 2 and 8 W at 43 and 2000 kHz, respectively. Thereafter, the reaction rate accelerates along with the increment of electric power. The former behavior reveals that KI reaction starts to take place at the electric power of 2 W at 43 kHz and 8 W at 2000 kHz.

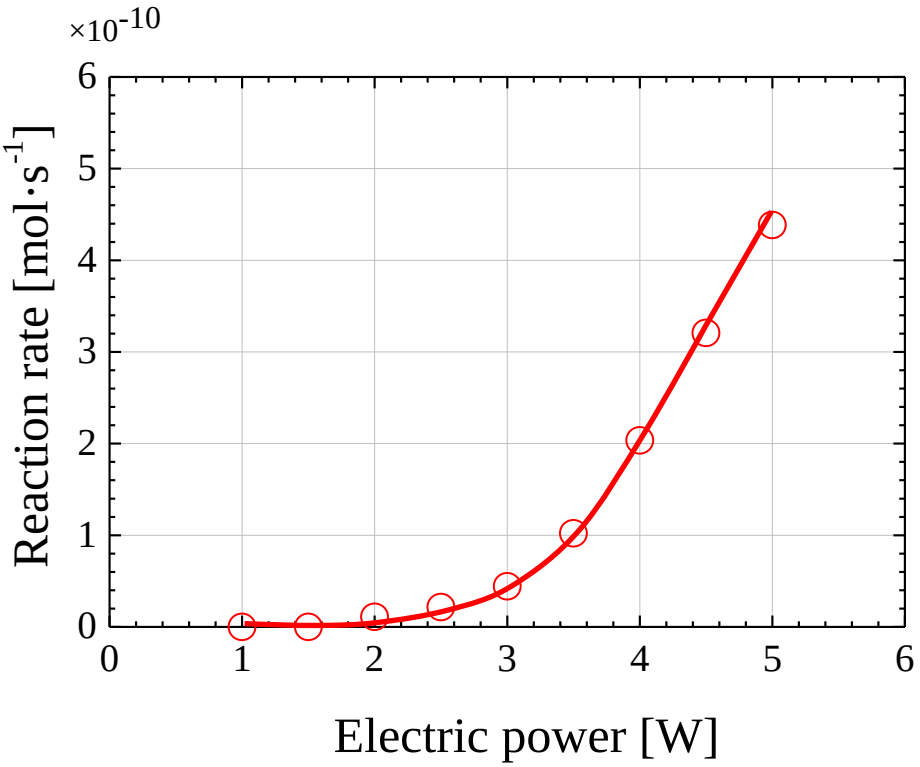

Fig 4. 1. Effect of electric power on reaction rate of I_3^- ion formation at 43 kHz

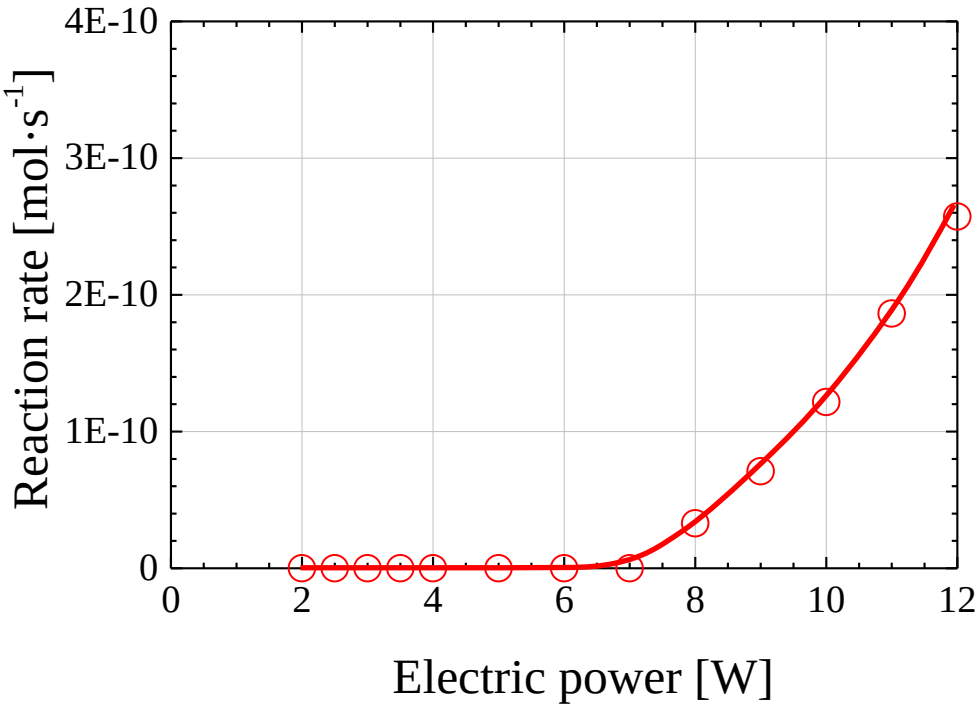

Fig 4. 2. Effect of electric power on reaction rate of I_3^- ion formation at 2000 kHz

For example, to calculate the chemical effect threshold at 43 kHz, the linear relationship between the sound pressure at the fundamental frequency and the square root of electric power at 43 kHz (Fig. 3. 6 (b), chapter 3) is utilized. Using the averaged value of this linear relationship from three independent experiments, the chemical effect threshold is proved to be obtained at 39.0 kPa. As calculated in the same way, the chemical effect threshold at 2000 kHz is 362 kPa. It means that chemical effect threshold is regarded as an acoustic pressure when KI oxidation first takes place by increasing electric power applied to the transducer. Table 4. 1 summarizes the chemical effect thresholds at all frequencies.

Table 4. 1 Thresholds of chemical and mechanical effects

Frequency [kHz]	22	43	98	304	488	1000	2000	4880
Chemical effect [kPa]	22.4	39.0	84.2	156	197	188	362	723
Mechanical effect [kPa]	20.0	23.1	149	1840	3220			

Fig. 4. 3 indicates the dependence of chemical effect threshold on the ultrasonic frequency through the variables of sound pressure (kPa) and frequency (kHz) which are drawn from results of this study and other references. Data of this study show that increasing frequency results in the increasing of chemical effect threshold. Yanagita *et al.* used luminol aqueous solution and measured the threshold of sonochemical luminescence [10]. The thresholds were achieved as 130 and 180 kPa at 1100 and 1700 kHz, respectively. It indicated that there is a frequency dependence of sonochemical luminescence. The reason of this behavior lies in the fact that the maximum size of the cavitation bubble becomes smaller at high frequency. Therefore at higher frequency, lower temperature after cavies collapse is generated, consequently higher threshold is obtained. Besides of that at a frequency of 0.5 MHz, the threshold was reported at 70 kHz. This threshold value is considered as an experimental error because it is lower than the atmospheric pressure and much lower than data at 1100 and 1170 kHz as well as the data of this study. However, it should also be considered that chemical effect threshold is possible to be lower than atmospheric pressure because cavity occurs from cavity nuclei such as nanoscale bubble. In

his study, the diffraction intensity was measured, thereafter equation using Raman-Nath parameter was used to calculate the sound pressure. The obtained intensity is an averaged value and contains some contribution from the edge region of the sonication cell with low pressure. Pickworth measured sonoluminescence from water and possessed the threshold value as 126 kPa at 1000 kHz [18]. These findings seem to be in the same line with the chemical effect threshold measured by KI oxidation in this study.

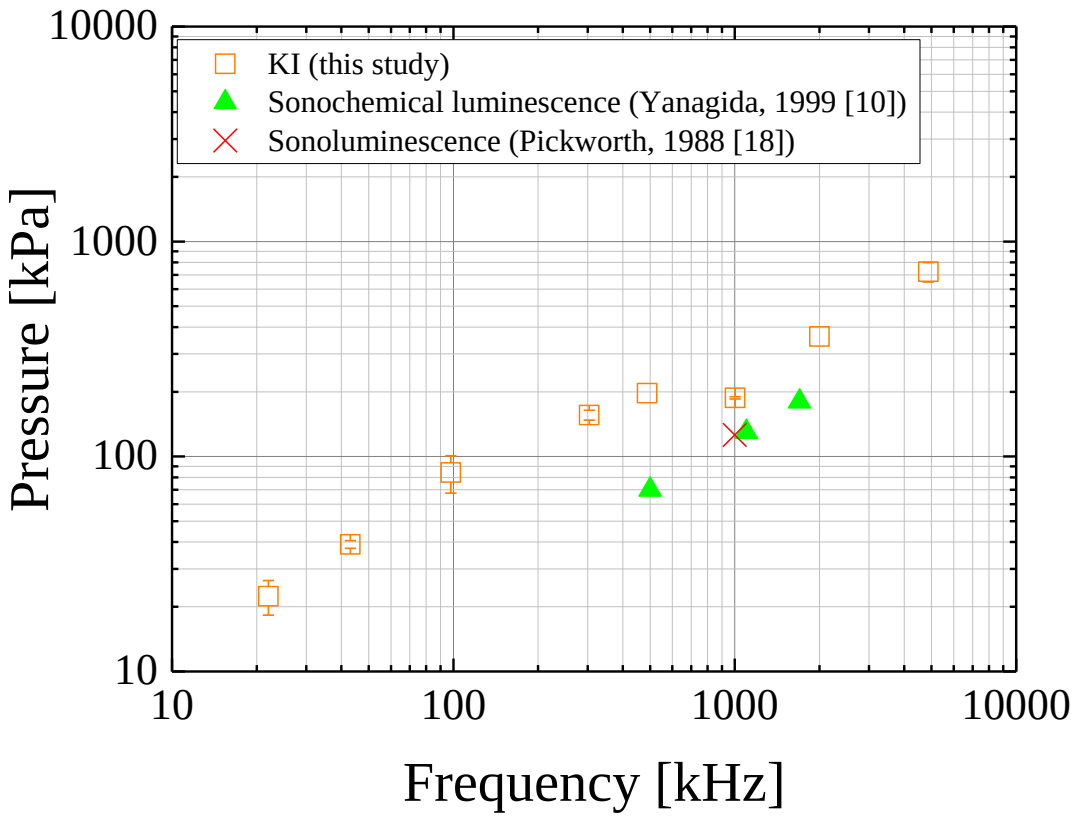

Fig 4. 3. Dependence of chemical effect threshold on ultrasonic frequency

4.3.2. Threshold of mechanical effect

In order to investigate mechanical effect threshold, the aluminum sheet which was fixed by a stainless steel frame was placed perpendicular to the transducer surface at the center of the transducer. The aluminum sheet was place in the reactor before ultrasound was applied, and then was irradiated within 180 minutes. The pitted points on the surface of aluminum sheet by ultrasound stand for mechanical effects of ultrasound. By increasing electric power applied to the transducer, aluminum foil was eroded at a certain electric power. Figure 4. 4 illustrates one example of the erosion of aluminum foil by the mechanical effect of acoustic cavitation. The driving frequency and electric power are 43 kHz and 1 W, respectively. The pit of aluminum foil is displaced by the white part in the diagram. The minimum sound pressure at the fundamental frequency which is capable of pitting aluminum foil is used to estimate the mechanical effect threshold. The mechanical effect threshold is obtained from the linear relationship between the sound pressure at the fundamental frequency and the square root of electric power. The data are shown in Table 4. 1.

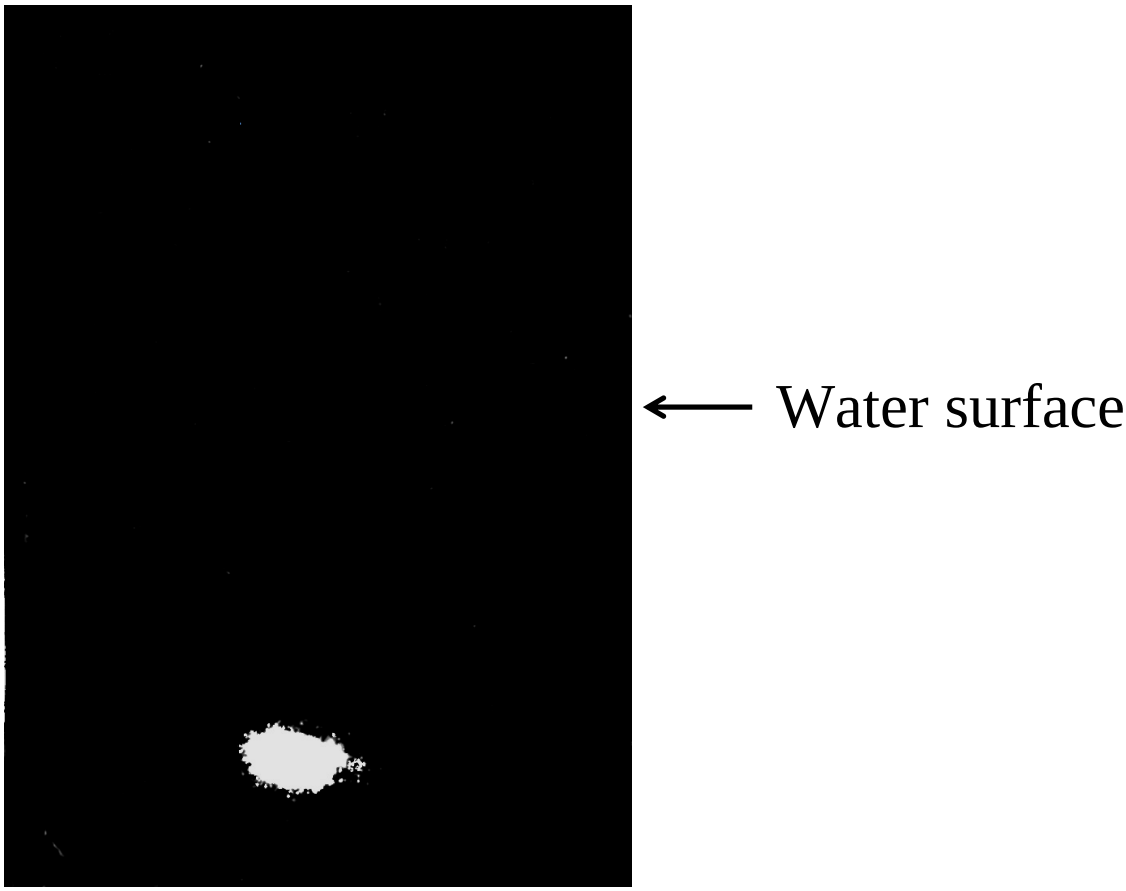

Fig 4. 4. Aluminum foil erosion at 43 kHz and 1 W

The dependence of mechanical effect threshold on the ultrasonic frequency can be seen on Fig. 4. 5. From 22 kHz to 488 kHz frequency ranges, the erosion of aluminum foil caused by acoustic cavitation is observed. However, above 1000 kHz, the erosion process of aluminum foil by ultrasound with the electric power applied to transducer of 100 W and irradiation time of 180 minutes is not observed. This result indicated that the increasing of ultrasonic frequency leads to the increasing of mechanical effect threshold. Gaete-Garreton et al. carried out the erosion of a thin aluminum film at 20 kHz, which is nearly same the frequency of this study at 22 kHz [16]. This threshold of aluminum film erosion behaves in a close manner with the performance at 20 kHz from the study of Gaete-Garreton. As illustrated in Fig. 4. 5, their threshold seems to be close to the mechanical effect threshold in this study.

Kling and Hammitt [19] carried out their research about the damage of aluminum foil by cavitation bubbles. Their observation indicated that when the jet velocity produced by collapse of cavitation bubbles reached 120 m/s, the damage of aluminum foil with 50 μm in thickness was recorded. With the focus on frequency dependence, Wang and Manmi [20] simulated microbubble dynamics near a wall subject to high intensity ultrasound. Their experiment revealed that the maximum bubble radius just before collapse and the jet velocity generated by the collapse of cavitation bubbles decreased as the frequency became higher. In the low frequency region, the size of bubbles is comparatively large because their radii are likely to be in the order of the bubble resonant radius in the acoustic field given by next equation [17]:

$$R = (3\gamma p/\rho\omega^2)^{1/2} \quad (4.3)$$

where γ is the ratio of specific heats of the gas in the bubble, ρ is the density of water, ω is the radical frequency of the ultrasound and p is the pressure. Therefore, the lower the frequency the larger the bubble size. The collapse behavior of cavitation bubble near a gelatin surface using a high-speed framing photography was investigated by Kodama and Tomita [21]. Their results indicated that the liquid jet had the potential to damage the gelatin. As the initial bubble radius increased from 0.33 to 1.12 mm, the penetration depth of the liquid jet increased. That means at low frequencies with larger bubble size, the liquid jet showed more violent damage on gelatin surface due to higher liquid jet velocity. In the same vein, Mason and Lorimer [22] reported that bubbles tended to be smaller by an increase of frequency and therefore the bubble collapse was less strong. The above-mentioned studies proved that the ultrasonic erosion at higher frequency needs higher sound pressure because the generated jet velocity decreases. That is the reason why the mechanical effect threshold greatly increases with increasing frequency. In another word, the mechanical effect threshold and frequency is closely related to each other.

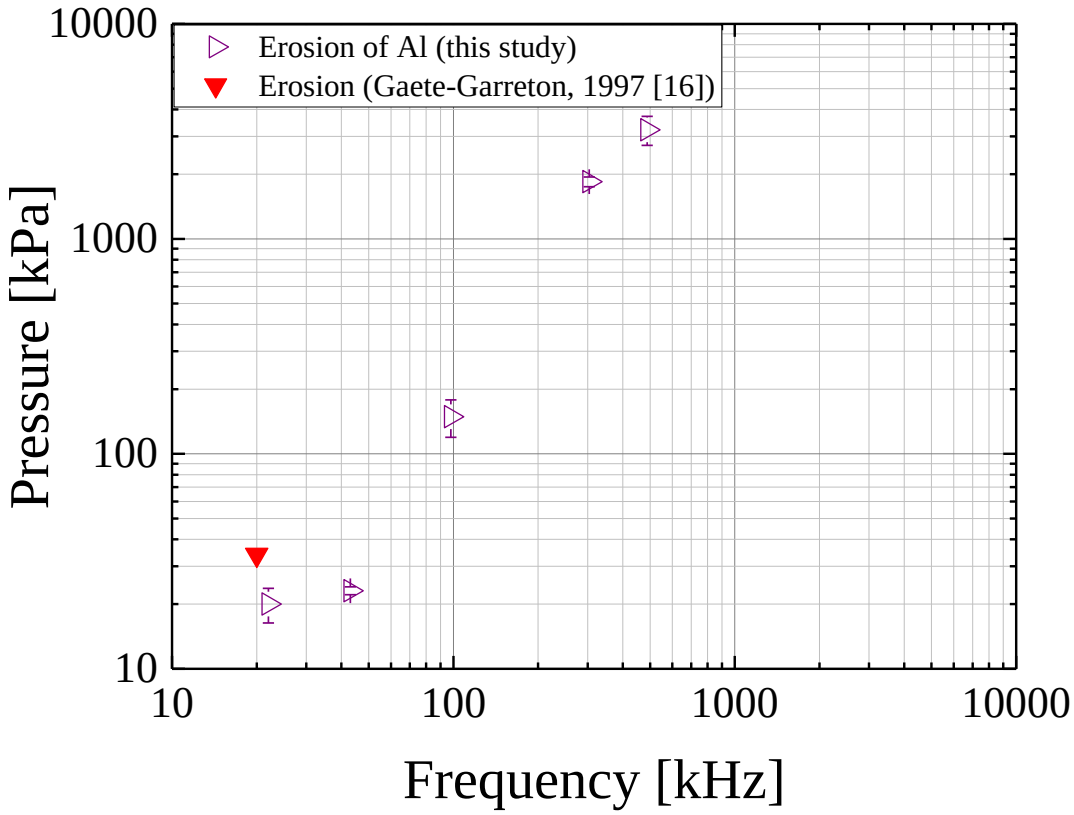

Fig 4. 5. Dependence of mechanical effect threshold on ultrasonic frequency

4.3.3. Comparisons of cavitation, chemical effect, and mechanical effect thresholds

Figure 4. 6 is the summary on the comparison of chemical effect and mechanical effect thresholds, as well as the cavitation threshold from Chapter 3. Data show that increasing frequency leads to the increasing of all thresholds. For instance, on the wide range of frequency from 22 kHz to 4880 kHz, the chemical effect threshold is close to the

cavitation threshold. This result indicated that the sonochemical reaction commences to occur almost under the same condition for acoustic cavitation generation. On the other hand, at lower frequency range of 22 and 43 kHz, the mechanical effect threshold is nearly equal to the cavitation threshold. However, in the higher range of ultrasonic frequency from 98 kHz to 488 kHz, mechanical effect threshold is much higher than cavitation and chemical effect thresholds. The reason of this phenomenon is that the jet velocity generated by cavitation is low. The ultrasonic cleaner used the sound pressure range between cavitation threshold and mechanical effect threshold are effective for non-damage cleaning.

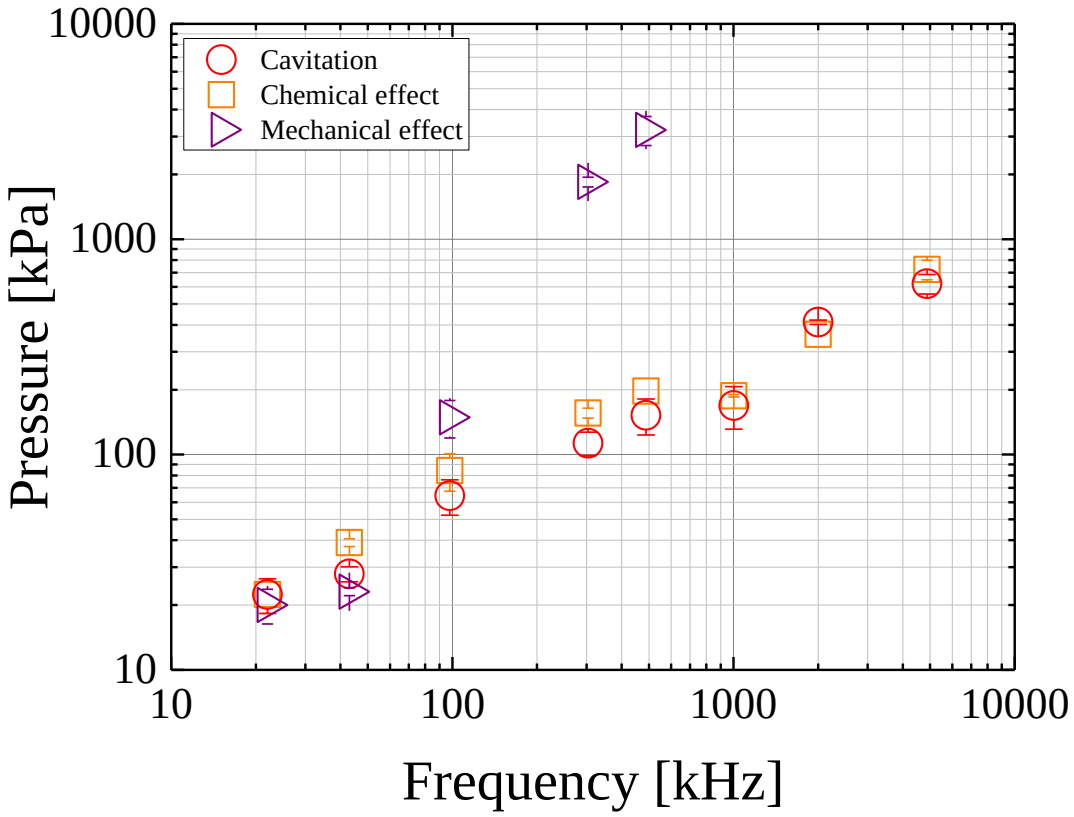

Fig 4. 6. Comparison of cavitation, chemical effect, and mechanical effect thresholds

4. 4. Conclusion

In this chapter, threshold of chemical effect was investigated by KI oxidation and threshold of mechanical effect was investigated by aluminum erosion. Those data were combined with cavitation threshold from chapter 3 to show the frequency dependence of cavitation, chemical effect and mechanical effect thresholds. The results showed a tendency of increasing thresholds of cavitation, chemical effect, and mechanical effect as ultrasonic frequency increased. Specifically, on the whole range of frequency, the chemical effect threshold was confirmed to be close to the cavitation threshold. For the case of mechanical effect threshold, two different tendencies were found. Mechanical effect threshold was almost equal to the cavitation threshold at frequencies below 98 kHz, but greatly higher than the cavitation threshold at high frequencies.

References

1. A.B. Michael, H. Inez, Impact of ultrasonic frequency on aqueous sonoluminescene and sonochemistry, J. Phys. Chem. A 105(15) (2001) 3796 – 3802.
2. T.J. Mason, A.J. Cobley, J.E. Graves, D. Morgan, New evidence for the inverse dependence of mechanical and chemical effects on the frequency of ultrasound, Ultrason. Sonochem. 18(1) (2011) 226 – 230.
3. K.S. Suslick, The chemical effects of ultrasound, Sci. Am. 260(2) (1989) 80 – 86.
4. K.S. Suslick, J.M. Thomas, Ultrasonic Physical Mechanisms and Chemical Effects. In K.S. Suslick, T.J. Matula, Wiley Encyclopedia of Electrical and Electronics Engineering, John Wiley & Sons, New York, 1999, pp. 647 – 657.
5. H. Fricke, E.J. Hart, The oxidation of Fe^{++} to Fe^{+++} by the irradiation with X-rays of solutions of ferrous sulfate in sulfuric acid, J. Chem. Phys. 3(1) (1935) 60 – 61.
6. T. Kimura, T. Sakamoto, J.M. Leveque, H. Sohmiya, M. Fujita, S. Ikeda, T. Ando, Standardization of ultrasonic power for sonochemical reaction, Ultrason. Sonochem. 3(3) (1996) S157-S161.
7. A. Weissler, H. W. Cooper, S. Snyder, Chemical effect of ultrasonic waves: oxidation of potassium iodide solution by carbon tetrachloride, J. Am. Chem. Soc. 72(4) (1950) 1769 – 1775.
8. O. Lindström, Physico‐chemical aspects of chemically active ultrasonic cavitation in aqueous solutions, J. Acoust. Soc. Am. 27(4) (1955) 654 – 671.
9. M. Sato, H. Itoh, T. Fujii, Frequency dependence of H_2O_2 generation from distilled water, Ultrasonics 38(1) (2000) 312 – 315.
10. H. Yanagida, Y. Masubuchi, K. Minagawa, J.I. Takimoto, K. Koyama, Effect of ultrasound frequency on sonochemical luminescence under well-determined sound pressure, Jpn. J. Appl. Phys. 38(5S) (1999) 3103 – 3104.
11. L. Rong, Y. Kojima, S. Koda, H. Nomura, Simple quantification of ultrasonic intensity using aqueous solution of phenolphthalein, Ultrason. Sonochem. 8(1) (2001) 11 – 15.
12. H. Nomura, S. Koda, K. Yasuda, Y. Kojima, Quantification of ultrasonic intensity based on the decomposition reaction of porphyrin, Ultrason. Sonochem. 3(3) (1996) S153 – S156.
13. M. Sivakumar, A.B. Pandit, Ultrasound enhanced degradation of Rhodamine B: optimization with power density, Ultrason. Sonochem. 8(3) (2001) 233 – 240.
14. E.J. Hart, A. Henglein, Free radical and free atom reactions in the sonolysis of aqueous iodide and formate solutions, J. Phys. Chem. 89(20) (1985) 4342 – 4347.
15. S. Koda, T. Kimura, T. Kondo, H. Mitome, A standard method to calibrate sonochemical efficiency of an individual reaction system, Ultrason. Sonochem. 10(3) (2003) 149 – 156.
16. L. Gaete-Garretón, Y. Vargas-Hernández, R. Vargas-Herrera, J.A. Gallego-Juárez, F. Montoya-Vitini, On the onset of transient cavitation in gassy liquids, J. Acoust. Soc. Am. 101(5) (1997) 2536 – 2540.

17. S. Merouani, O. Hamdaoui, F. Saoudi, M. Chiha, Influence of experimental parameters on sonochemistry dosimetries: KI oxidation, Fricke reaction and H_2O_2 production, J. Hazard. Mater. 178(1) (2010) 1007 – 1014.
18. M.J.W. Pickworth, P.P. Dend, T.G. Leighton, A.J. Walton, Studies of the cavitational effects of clinical ultrasound by sonoluminescence: 2. Thresholds for sonoluminescence from a therapeutic ultrasound beam and the effect of temperature and duty cycle, Phys. Med. Biol. 33(11) (1988) 1249 – 1260.
19. C.L. Kling, F.G. Hammitt, A photographic study of spark-induced cavitation bubble collapse, *J. Basic Eng.* 94(4) (1972) 825 – 832.
20. Q.X. Wang, K. Manmi, Three dimensional microbubble dynamics near a wall subject to high intensity ultrasound, Phys. Fluids 26(3) (2014) (032104-1-23).
21. T. Kodama, Y. Tomita, Cavitation bubble behavior and bubble–shock wave interaction near a gelatin surface as a study of in vivo bubble dynamics, Applied Physics B, 70(1) (2000) 139 – 149.
22. T. J. Mason, J. P. Lorimer, Theory, Applications and Uses of Ultrasound in Chemistry, Ellis Harwood Limited, John Wiley, New York (1988).

Chapter 5

Measurement of distribution of broadband noise and sound pressures in sonochemical reactor

5.1. Introduction

Ultrasonic cavitation is a phenomenon that originated from irradiation of high intensity ultrasound, consequently generating fine bubbles are, which oscillated and collapsed in the liquid. Ultrasonic cavitation causes localized fields with high temperature, pressure and fluid velocity. In these localized fields, chemical and mechanical effects are generated. Sonochemistry is chemical effect of ultrasonic cavitation that attracts attention because it applies to many areas such as synthesis of nanoparticles with high catalyst activity [1-3] and decomposition of harmful material in water under normal temperature and pressure [4-6]. It is proven that sonochemical technique shows advantages in low environmental load and safety operation.

To put sonochemical method into practical use, it is necessary to develop a high-efficiency sonochemical reactor which has high reaction rate per unit ultrasonic energy. The enlargement of reaction fields in the reactor is important for the development of the high-efficiency sonochemical reactor. Simultaneously, an accurate method of evaluating reaction fields should be developed. So far, fields of sonochemical reaction and ultrasound were evaluated by several methods such as distribution of sound pressure at the fundamental frequency [7-9], observation of bubble clouds [10-12], distribution of aluminum foil erosion [13-15], observation of sonochemical luminescence [16-18], and distribution of broadband noise [19-21].

Distribution of sound pressure at the fundamental frequency was measured using a hydrophone and an XYZ-stage. The obtained sound pressure is accurate and can compare

with that by numerical simulation [7, 9, 22-24]. However, fields with high sound pressure do not necessarily correspond to those with high reaction [20, 21] since cavitation generation is influenced by bubble behavior under ultrasound. Bubble clouds have been often observed by high-speed video camera. Mettin classified several bubble clouds in terms of shapes and explained its formation mechanism [10]. However, it is difficult to distinguish bubbles contributing to reaction from other bubbles. In the distribution of aluminum foil erosion, an aluminum foil tailored to the size of the reactor is immersed into a sample. After ultrasonic irradiation, erosion positions and areas are measured [13, 15]. This method is simple and requires short measurement time. Nevertheless, there is a concern that sound fields may change by immersion of the aluminum foil. Observation of sonochemical luminescence by luminol solution is the most frequently used method since sonochemical luminescence directly originates from sonochemical reaction and it is easy to observe reaction fields in the whole reactor. However, it is impossible to estimate cross-sectional area distribution of reaction field in the reactor because the observation could be only taken from a window or wall of the reactor. In the case of a sonochemical reactor surrounded by cooling water, measurement of reaction fields is difficult.

The sound emissions generated by cavitation bubbles are composed of its characteristic noise and frequency components. A significant contributor to broadband noise comes from shockwaves arising from collapse of cavitation bubbles. Extent of broadband noise relates to the amount of bubble collapse at a certain measurement point in the reactor. The broadband noise ranging from kilohertz to megahertz frequencies is measured using the hydrophone and a spectrum analyzer. This method is possible to

estimate cross-sectional area distribution of reaction fields in the reactor since sonochemical reaction originates from collapse of cavitation bubbles. Still, the distribution of broadband noise in the reactor has been only conducted one-dimensional measurement [20, 21]. The value of broadband noise is a relative value varied according to the type of hydrophone. Recently, Shiiba et al. [25] have developed a tough needle-type hydrophone fabricated by a hydrothermal synthesis method. This hydrophone can measure high sound pressures in a wide range of frequencies under ultrasonic cavitation.

In this chapter, the cross-sectional area distribution of broadband noise in the sonochemical reactor was measured to estimate reaction fields. The tough needle-type hydrophone fabricated by a hydrothermal synthesis method scanned the reactor in horizontal and vertical directions at one-millimeter interval. Average of broadband sound pressure was defined to show an absolute value of broadband noise. The sonochemical reactor surrounded by cooling water was driven at 130 and 43 kHz. The cross-sectional area distribution of sound pressures at the fundamental and second harmonic frequencies were also measured to clarify effects of sound pressure and bubbles on reaction fields.

5.2. Experiments

Figure 5. 1 shows dimensions of the double layer - sonochemical reactor. Sample was put in inner layer and cooling water was circulated in outer layer of the stainless steel reactor. Inner diameter and height of the reactor were 56.8 and 120 mm, respectively. A Langevin transducer 45 mm in diameter was fixed at the bottom of the reactor, and

ultrasound was irradiated to the sample in the reactor. The transducer was driven at ultrasonic frequencies of 130 and 43 kHz. The sample heights in the reactor at 130 and 43 kHz were 40 and 100 mm, respectively. Air-saturated distilled water was used as a sample. The sample temperature was kept constant at 298 K using a water bath.

The detail explanation of apparatus and experimental setup were shown in chapter 3. The hydrophone scanned the reactor in horizontal and vertical directions at one-millimeter interval by an XYZ-axis stage and a stage controller to get the cross-sectional area distribution of sound pressure and broadband noise in the sonochemical reactor. The origin position of distribution measurement was decided at the center of the transducer surface, and the x and z axes were defined as the horizontal and vertical directions, respectively.

Using calibration data, sound pressures at the fundamental and second harmonic frequencies were obtained from their sound signals. The average of broadband sound pressure was calculated using the next equation,

$$ABP = \frac{\int_{f_2}^{f_1} P(f)df}{f_2 - f_1} \qquad (5.\ 1)$$

where $P(f)$ is broadband sound pressures excluding the fundamental, subharmonic, harmonic, and ultraharmonic components [26]. The start frequency of the integration region f_1 was 20 kHz and the end frequency f_2 was 10 MHz. Average of broadband sound pressure shows the absolute value of a broadband noise.

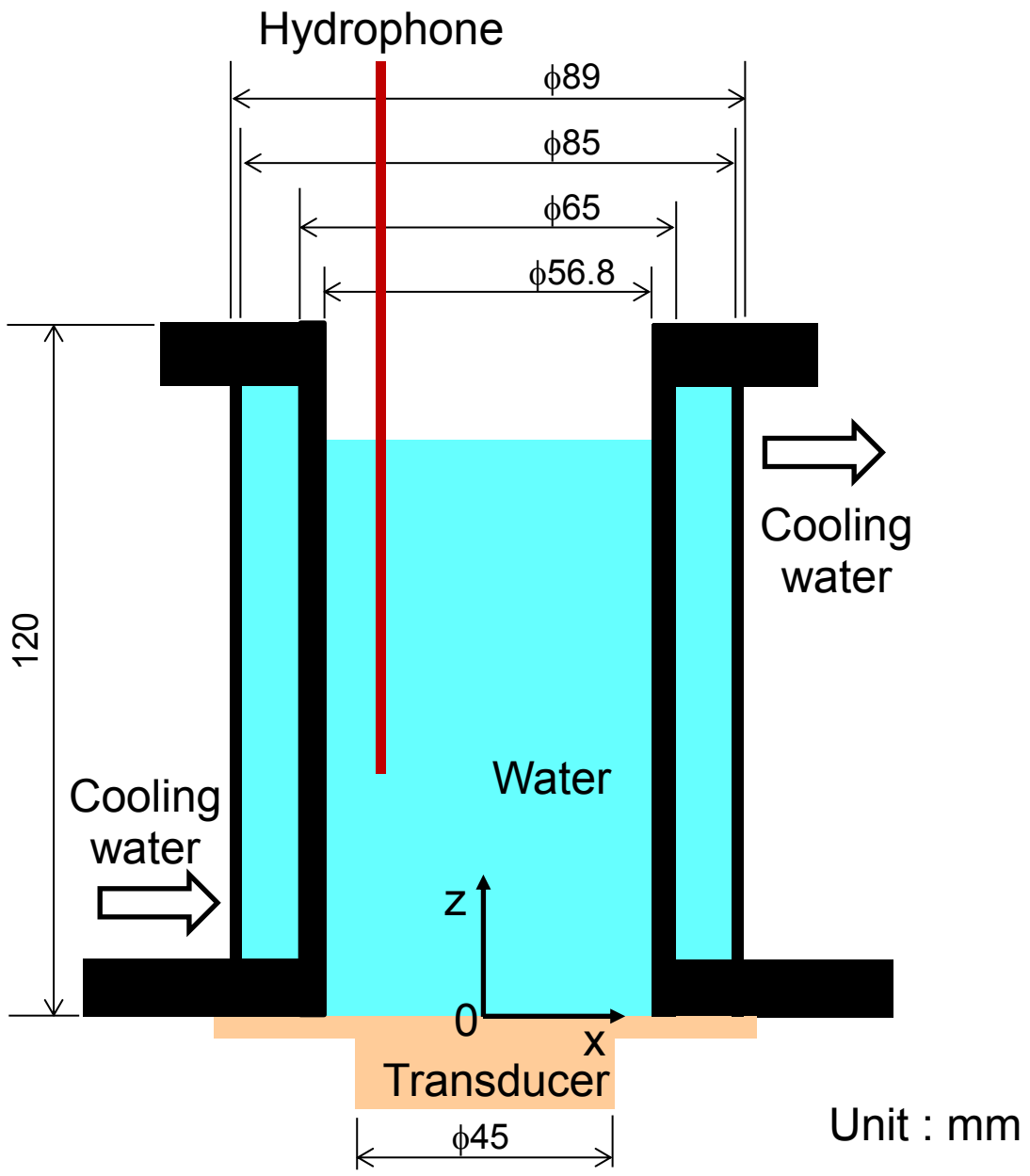

Fig. 5. 1 Dimensions of the sonochemical reactor

5.3. Results and discussion

5.3.1. Distribution at 130 kHz

In order to determine the effects of sound pressure and bubbles on reaction fields in the sonochemical reactor, the experiments for investigating the cross-sectional area distribution of sound pressures took place at the fundamental frequencies of 130 and 43 kHz by hydrophone measurement. The distribution of sound pressure at the former driving frequency is shown in Fig. 5. 2. The stripe patterns of standing wave are observed between the transducer and the water surface at the positions of sound pressure antinodes at z = 12, 19, 26, 32, and 38 mm. The ultrasound wavelength in water is 11.5 mm. Due to a coupled vibration so-called phenomenon in which the vibration of the progressive wave is influenced by the radial vibration, the interval between two nearest peaks at high sound pressure is observed as being pretty longer than a half wavelength [27].

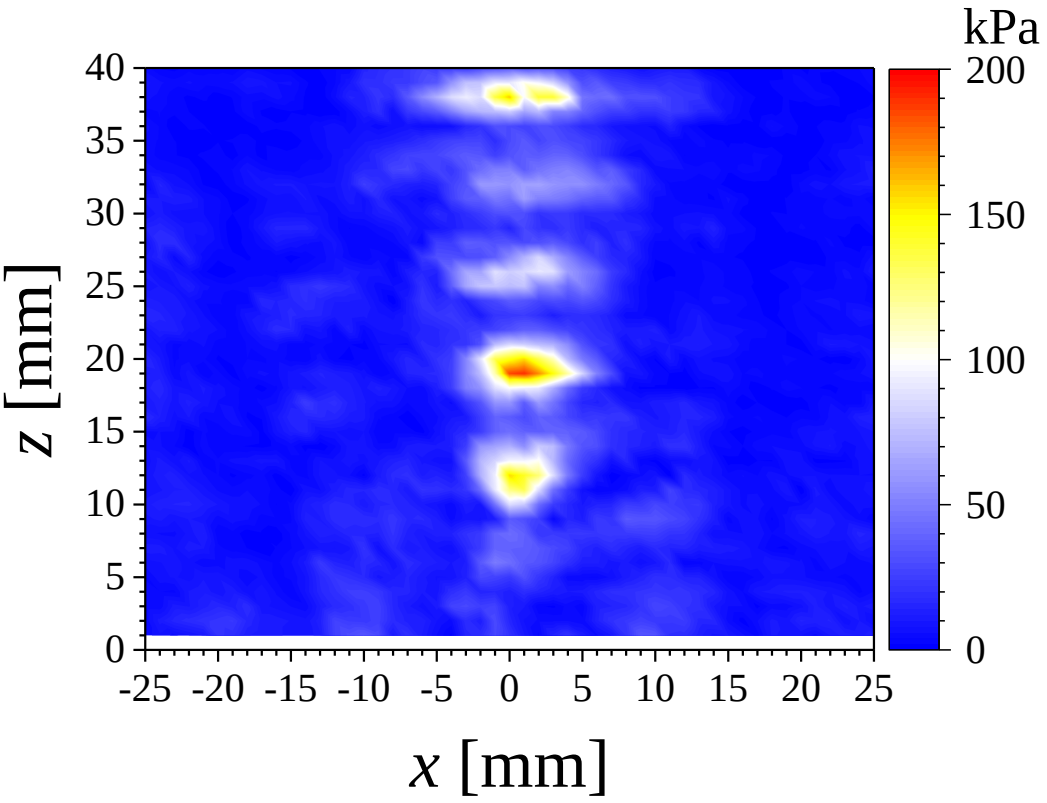

Fig 5. 2. Distribution of sound pressure at the fundamental frequency at the driving frequency of 130 kHz.

In many related studies, the broadband noise is often used for the cavitation detection due to the fact that it is directly attributed to the collapse of cavitation bubbles [19, 20]. The hydrophone used in these experiments for the sound pressure can detect a wide range of ultrasonic frequency under cavitation as it is tough [25] and calibrated for the range of 20 kHz to 20 MHz. Since the collapse of cavitation bubbles generated sonochemical reaction, thus the average of broadband sound pressure derived from equation (1) reflected sonochemical reaction fields. In Fig. 5. 3, the distribution of average broadband sound pressure is illustrated with the display of which pressure is upper than 40

Pa to improve the visualization of reaction fields. As shown in the figure, the sonochemical reaction fields are observed above the transducer and have several ellipse shapes centered at points of (x, z) = (0, 12), (0, 19), (0, 26), (0, 32), (0, 38). Observing from the figure, reaction fields are powerful in upper part of the reactor which indicates the existence of many bubbles in this area. Furthermore, the reaction fields are different from the sound pressure at the fundamental frequency which is shown in Fig. 5. 2. Especially, a turnover performance was recognized at areas with very high sound pressure such as (x, z) = (0, 12), (0, 19), (0, 26), (0, 38) where the reactions fields are weak.

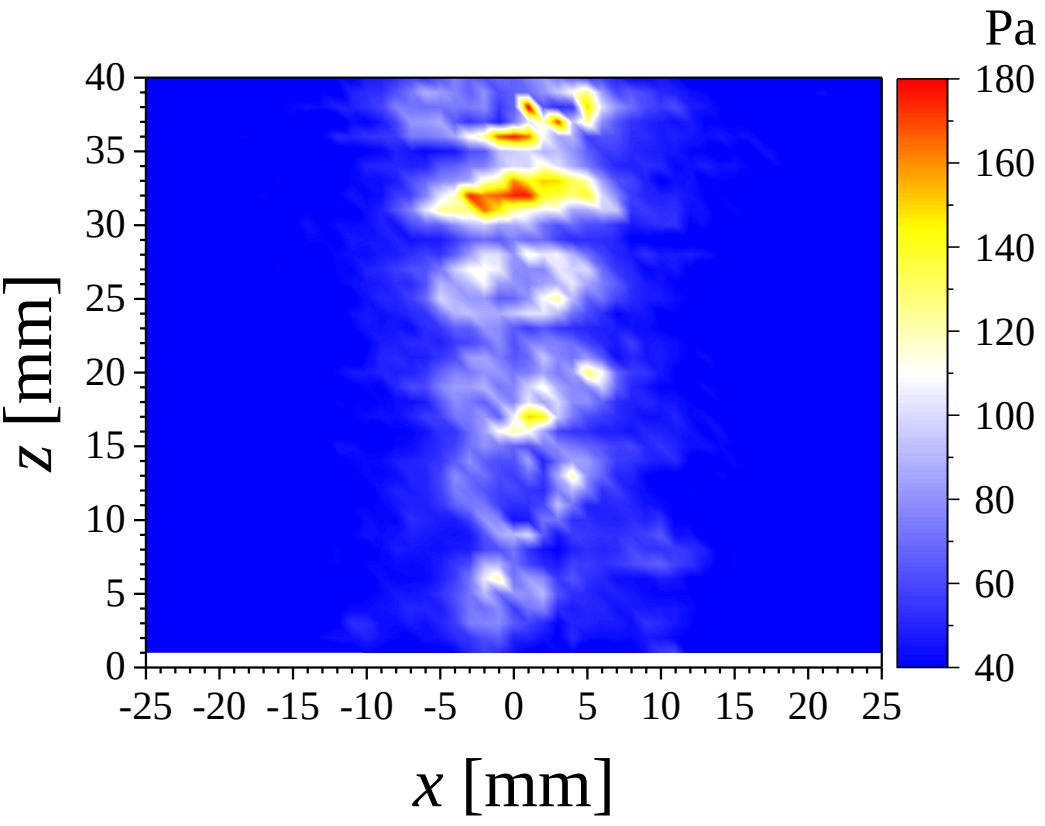

Fig 5. 3. Distribution of average of broadband sound pressure at the driving frequency of 130 kHz.

Mettin conducted the experiment of observing bubble structure at 20 kHz and observed double layer structure of bubbles in plate-like standing wave. He clarified that the bubbles were repelled from the pressure antinode due to primary Bjerknes force and settled at locations between the pressure antinode and node. Since this force departs bubbles from the pressure antinode, in Fig. 5. 3, hollow ellipse shape reaction fields can be observed at points of (x, z) = (0, 12), (0, 19), (0, 26).

The harmonic signals are mainly originated from nonlinear oscillations of bubbles in water [28]. The distribution of sound pressure at the second harmonic frequency is used to indicate distribution of bubbles with nonlinear oscillations. Fig. 5. 4 shows the distribution of sound pressure at the second harmonic frequency. To eliminate noise, the sound pressure at the second harmonic frequency above 5 kPa is displayed. It is noticed in the figure that the amount of bubbles are enormous in upper part of the reactor. One explanation can be drawn out that the bubbles move to the upper part by the difference of radiation force between progressive wave and reflective wave [29]. The fact that the former sort of force which is generated from the transducer is higher than that of the latter which is produced from water surface because of the absorbance of ultrasound into water. It should be noticed in the figure that bubble clouds with hollow ellipse shape are observed at points of (x, z) = (0, 12), (0, 19), (0, 26) because of repulsive force at the pressure antinode and the distribution patterns of bubbles resembles to that of reaction fields closely. In comparison with distribution of sound pressure in Fig. 5. 2, there is a small amount of bubbles at the positions of very high sound pressures such as (x, z) = (0, 12), (0, 19), (0, 26), (0, 38).

Since the measurement of sound pressure at the second harmonic frequency is

suffered by nonlinear propagation of ultrasound above 1 MHz [30], applying the average of broadband sound pressure to measure the distribution of sonochemical fields is an apparently effective method.

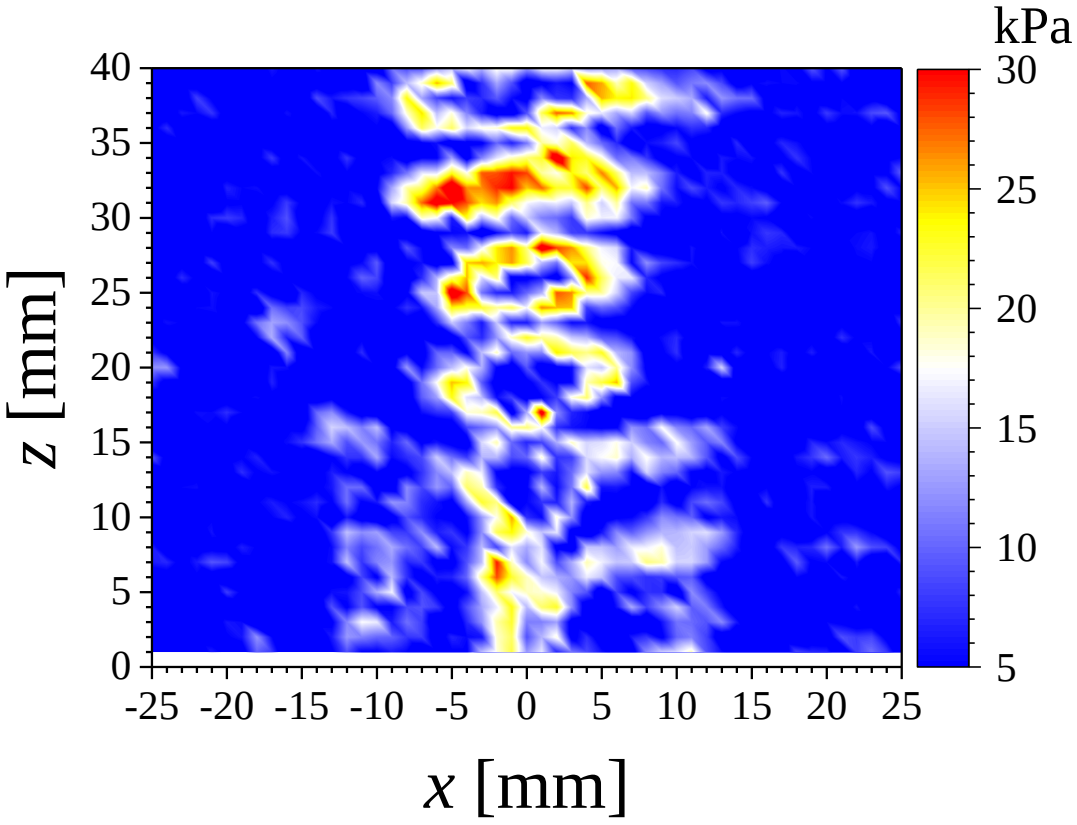

Fig. 5. 4. Distribution of sound pressure at the second harmonic frequency at the driving frequency of 130 kHz.

5.3.2. Distribution at 43 kHz

When the distribution of sound pressure at the driving frequency of 130 kHz is examined to understand the behavior of reaction fields in the sonochemical reaction, the similar investigation at the driving frequency of 43 kHz is also implemented to get the deeper insight of reaction fields at different frequencies (Fig. 5. 5). This result raises a notice about the complex distribution of the sound pressure at 43 kHz comparing with that at 130 kHz. To discuss the distribution of sound pressure at 43 kHz, the simulation is conducted using a software (Femtet, Murata Software). This software is a kind of finite method based on linear acoustic. Dimensions and material of reactors imitated in the simulation were the same as those used in empirical experiments. In the calculation, the tetrahedral mesh was used and its mesh was set to be less than 1/70 of the ultrasound wavelength in water. The transducer was assumed to vibrate in a piston motion at a constant velocity. Figs. 5. 6 (a) and (b) show distributions of sound pressure at the fundamental frequency by numerical simulation. In this simulation, the dimensions of the reactor are as same as those of the one shown in Fig. 5. 1. In Fig. 5. 6 (a), the reactor material is made from stainless steel. The reactor is enclosed with cooling water in the outer layer. A similar appearance of this result to that by hydrophone measurement (Fig. 5. 5) is remarked which can contribute to the reliability of the sound pressure distribution measurement. The ultrasound wavelength in water at 43 kHz is 34.8 mm which closely fit with the inner diameter of the reactor (56.8 mm). This significantly affects the distribution behavior of sound pressure by the large effect of coupled vibration and causes a complex distribution

behavior.

On the other hand, the second simulation with the glass reactor and the air cooling system was conducted (Fig. 5. 6 (b)). From a glance at both Figs. 5. 6 (a) and (b), it is clear that there is a much difference in the sound pressure distribution when the reactor system is changed. When the reactor material is made from stainless steel with a water cooling system, a part of ultrasound transmitted from the reactor wall out to water (Fig. 5. 6 (a)) whereas total ultrasound can be reflected on the interface between glass and air in the latter system (Fig. 5. 6 (b)). Normally, to estimate sonochemical reaction fields, the measurement of sonochemical luminescence by luminol solution has been conducted using a reactor surrounded by air [17]. Hence, it should be concluded that the estimation of sonochemical reaction fields by luminol method is not suitable for the sonochemical reactor surrounded by cooling water.

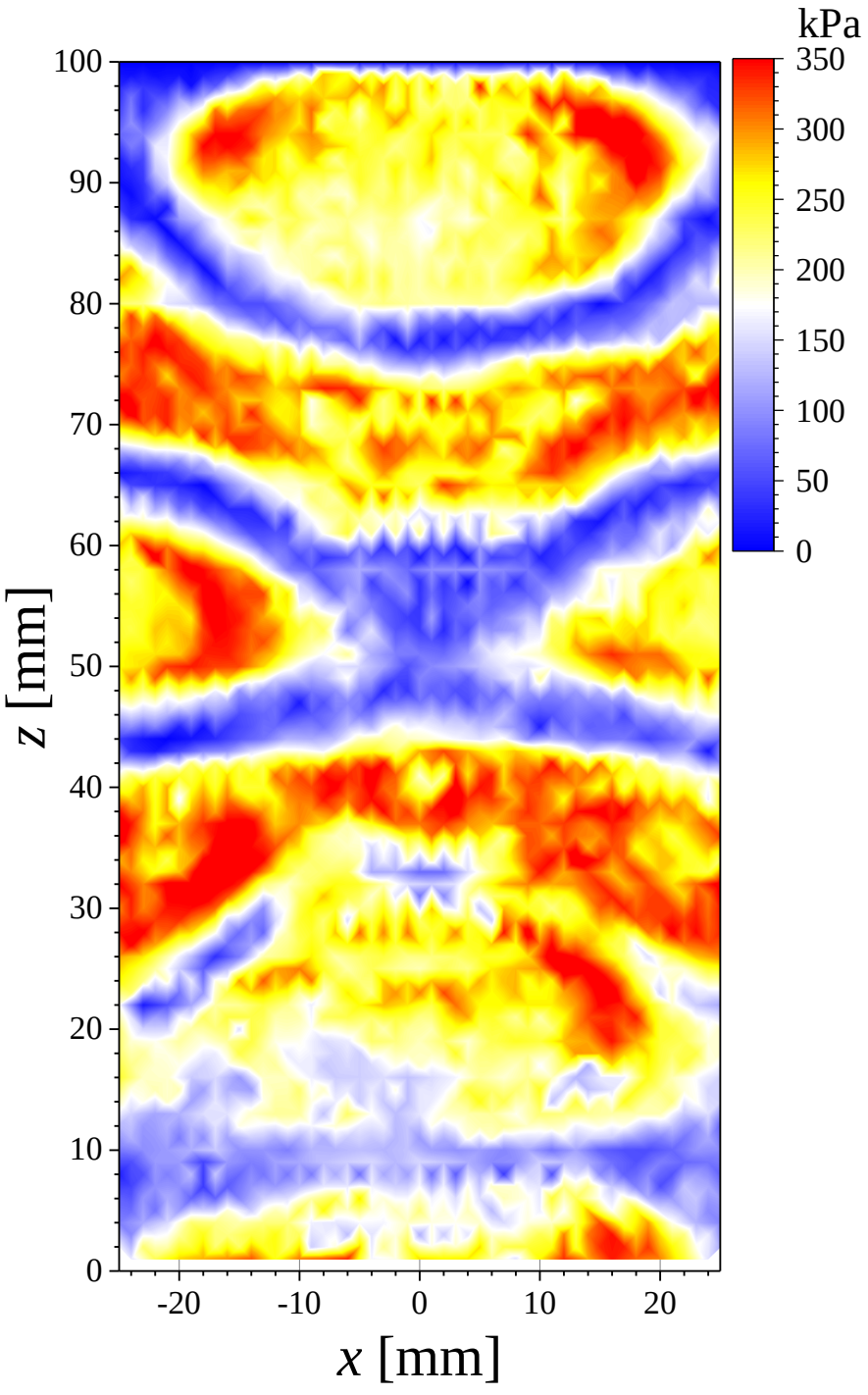

Fig. 5. 5. Distribution of sound pressure at the fundamental frequency by measurement at the driving frequency of 43 kHz.

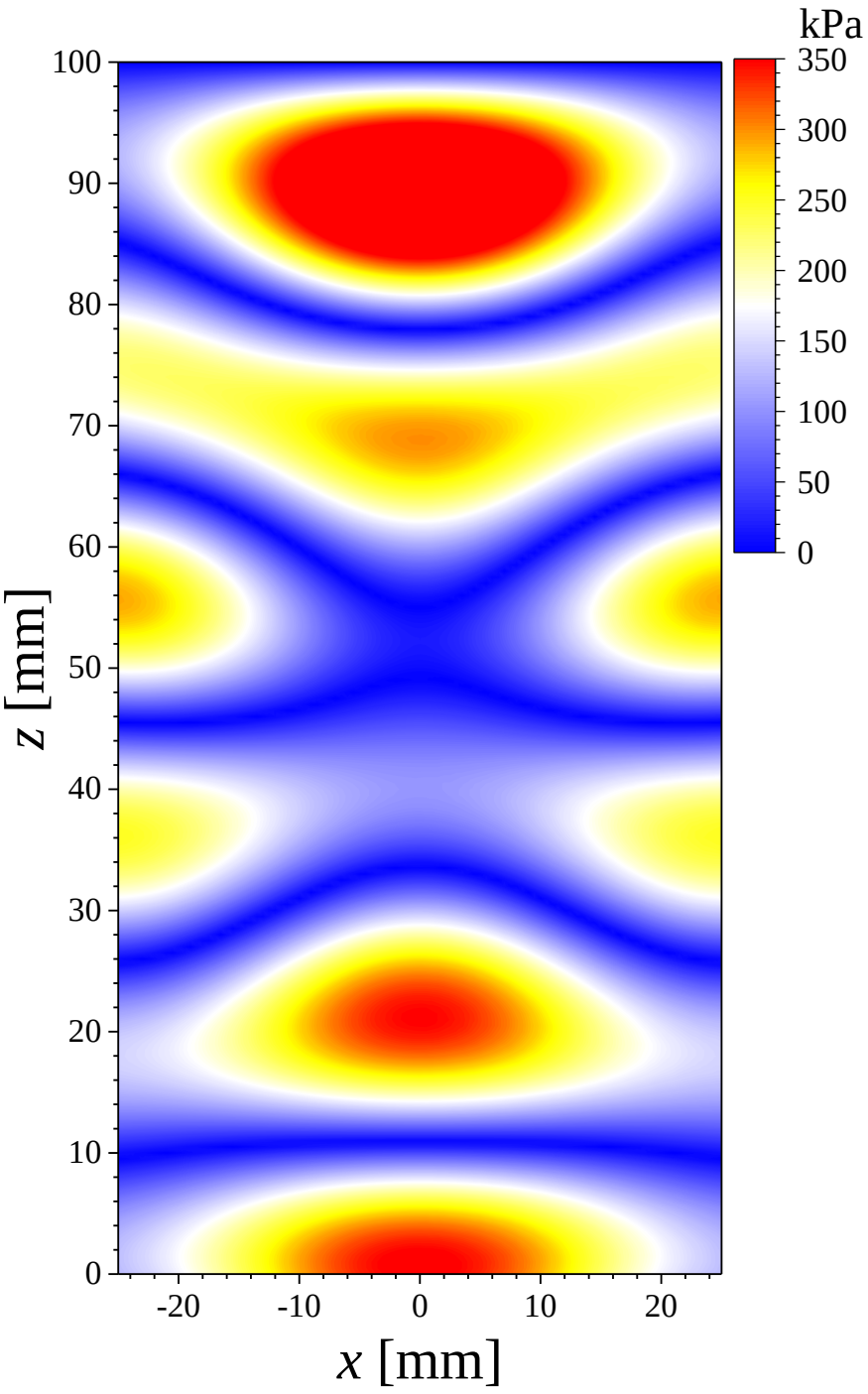
kPa
350
300
250
200
150
100
50
0
100
90
80
70
60
50
40
30
20
10
0
z [mm]
-20
-10
0
10
20
x [mm]

(a)

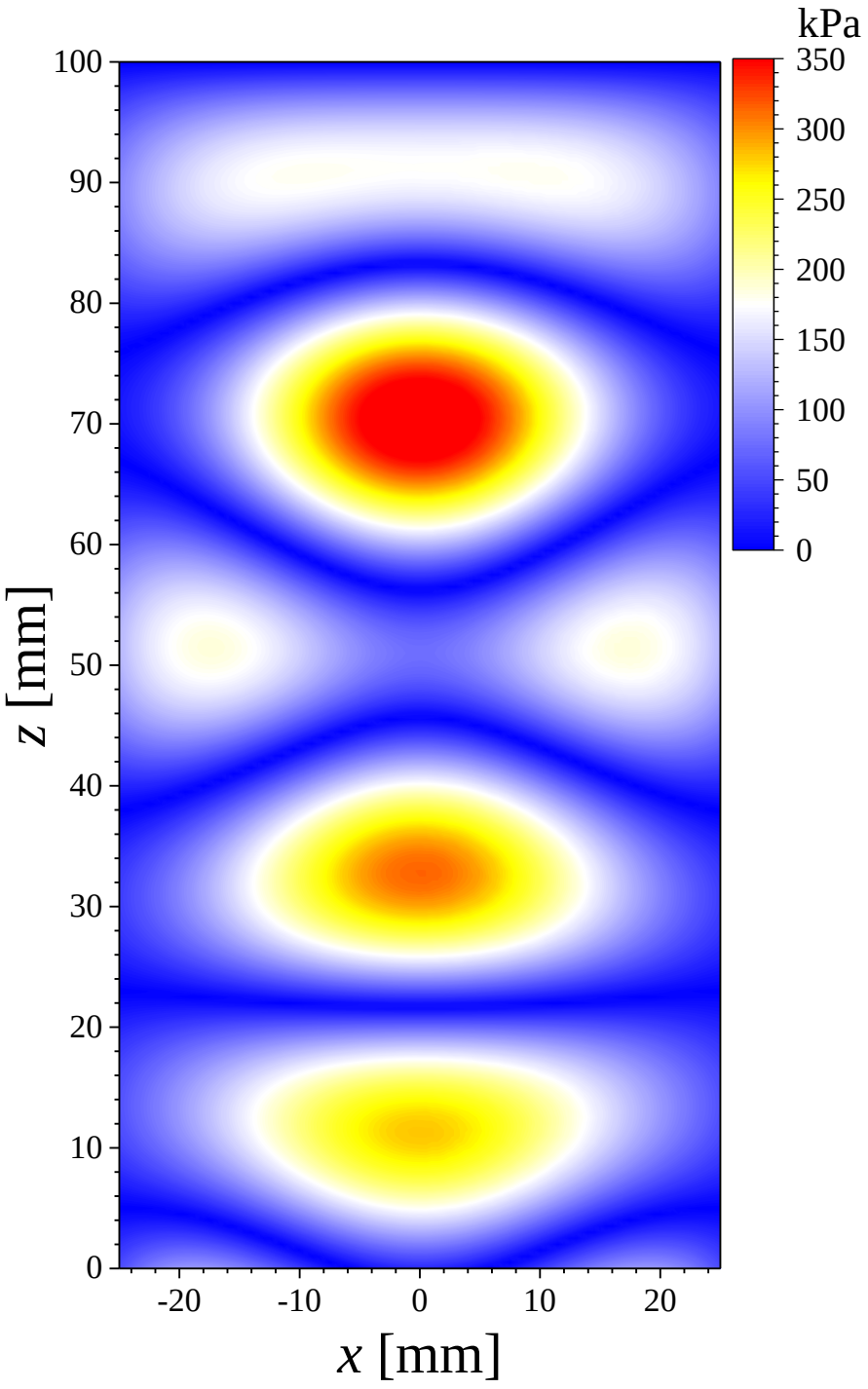

(b)

Fig 5. 6. Distribution of sound pressure at the fundamental frequency by numerical simulation at the driving frequency of 43 kHz, (a) stainless steel reactor and(b) glass reactor

Figure 5. 7 shows the distribution of average of broadband sound pressure at 43 kHz. It can be seen in the figure that the reaction fields are powerful at roughly z = 20 and 90 above the transducer. The reaction fields are relatively feeble in areas where have very high sound pressures in Fig. 5. 5. This tendency seems like the appearance at 130 kHz as shown in Figs. 5. 2 and 5. 3. This phenomenon can be explained by the effect of the primary Bjerknes force to the movement of bubbles from the pressure antinodes.

In this chapter, the distribution of average of broadband sound pressure by the hydrophone was measured to estimate the cross-sectional area distribution of reaction field in the reactor. From the comparison between the distributions of sonochemical reaction fields and those of sound pressure at the fundamental frequency, a significant difference is observed. The reasons for this discrepancy are that cavitation bubbles move toward the upper part of the reactor by the radiation force and repel from the pressure antinode by primary Bjerknes force.

By optimizing the distribution of sound pressure and bubbles, the sonochemical reaction fields will be enhanced. For the sake of enhancing the efficiency of the sonochemical reactor, the method of measurement of distribution of average of broadband sound pressure can be highly adapted in evaluating the sonochemical reaction field.

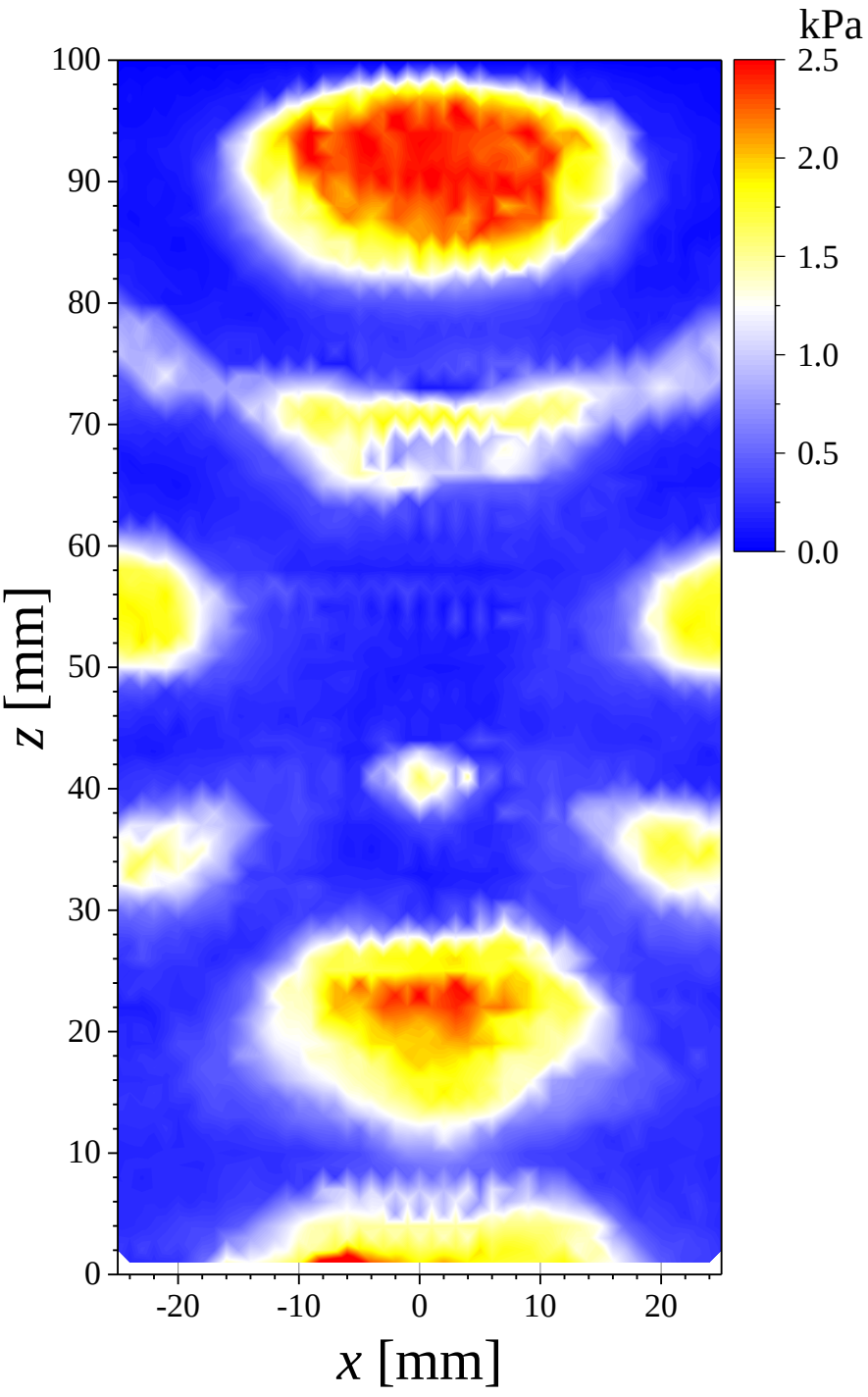

Fig. 7. Distribution of average of broadband sound pressure at the driving frequency of 43 kHz.

5.4. Conclusion

The reaction field in a sonochemical reactor was investigated by the cross-sectional area distribution of broadband noise using a needle-type hydrophone to scan the sonochemical reactor in both horizontal and vertical directions at one-millimeter interval. The average of broadband sound pressure was defined with the aim of showing an absolute value of broadband noise. Besides, the distribution of sound pressures at the fundamental and second harmonic frequencies were also measured to know the high zones of sound pressure in the sonochemical reactor. At 130 kHz, the sonochemical reaction fields in ellipse shape were observed and showed to be strong in upper part of the reactor. It is known that within the reactor, cavitation bubbles move up by radiation force. The sound pressure distribution at the fundamental frequency showed existence of standing waves and reaction fields were weak at pressure antinodes because cavitation bubbles were repelled by primary Bjerknes force. The sound pressure distribution at the second harmonic frequency indicated that the pattern of bubbles distribution resembled to that of reaction fields closely. Compared with 130 kHz, distributions of reaction fields and sound pressures at 43 kHz were complex due to coupled vibration. The reaction fields were relatively weak in areas which had very high sound pressures at the fundamental frequency.

References

1. K.S. Suslick, S.B. Choe, A.A. Cichowlas, M.W. Grinstaff, Sonochemical synthesis of amorphous iron, Nature 353(6343) (1991) 414 – 416.
2. T. Hyeon, M. Fang, K.S. Suslick, Nanostructured molybdenum carbide: sonochemical synthesis and catalytic properties, J. Am. Chem. Soc. 118(23) (1996) 5492 – 5493.
3. K. Okitsu, A. Yue, S. Tanabe, H. Matsumoto, Sonochemical preparation and catalytic behavior of highly dispersed palladium nanoparticles on alumina, Chem. Mater. 12(10) (2000) 3006 – 3011.
4. A. Kotronarou, G. Mills, M.R. Hoffmann, Decomposition of parathion in aqueous solution by ultrasonic irraidaition, Eviron. Sci. Technol. 26(7) (1992) 1460 – 1462.
5. Y. Kawase, T. Masuya, K. Yasuda, M. Nakamura, Development of small ultrasonic reactor for on-site treatment of wastewater including chlorinated hydrocarbon, J. Chem. Eng. Jpn, 39(1) (2006) 95 – 98.
6. M. Chiha, S. Merouani, O. Hamdaoui, S. Baup, N. Gondrexon, C. Pétrier, Modeling of ultrasonic degradation of non-volatile organic compounds by Langmuir-type kinetics, Ultrason. Sonochem. 17(5) (2010) 773 – 782.
7. S. Dähnke, K.M. Swamy, F.J. Keil, Modeling of three-dimensional pressure fields in sonochemical reactors with an inhomogeneous density distribution of cavitation bubbles. Comparison of theoretical and experimental results, Ultrason. Sonochem. 6(1-2) (1999) 31 – 41.
8. S. Nomura, S. Mukasa, M. Kuroiwa, Y. Okada, K. Murakami, Cavitation bubble streaming in ultrasonic-standing-wave field, Jpn. J. Appl. Phys. 44(5A) (2005) 3161 – 6164.
9. Z. Wei, L.K. Weavers, Combining COMSOL modeling with acoustic pressure maps to design sono-reactors, Ultrason. Sonochem. 31 (2016) 490 – 498.
10. R. Mettin, Bubble structures in acoustic cavitation, in: A.A. Doinikov, Bubble and particle dynamics in acoustic fields: modern trends and applications, Research Signpost, Trivandrum (India), 2005, 1 – 37.
11. T. Tuziuti, K. Yasui, Y. Iida, Spatial study on a multibubble system for sonochemistry, Ultrason. Sonochem. 12(1-2) (2005) 73 – 77.
12. X. Ma, B. Huang, G. Wang, M. Zhang, Experimental investigation of conical bubble structure and acoustic flow structure in ultrasonic field, Ultrason. Sonochem. 34 (2017) 164 – 172.
13. G. Servant, J.-L. Laborde, A. Hita, J.-P. Caltagirone, A. Gérard, Spatio-temporal dynamics of cavitation bubble clouds in a low frequency reactor: comparison between theoretical and experimental results, Ultrason. Sonochem. 8(3) (2001) 163 – 174.
14. Z. Liang, G. Zhou, Y. Zhang, Z. Li, S. Lin, Vibration analysis and sound field characteristics of a tubular ultrasonic radiator, Ultrasonics 45(1-4) (2006) 146 – 151.
15. L. Liu, J. Wen, Y. Yang, W. Tan, Ultrasound field distribution and ultrasonic oxidation desulfurization efficiency, Ultrason. Sonochem. 20(2) (2013) 696 – 702.
16. K. Yasuda, T. Torii, K. Yasui, Y. Iida, T. Tuziuti, M. Nakamura, Y. Asakura, Enhancement of sonochemical reaction of terephthalate ion by superposition of ultrasonic fields of various frequencies Ultrason. Sonochem. 14(6) (2007) 699 – 704.

17. Y. Asakura, T. Nishida, T. Matsuoka, S. Koda, Effects of ultrasonic frequency and liquid height on sonochemical efficiency of large-scale sonochemical reactors, Ultrason. Sonochem. 15(3) (2008) 244 – 250.
18. M. Kauer, V. B.-Magri, C. Cairós, H.-J. Schreier, R. Mettin, Visualization and optimization of cavitation activity at a solid surface in high frequency ultrasound fields, Ultrason. Sonochem. 34 (2017) 474 – 483.
19. M. Hodnett, B. Zeqiri, Toward a reference ultrasonic cavitation vessel: Part 2 - Investigating the spatial variation and acoustic pressure threshold of inertial cavitation in a 25 kHz ultrasound field, IEEE Trans. Ultrason. Ferroelectr. Freq. 55(8) (2008) 1809 – 1822.
20. T. Uchida, S. Takeuchi, T. Kikuchi, Measurement of amount of generated acoustic cavitation: investigation of spatial distribution of acoustic cavitation generation using broadband integrated voltage, Jpn. J. Appl. Phys. 50 (2011) 07HE01 – 1 – 4.
21. D. Sarno, M. Hodnett, L. Wang, B. Zeqiri, An objective comparison of commercially-available cavitation meters, Ultrason. Sonochem. 34 (2017) 354 – 364.
22. R. Jamshidia, B. Pohlb, U. A. Peukerb, G. Brenner, Numerical investigation of sonochemical reactors considering the effect of inhomogeneous bubble clouds on ultrasonic wave propagation, Chem. Eng. J., 189-190 (2012) 364 – 375.
23. Z. Xu, K. Yasuda, S. Koda, Numerical simulation of liquid velocity distribution in a sonochemical reactor, Ultrason. Sonochem. 20(1) (2013) 452 – 459.
24. I. Tudela, V. Sáez, M. D. Esclapez, M. I. D.-García, P. Bonete, J. G.-García, Simulation of the spatial distribution of the acoustic pressure in sonochemical reactors with numerical methods: A review, Ultrason. Sonochem. 21(3) (2014) 909 – 919.
25. M. Shiiba, N. Okada, T. Uchida, T. Kikuchi, M. Kurosawa, S. Takeuchi, Frequency characteristics of receiving sensitivity and waveform of an anti-acoustic cavitation hydrophone, Jpn. J. Appl. Phys. 53(7S) (2014) 07KE06 – 1 – 6.
26. T. T. Nguyen, Y. Asakura, N. Okada, S. Koda, K. Yasuda, Effect of ultrasonic cavitation on measurement of sound pressure using hydrophone, Jpn. J. Appl. Phys. 56(7S1) (2017) 07JE06 – 1 – 5.
27. S. Hatanaka, H. Mitome, T. Tuziuti, T. Kozuka, M. Kuwabara, S. Asai, Relationship between a standing-wave field and a sonoluminescing field, Jpn. J. Appl. Phys. 38(5B) (1999) 3053 – 3057.
28. E.A. Neppiras, Measurement of acoustic cavitation, IEEE Trans. Sonics Ultrason. 15(2) (1968) 81 – 88.
29. J. Lee, K. Yasui, T. Tuziuti, T. Kozuka, A. Towata, Y. Iida, Spatial distribution enhancement of sonoluminescence activity by altering sonication and solution conditions, J. Phys. Chem. B 112(48) (2008) 15333 – 15341.
30. T. T. Nguyen, Y. Asakura, S. Koda, K. Yasuda, Dependence of cavitation, chemical effect, and mechanical effect thresholds on ultrasonic frequency, Ultrason. Sonochem. 39 (2017) 301 – 306.

Chapter 6

Application of ultrasonication and silica gel on removal of silicic acid in geothermal water

6.1. Introduction

Geothermal power is a renewable and environmentally friendly energy resource, which is generated by geothermal energy that has been harnessed in many facilities that require heat. It does not create pollution and is not dependent on weather conditions. However, geothermal power plant is challenged by formation of silica scale, which adhere to solid surfaces of process equipment and wells that consequently results to a reduction of the heat exchange efficiency of geothermal energy plants and increase pressure losses in pipelines for geothermal water by clogging pipelines. It is therefore beneficial to prevent silica scale formation while operating geothermal energy plants.

Prevention methods to restrain deposition of silica scales include hot water re-injection [1], aging or pond retention [2], dilution with low silica content water [3], and gravity filtration [4]. These processes are easy to operate and control, however, they require a large amount of water and energy resources as well as large plant areas. Methods, which do not require substantial natural resources, include the addition of cationic surfactants [5] or organic compounds [6] to control silica scale. Cationic surfactant and organic material inhibitors showed high potential in the prevention of silica scale formation. The use of chemical compounds, however, causes water pollution and requires extra water treatment. On the other hand, the seeding method, a technique based on the adsorption or precipitation of excess silicic acid on the surface of the added reagents with the extra silicic acid being removed from the liquid phase, has been proven to be effective and environmentally friendly. It prevents silica scale formation since the seeds can be separated from the

geothermal water after removal of the silicic acid. Silica gels are high potential seeds because they have a high specific surface area [7]. The silica gel seed method is based on the polymerization reaction between the silica gel surface and silicic acid in geothermal water, so the reaction products are useful as high-quality silica resources [8]. Compared with other seeds such as calcium, aluminum, or iron compounds [9, 10], the silica gels are relatively large seeds that are easy to separate from the liquid phase and do not absorb arsenic which requires secondary treatment. Nevertheless, in order to put this method to practical use, there is a need to reduce the quantity of silica gel consumed and enhance the removal performance of the silicic acid.

Chemical reaction by ultrasonication has been applied in many applications, including synthesis [11], degradation [12], and polymerization [13, 14]. When ultrasound is irradiated into a solution, the reaction is caused by cavitation. Polymerization by ultrasonication has been studied for a number of compounds that involved bromobenzene, styrene, isoprene, and methyl methacrylate [13, 15]. Previously, the effect of ultrasonic irradiation on the polymerization of silicic acid was examined [16]. An ultrasonic frequency of 500 kHz with ultrasonic intensity of 3.6 W enhanced polymerization rate of monosilicic acid. Ultrasonication does not harm the environment and ultrasonic irradiation at low intensity could become a low-cost method.

The removal of silicic acid in water by ultrasonication and silica gel is examined with the goal of preventing silica scale formation. The effects of ultrasonic frequency, initial concentration of monosilicic acid, pH, concentration, particle diameter and pore size of the silica gel on the reduction of silicic acid concentration were examined.

6.2. Polymerization of silicic acid

Silicic acid is dissolved in geothermal water under conditions of elevated temperature and pressure in groundwater, and is in equilibrium with quartz in the rock to exist as monosilicic acid.

$$SiO_2 + 2H_2O \rightleftarrows Si(OH)_4 \qquad (6.\ 1)$$

Monosilicic acid solubility decreases due to the fall in temperature when geothermal water flows from the underground to the surface, resulting to the supersaturation of geothermal water with it. The polymerization of monosilicic acid occurs as shown in the following steps [17, 18] below with the monosilicic acid first ionized by the following reaction.

$$Si(OH)_4 \rightleftarrows Si(OH)_3O^- + H^+ \qquad (6.\ 2)$$

The polymerization between the monosilicic acid and the ion of monosilicic acid arises in the supersaturated solution, referred as a monomer – monomer reaction.

$$Si(OH)_4 + Si(OH)_3O^- \rightleftarrows (HO)_3SiOSi(OH)_3 + OH^- \qquad (6.\ 3)$$

The silanol group on the surface of polysilicic acid then reacts with hydroxide ion to form

the active site of the silanol group and water.

$$\equiv Si(OH) + OH^- \rightleftarrows \equiv SiO^- + H_2O \qquad (6.\ 4)$$

This active site polymerizes with monosilicic acid and the growth of polysilicic acid proceeds. This polymerization is referred to as a monomer – polymer reaction.

$$\equiv SiO^- + Si(OH)_4 \rightleftarrows \equiv SiOSi(OH)_3 + OH^- \qquad (6.\ 5)$$

The polymerization between the polysilicic acid and the ion of polysilicic acid also occurs. This polymerization is referred to as a polymer – polymer reaction.

$$\equiv SiO^- + HOSi\equiv \rightleftarrows \equiv SiOSi\equiv + OH^- \qquad (6.\ 6)$$

In geothermal water that includes supersaturated monosilicic acid, the reactions from Eqs. (6. 2) to (6. 6) are repeated, and polysilicic acid forms.

Tarutani (1989) measured the pH value giving a maximum rate of polymerization of the above three types of reactions using spectrophotometry, gas – liquid chromatography, and gel permeation chromatography [19]. The pH values giving a maximum rate of polymerization for the monomer – monomer reaction (Eq. (6. 3)), monomer – polymer reaction (Eq. (6. 5)), and polymer – polymer reaction (Eq. (6. 6)) are 9.5 – 8.1, 8.9 – 7.5, and 7.0 – 6.1 at 275 – 363 K, respectively.

6.3. Experiment

The experimental apparatus for ultrasonication at 500 kHz consisting of a signal generator, a power amplifier, a transducer, a glass vessel, a liquid pump, and a constant-temperature bath is shown in Fig. 6. 1. A power amplifier (AP-400B, ENI) and a signal generator (1941, NF Corp.) drives the plate-type transducer at 500 kHz (PZT, Honda Electronics Co., Ltd.).The sample was placed into a glass vessel with 45 mm in diameter and 75 mm in height. Afterwhich, an ultrasound was indirectly irradiated into the sample at an ultrasonic intensity of 3.6 W. The ultrasonic intensity was measured by a calorimetric method. The sample temperature was maintained at 308 ± 1 K. For comparison, ultrasonication at 28 kHz by a horn-type transducer (SONAC 150, Honda Electronics Co., Ltd.) at an ultrasonic intensity of 15.3 W and non-ultrasonication with stirring were performed. As reported in chapter 4, the threshold of chemical effect was in harmony with the cavitation threshold at all frequencies used from 22 to 4880 kHz. In this experiment, the ultrasound showed high potential in polymerization of the monosilicic acid. It means that the chemical effect is generated in the solution, that is the generation of OH radicals. Therefore, it should be noted that the ultrasonic intensity utilized in this experiment was higher than the ultrasonic intensity of cavitation threshold.

The sample was a liquid glass (Wako Pure Chemical Industries, Ltd.) aqueous solution with a volume of 75 mL. The initial concentration of monosilicic ranged from 0.5 to 1.1 g/L. The pH of the solution was changed by the addition of hydrochloric acid and sodium hydroxide. The total silica concentration was measured by the molybdate yellow

method (JIS K 0101) using a spectrophotometer (UV-1600, Shimadzu Corp.) after the sample was filtered using a paper filter of 1 μm pore size to remove the silica gel. The polysilicic acid was depolymerized by adding sodium bicarbonate and distilled water to the filtrate, which was then boiled for 30 min. The filtrate was cooled to room temperature, and the silica concentration was measured [7]. Six types of silica gel (Wako Pure Chemical Industries, Ltd.) were used. The diameters of the silica gel were 60, 95, and 180 μm and the pore sizes of the silica gel were 6 and 7 nm. The silica gel concentration was changed from 0 to 2.5 g/L. The concentrations of *t*-butanol and hydrogen peroxide were 11 and 74 g/L, respectively.

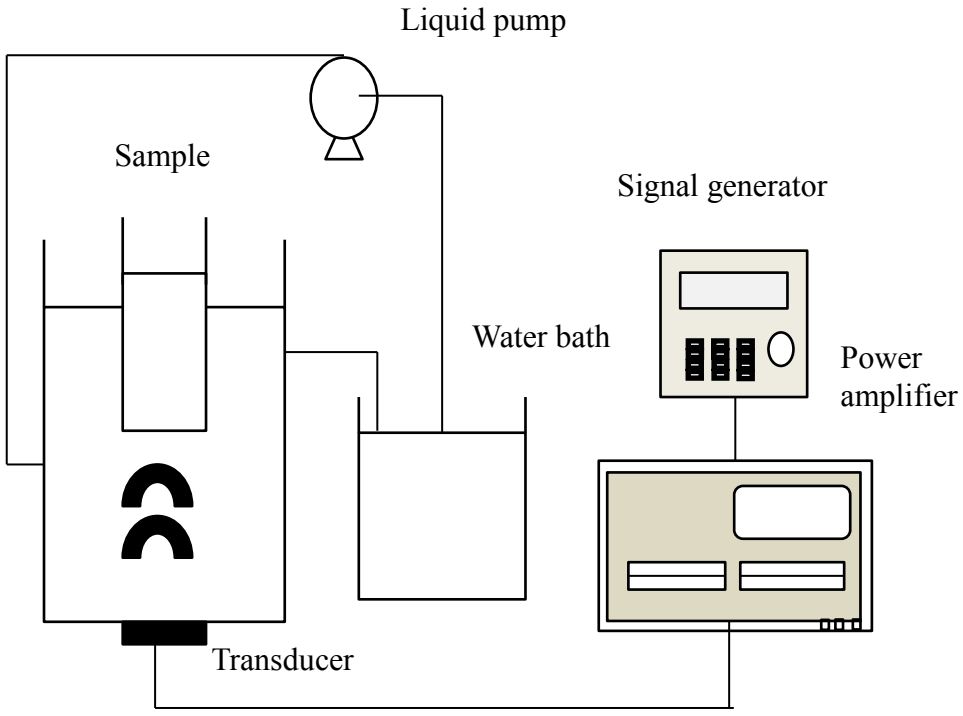

Fig. 6. 1 Setup of experimental apparatus

6.4. Results and discussion

6.4.1. Effects of silica gel and samples condition

At two conditions of stirring and ultrasonication, the total silicic acid concentration varies with time is shown in Fig. 6. 2. The experimental conditions are listed as follow:

- The particle diameter of silica gel is 60 μm.
- The pore size of silica gel is 7 nm.
- The silica gel concentration is 1.5 g/L.
- The initial concentration of monosilicic acid is 1.1 g/L
- pH is 6.0

Firstly, for comparison, the experiment of stirring without silica gel is conducted, and the total silicic acid concentration does not decrease. Lately, with the addition of silica gel, the total silicic acid concentration decreases because silicic acid in solution polymerizes with silica gel [8]. When the concentration of silicic acid and silica gel reduce by their reaction, the reaction rate decreases. Therefore, in this experiment, after 90 -120 min, the total silicic acid concentration becomes constant due to that decrease of reaction rate. The experimental result also shows that the ultrasonic irradiation greatly enhances the removal of silicic acid in solution. Moreover, the reaction efficiency is obtained higher at 28 kHz than that at 500 kHz. In other words, the total silica concentration with ultrasound at 28 kHz is higher than that at 500 kHz. In the case of not using silica gel, ultrasound was irradiated into monosilicic acid solution in the previous study [16], the total silicic acid concentration decreased only slightly.

In general, the silica removal ratio is defined as the ratio of the removed silica concentration to the initial silica concentration (C_0 - C_T) / C_0. The aim of this study is to inhibit silica gel formation, therefore, the removal ratio of total silica concentration, that is, the silica removal ratio was estimated using the next equation

$$R = \frac{C_0 - C_T}{C_0 - C_e} \quad (6.\ 7)$$

where C_0 is the initial concentration of monosilicic acid, C_T is the average concentration of total silicic acid from 120 to 180 min and C_e is the equilibrium concentration of monosilicic acid. The excess monosilicic acid concentration (C_0 - C_e) indicates the potential for silica scaling.

The next experiment was performed at 500 kHz to investigate the effect of silica gel concentration on the removal ratio of total silicic acid concentration, and at the same time experiment under the condition of stirring also was performed for comparison. The total irradiation time the experiment is 180 min. Figure 6. 3 demonstrates how silica gel effect the removal ratio of total silicic acid. In the case without the silica gel, the silica removal ratio for ultrasonication at 500 kHz is 0.1 since large silica particles were formed [16]. However, in the case of the addition of silica gel, large silica particles were not observed. The removal ratio of silicic acid increases as the silica gel concentration increased to 1.5 g/L. The removal ratios for ultrasonication are higher than those for stirring. The removal ratio difference between ultrasonication and stirring is also plotted in Fig. 6. 3. As the gel

concentration increases, the difference of removal ratio increases. Therefore, it could be deduced that ultrasonication is effective for the reaction enhancement between silicic acid and silica gel.

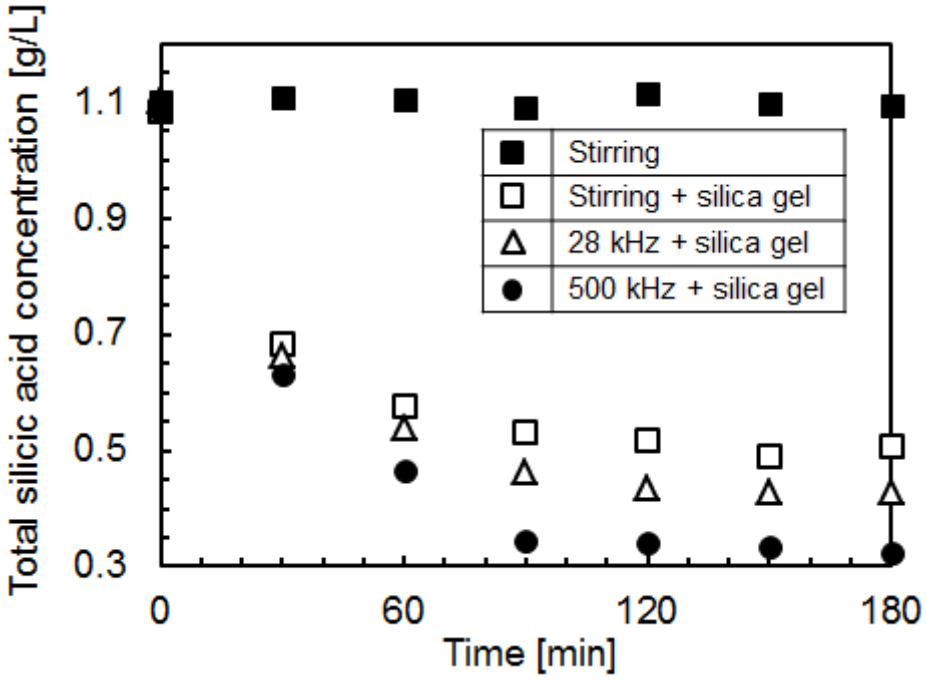

Fig. 6. 2 Changes in total silicic acid concentration with time for stirring, stirring with silica gel, ultrasonication at 28 kHz with silica gel, ultrasonication at 500 kHz with silica gel at pH = 6. Particle size of silica gel is 60 μm. Pore size of silica gel is 7 nm. Initial concentration of monosilicic acid is 1.1 g/L

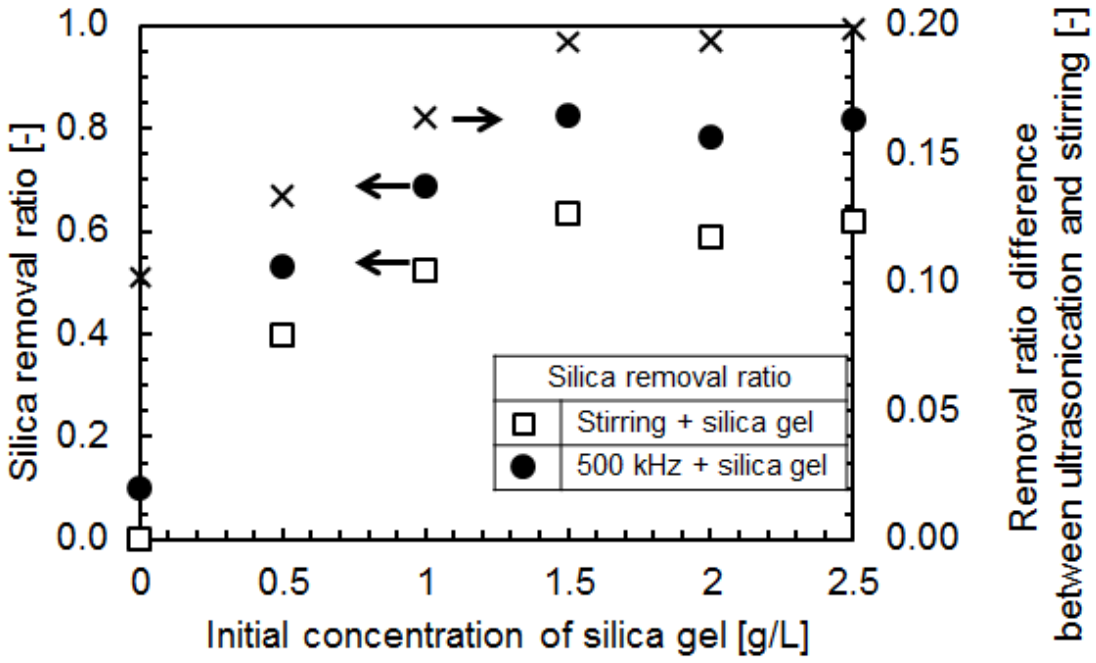

Fig. 6. 3 Effect of silica gel concentration on removal ratio of total silicic acid concentration for stirring, ultrasonication at 500 kHz with silica gel at pH = 6. Particle size of silica gel is 60 μm. Pore size of silica gel is 7 nm. Initial concentration of monosilicic acid is 1.1 g/L

Variety of silica gel types was utilized to investigate the effect of silica gel characteristics on the silica removal ratio. The result is shown in Fig. 6. 4. The experiment was conducted at 500 kHz. The upper and lower columns in horizontal axis are particle diameter and pore size of silica gel, respectively. The silica gel concentration is 1.5 g/L. The silica removal ratio increases as the particle diameter of silica gel decreases. The reason lies in the fact that the surface area of the silica gel becomes larger with the decreasing of silica gel diameter. The silica removal ratios of silica gel with pore size at 7 nm are higher than those at 6 nm. As the pore size of the silica gel increases, it might be

easier for silicic acid to enter into the pores of the silica gel with silicic acid reacting at the surface of the silica pores.

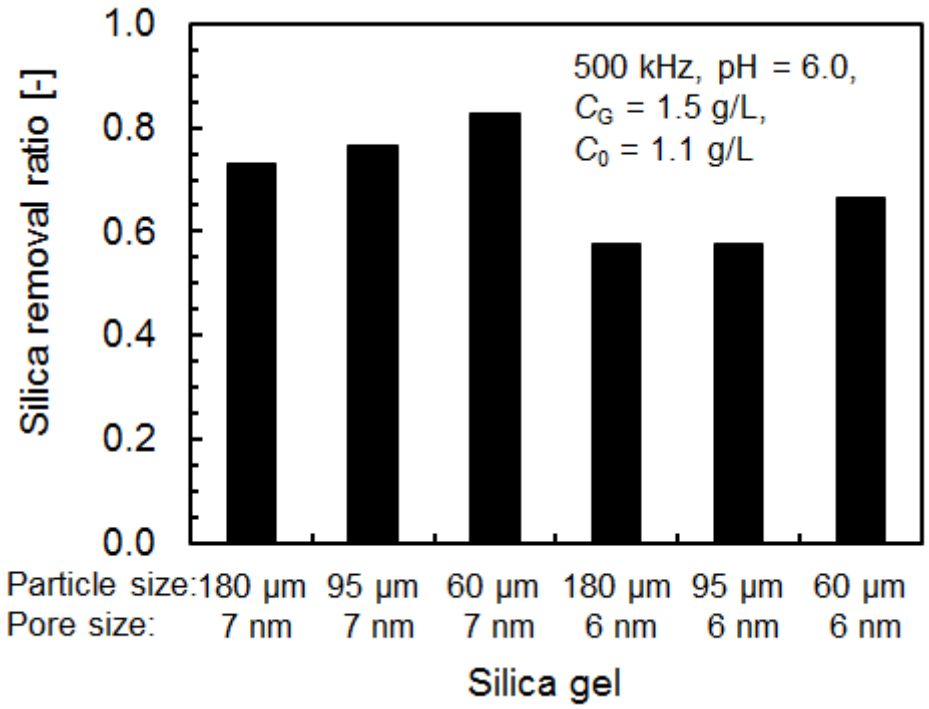

Fig. 6. 4 Effect of silica gel concentration on removal ratio of total silicic acid concentration for stirring and ultrasonication at 500 kHz at pH = 6. Initial concentration of monosilicic acid is 1.1 g/L. Initial concentration of silica gel is 1.5 g/L.

Next, the effect of pH on the silica removal ratio was examined. Figure 6. 5 shows the effect of pH on the silica removal ratio for various silica gel concentrations under ultrasonication at 500 kHz. The initial concentration of monosilicic acid is 1.1 g/L. In this study, at the lowest pH (pH = 4), the removal ratios are comparatively small since the ionization reaction (Eq. (6. 2)) occurrence is difficult in strong acid conditions. It is well known that the rate of silica polymerization is slow in high and low pH solution [20]. At

low pH, there is a majority of un-ionized silicic acid in solution, consequently, the reaction takes place slowly. In the case of the silica gel concentration at 1.5 g/L, the silica removal ratio is highest at pH 6 and decreases with increasing pH. The pH value giving a maximum rate of polymerization for polymer – polymer reactions (Eq. 6. 6) is around pH 6.5 [19]. The mechanism of silicic acid reduction by silica gel methods is polymerization between silica gel and silicic acid because silica gel is regarded as a silica polymer [8].

In the experimental condition of high monosilicic acid concentration and low silica gel concentration, it is considered that the monosilicic acids react by a monomer – monomer reaction (Eq. 6. 3) at first and then form polysilicic acid. Next, the polymer – polymer reaction (Eq. 6. 6) between polysilicic acid and silica gel is dominant. In the case of low silica gel concentration at 1.5 g/L, the silica removal ratio is at a maximum when the reaction rate between polymer and polymer is at its maximum value. In contrast, in the case of high silica gel concentration at 2.5 g/L, the removal ratios are high in the pH range from 6 to 9. The pH value giving the maximum rate of polymerization between monomer and polymer reaction (Eq. 6. 5) is around pH 8.5 [19]. When the concentrations of both monosilicic acid and silica gel are high, it is thought that the silica removal ratio becomes high when the polymerization rate between monosilicic acid and silica gel (monomer – polymer) is high or the polymerization rate between polysilicic acid and silica gel (polymer – polymer) is high.

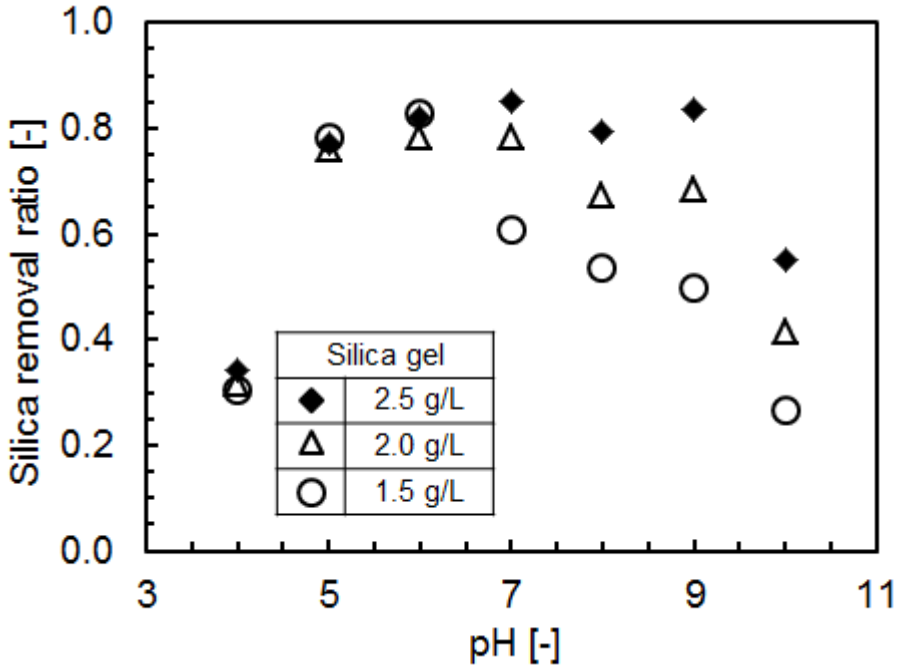

Fig. 6. 5 Effect of pH on the silica removal ration for several silica gel concentrations at 500 kHz. Initial concentration of monosilicic acid is 1.1 g/L. Particle size of silica gel is 60 μm. Pore size of silica gel is 7 nm.

The previous experimental data which were shown in Fig. 6. 5 were performed under ultrasonic irradiation with the driving frequency of 500 kHz at various pH and silica gel concentrations. In Fig. 6. 6, the similar experimental conditions are used, but instead of changing the silica gel concentration, the monosilicic acid alters in this experiment. In the case of the initial concentration of monosilicic acid at 0.5 g/L, with increasing pH, the removal ratio increases and the maximum value, which is 0.96, is obtained at pH 9. When the initial concentration of monosilicic acid is low, the reaction rate between monosilicic acids is small and the polymerization of monosilicic acid and silica gel (monomer - polymer) is dominant. The reaction rate between monomer and polymer peaks around pH 8.5 [19]. As the initial monosilicic acid concentration becomes higher, the pH at maximum

removal ratio becomes lower. It can be explained that the concentration of polysilicic acid increases due to the high polymerization rate of monosilicic acid. It is thought that the polymerization rates between monosilicic acid and silica gel (monomer – polymer) decrease and those between polysilicic acid and silica gel (polymer – polymer) increase. The rate of polymer – polymer reaction peaks around pH 6.5 [19].

Another possible reason for the lowering of the silica removal ratios at high pH in both Figs. 6. 5 and 6. 6 is that the solution mainly consists of silicic acid ions. Silicic acid ions tend to repel each other. The produced polysilicic acid would be depolymerized in the solution.

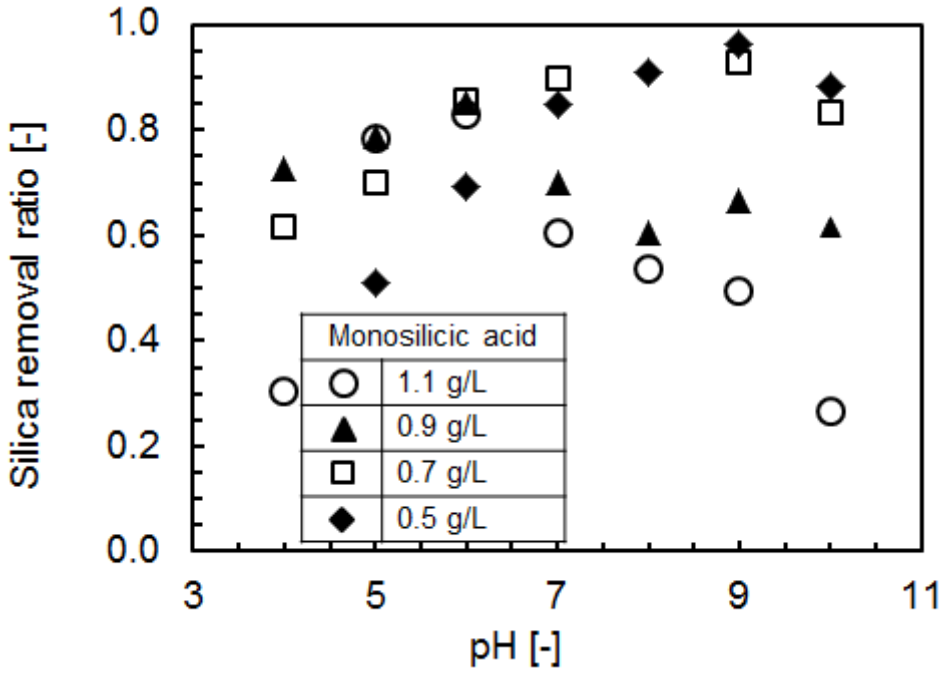

Fig. 6. 6 Effect of pH on the silica removal ratio for different initial concentration of monosilicic acid under ultrasonication at 500 kHz. Initial concentration of silica gel is 1.5 g/L. Particle size of silica gel is 60 µm. Pore size of silica gel is 7 nm.

6.4.2. Effect of ultrasonic conditions

In this part, stirring, ultrasonication, and ultrasonication with the adding of a chemical substance are performed. Figure 6. 7 shows the silica removal ratio with silica gel for those experimental conditions. There are five separately experiments are carried out namely stirring, ultrasonication at 28 kHz, ultrasonication at 500 kHz, ultrasonication at 500 kHz in hydrogen peroxide solution, and ultrasonication at 500 kHz in t-butanol solution. It is found that the removal ratios are in the range 0.6 to 0.9. In the case of stirring, the removal ratio is 0.63 and is the lowest value as compared to those of other experiments. It is also shown that ultrasonication enhances silica removal. Besides that the ultrasonication at 500 kHz is effective compared to that at 28 kHz. The addition of hydrogen peroxide for ultrasonication at 500 kHz increases the silica removal ratio. The silica removal ratio for ultrasonication at 500 kHz with *t*-butanol is lower than that without *t*-butanol and is higher than that for stirring.

Yasuda et al. carried out a research using the same ultrasonic frequency and power, but without using silica gel [16]. Ultrasound was irradiated into monosilicic acid with the initial concentration of 1.1 g/L. The silica monosilicic acid concentration decreased to a quasi-stable concentration because of polymerization. Compared with stirring, the rate of reduction in the monosilicic acid concentration for ultrasonication at 28 kHz was almost the same and the rate of reduction for ultrasonication at 500 kHz was higher. The addition of hydrogen peroxide for ultrasonication at 500 kHz enhanced the polymerization of monosilicic acid. It is known that the formation rate of OH radicals due to ultrasonic

cavitation becomes higher by the addition of hydrogen peroxide [21]. However, the addition of *t*-butanol reduced the rate of reduction in the monosilicic acid compared to that for stirring. The formation of OH radicals was suppressed by the addition of *t*-butanol [22]. The chemical effect of ultrasonic cavitation is maximum in the frequency range from 200 kHz and 600 kHz [23]. The mechanical effect of ultrasonic cavitation is large at frequencies below 100 kHz [24]. Therefore, it is proven that the enhancement of polymerization of the monosilicic acid by ultrasonication without silica gel is mainly due to the generation of OH radicals, that is, the chemical effect of ultrasonication is as noted by Yasuda et al. [16].

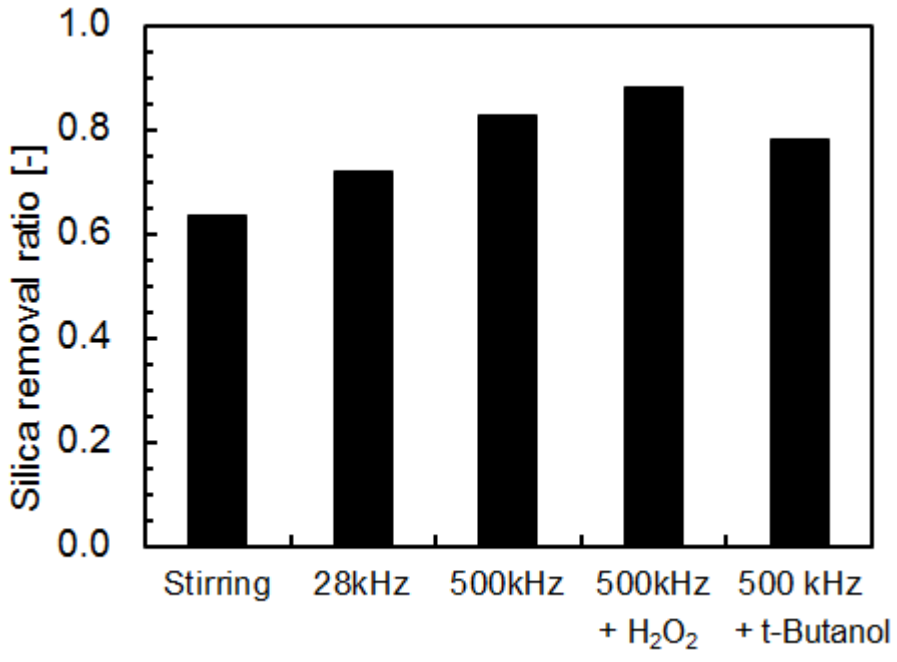

Fig. 6. 7 Silica removal ratio by stirring, ultrasound and addition of H_2O_2 and t-Butanol at pH = 6. Particle size of silica gel is 60 μm. Pore size of silica gel is 7 nm.
Initial concentration of monosilicic acid is 1.1 g/L.
Initial concentration of silica gel is 1.5 g/L

From the results in Fig. 6. 7, it is obvious that the enhancement of silica removal by ultrasonication is due to the chemical and mechanical effects of ultrasonication. The silica polymerization reaction is enhanced by the chemical effect, that is, the generation of OH radicals. The OH radicals might promote reactions of Eqs. (6. 5) and (6. 6) by initiation of a subsequent scission reaction [16]:

$$\equiv SiOSi\equiv + HO\cdot \longrightarrow \equiv SiO\cdot + HOSi\equiv \qquad (6.\ 8)$$

The site of ≡SiO is active in polymerization. The mechanical effect is mainly known as a high velocity field after cavitation collapse. When a bubble collapses near a solid surface, a liquid jet is directed toward the solid wall [25, 26]. The removal of silicic acid by silica gel is also enhanced by ultrasonication at 28 kHz. It is suggested that the liquid jet enhances the movement of silicic acid into the pores in the silica gel.

Because both chemical and mechanical effects induced from ultrasonic irradiation play the important roles in the silica removal efficiency, and each effect is powerful at different frequency, a combining ultrasonication is examined. Ultrasonic irradiation at 500 kHz and 28 kHz is combined. The data is shown in Fig. 6. 8 which indicated the frequency switching effect on the silica removal ratio. At first, ultrasonication at 500 kHz was conducted followed by ultrasonication at 28 kHz. The total time for ultrasonication is fixed at 180 min. Both ends of the horizontal axis indicate ultrasonication without frequency switching. Compared with single frequency ultrasonication, the silica removal ratio becomes higher with frequency switching. When the ultrasonic irradiation times at 500 and

28 kHz are 90 min, the silica removal ratio has a maximum value. In Fig. 6. 2, the total silicic acid concentration for ultrasonication at 500 kHz becomes almost constant after 90 min. Yasuda et al. reported that the monosilicic acid concentration decreased to a quasi-stable concentration until 90 min [16]. From these results, it is suggested that the chemical effect of ultrasonication through 90 min enhances the polymerization of silicic acid and silica gel. The polymerization is first enhanced by OH radicals generated at 500 kHz, and then the polysilicic acid in solution moves into pores by strong cavitation collapse at 28 kHz. More optimization of frequency switching should be conducted in the near future to develop a high-performance apparatus for removal of silicic acid in geothermal water.

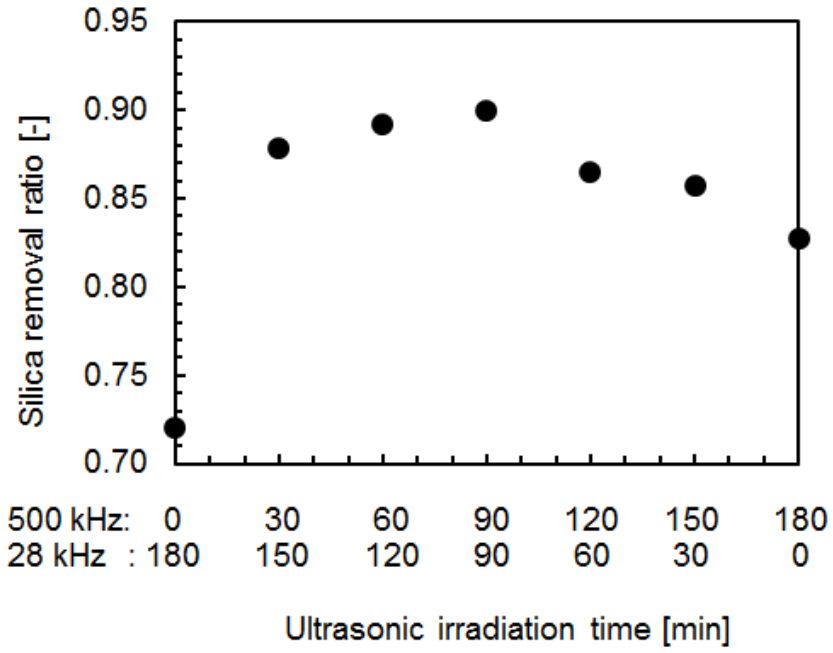

Fig. 6. 8 Changes in silica removal ratio by frequency switching ultrasound at pH = 6.
Particle size of silica gel is 60 μm. Pore size of silica gel is 7 nm.
Initial concentration of monosilicic acid is 1.1 g/L.
Initial concentration of silica gel is 1.5 g/L.

6. 5. Conclusion

A method combining ultrasonication and silica gel seed was used in this study in an effort to find a suitable and sufficient condition for removal of silicic acid in geothermal water. The findings of this research are as follows:

1. Ultrasonication enhanced the removal of silicic acid by silica gel seed. The enhancement by ultrasonication increased with increasing silica gel concentration.

2. The removal ratio of silicic acid strongly depended on the pH of the solution and, concentrations of silica gel and silicic acid. When the initial monosilicic acid concentration was 1.1 g/L and the silica gel concentration was 1.5 g/L, the silica removal ratio was highest at pH 6. However, in the case of initial monosilicic acid concentration at 0.5 g/L, the silica removal ratio was highest at pH 9.

3. The ultrasonic frequency is also an important parameter affecting removal of silicic acid. The higher frequency of 500 kHz proved to be more efficient in polymerizing of silicic acid than 28 kHz.

4. The particle diameter and pore size of silica gel affected the removal of silicic acid. The smaller particle diameter and larger pore size of silica gel indicated better results in the removal of silicic acid.

5. The ultrasonication using frequency switching between 500 kHz and 28 kHz enhanced the silica removal ratio compared to that at a single frequency. This can be explained by the high chemical effect at 500 kHz and the strong mechanical effect at 28 kHz, as both contribute to the removal of silicic acid.

References

1. R.W. Henley, pH and silica scaling control in geothermal field development, Geothermics, 12(4) (1983) 307 – 321.
2. T. Yanagase, Y. Suginohara, K. Yanagase, The properties of scales and methods to prevent them, Geothermics, 2 (1970) 1619 – 1623.
3. D. L. Gallup, J. L. Featherstone, Acidification of steam condensate for incompatibility control during mixing with geothermal brine, US Patent, 4, 522, 728 (1985).
4. J. L. Featherstone, D. R. Powell, Stabilization of highly saline geothermal brines, J. Petroleum Tech., 33(4) (1981) 727 – 734.
5. A. Ueda, K. Kato, K. Abe, T. Furukawa, K. Mogi, K. Ishimi, Recovery of silica from the sumikawa geothermal fluids by addition of cationic reagents, J. Geotherm. Res. Soc. Jpn., 22(4) (2000) 249 – 258.
6. J. E. Harrar, F. E. Locke, C. H. Otto Jr, L. E. Lorsensen, S. B. Monaco, W. P. Frey, Field tests of organic additives for scale control at the salt on sea geothermal field, Soc. Pet. Eng. J., 22(1) (1982) 17 – 27.
7. H. Sugita, Y. Bando, M. Nakamura, Removal of silica from geothermal brine by seeding method using silica gel, J. Chem. Eng. Jpn., 31(1) (1998) 150 – 152.
8. H. Sugita, I. Matsunaga, T. Yamaguchi, K. Kato, A. Ueda, Silica removal performance of seed from geothermal fluids, Geothermics, 32(2) (2003) 171 – 185.
9. E.J. Reardon, Complexing of silica by iron (iii) in natural waters, Chem. Geology, 25(4) (1979), 339 – 345.
10. T. Yokoyama, Y. Takahashi, T. Tarutani, Retarding and accelerating effects of aluminum on the growth of polysilicic acid particles, J. Colloid Interface Sci., 141(2) (1991), 559 – 563.
11. G.E.J. Poinern, X.T. Le, S. Shan, T. Ellis, S. Fenwick, J. Edwards, D. Fawcett, Ultrasonic synthetic technique to manufacture a pHEMA Nanopolymeric–based vaccine against the H6N2 avian influenza virus: a preliminary investigation, Int. J. Nanomedicine, 6 (2011) 2167 – 2174.
12. C. Petrier, B. David, S. Laguian, Ultrasonic degradation at 20 kHz and 500 kHz of Atrazine and Pentachlorophenol in aqueous solution: preliminary results, Chemosphere, 32(9) (1996) 1709 – 1718.
13. G. J. Price, D. J. Norris, P. J. West, Polymerization of Methyl Methacrylate initiated by ultrasound, Macromolecules, 25(24) (1992) 6447 – 6454.
14. S. Koda, A. Suzuki, H. Nomura, Ultrasonic polymerization of Poly(vinylpyrrolidone), Polym. J., 27(11) (1995) 1144 – 1146.
15. P. Kruus, Polymerization resulting from ultrasonic cavitation, Ultrasonics, 21(5) (1983) 201 – 204.
16. K. Yasuda, Y. Takahashi, Y. Asakura, Effect of ultrasonication on polymerization of silicic acid in geothermal water, Jpn. J. Appl. Phys., 53(7S) (2014) 07KE08.
17. B.A. Fleming, D.A. Crerar, Silicic acid ionization and calculation of silica solubility at elevated temperature and pH application to geothermal fluid processing and reinjection, Geothermics, 11(1) (1982) 15 – 29.
18. B.A. Fleming, Kinetics of reaction between silicic acid and amorphous silica surface in

NaCl solutions, J. Colloid Interface Sci., 110(1) (1986), 40 – 64.
19. T. Tarutani, Polymerization of silicic acid a review, Ana. Sci., 5 (1989) 245 – 252.
20. S.A. Greenberg, D. Sinclair, The polymerization of silicic acid, J. Phys. Chem., 59(5) (1955) 435 – 440.
21. A. Hwang, S. Na, J. Ha, J. Khim, Degradation of Diethyl Phthalate by sono–Fenton process and its dependence on the power density, Jpn. J. Appl. Phys., 49 (2011), 07HE09.
22. L. Rong, K. Yasuda, M. Nakamura, N. Kato, K. Kawakami, Y. Kitaide, Decomposition of p-Chlorophenol in aqueous solution by combination of ultrasound and ultraviolet light, J. Chem. Eng. Jpn., 36(9) (2003) 1045 – 1049.
23. S. Koda, T. Kimura, T. Kondo, H. Mitome, A standard method to calibrate sonochemical efficiency of an individual reaction system, Ultrason. Sonochem., 10(3) (2003) 149 – 156.
24. K.V.B. Tran, T. Kimura, T. Kondo, K. Koda, Quantification of frequency dependence of mechanical effects induced by ultrasound, Ultrason. Sonochem., 21(2) (2014) 716 – 721.
25. V. Minsier, J. De Wilde, J. Proost, Simulation of the effect of viscosity on jet penetration into a single cavitation bubble, J. Appl. Phys., 106(8) (2009) 084906.
26. C. D. Ohl, M. Arora, R. Dijkink, V. Janve, D. Lohse, Surface cleaning from laser–induced cavitation bubbles, Appl. Phys. Lett., 89(7) (2006) 074102.

Chapter 7

Summary

This study was conducted in the wide range of ultrasonic frequency from 22 kHz to 4880 kHz. Broadband noise determined by a tough needle-type hydrophone was used to investigate the cavitation threshold. It should be noted in this study that before BIP was calculated, all fundamental, harmonic, and subharmonic components were entirely removed from the signal spectrum. The result pointed out that the cavitation threshold got higher as ultrasonic frequency increased. Besides, thresholds of chemical and mechanical effects were determined by KI oxidation and aluminum foil erosion, respectively. The tendency of those thresholds showed to be same as the tendency of cavitation threshold. The chemical effect threshold was nearly same as the cavitation threshold at every frequency. The mechanical effect threshold and the cavitation threshold were almost close to each other at frequencies lower than 98 kHz, whereas the mechanical effect threshold was comparatively higher than the cavitation threshold at high frequencies.

The effect of occurrence of bubbles in a liquid was determined by measuring the thresholds of the second harmonic and the first ultraharmonic frequencies. The results of this study showed that the threshold of the second harmonic component was in harmony with the cavitation threshold below 1000 kHz. For the threshold of the first ultraharmonic frequency, there were two trends obtained. At low frequencies below 98 kHz, the threshold of the first ultraharmonic was greater than the cavitation threshold. At high frequencies, the threshold of the first harmonic was consistent with the cavitation threshold.

As regards the affect of ultrasonic cavitation in the solution, the sound pressures at various frequency components such as the fundamental, second harmonic and first ultraharmonic, and the BIP at 22, 43, 98, 304, and 488 kHz were investigated. For the

fundamental frequency, firstly if cavitation bubbles were not generated in the water yet, sound pressure rose linearly with the upward of the effective electric power applied to the transducer. Afterward as continually increasing the electric power, the sound pressure drastically dropped at around the electric power giving cavitation threshold. Finally, the sound pressure went up again when the electric power became higher than that of the cavitation threshold. At a high electric power, even the sound pressure increased, but its value was lower than the value extrapolated from the linear relationship between the sound pressure at the fundamental frequency and the square root of electric power below the electric power of cavitation threshold. The second harmonic signal began to appear at the electric power comparably lower than that of the cavitation threshold. The first ultraharmonic signal was noticed at the electric power near to that of cavitation threshold at 304 and 488 kHz. At lower frequencies, the first ultraharmonic component appeared at higher electric power compared with cavitation inception.

To study the sonochemical reaction field in a sonochemical reactor, the cross-sectional area distribution of broadband noise was measured using a needle-type hydrophone at 130 and 43 kHz. Two directions in the sonochemical reactor horizontal and vertical directions were scanned at one-millimeter interval. At 130 kHz, the ellipse shape of reaction fields were obtained. Along the vertical direction, the sonochemical reaction field were more powerful in the upper part of the reactor. In the distribution of the sound pressure at the fundamental frequency, standing waves were obtained and reaction fields were weak at pressure antinodes. In the distribution of the sound pressure at the second harmonic frequency, the data showed that the pattern of bubbles distribution resembled to

that of reaction fields closely. At 43 kHz, the distribution of reaction fields and sound pressures were more complicated. The data also pointed out that the areas of reaction fields were comparably weak in areas where high sound pressures at the fundamental frequency were obtained.

An experiment of application of ultrasonic cavitation on silicic acid removal was performed. Ultrasonication combining silica gel seed was used for removing silicic acid in geothermal water. Various experimental conditions were applied. Ultrasonication was proven the ability of enhancing the removal of silicic acid by silica gel seed and the enhancement ratio increased with increase silica gel concentration. All the parameters of pH, ultrasonic frequency, particle diameter of silica gel, and pore size of silica gel largely affect the removal of silicic acid. The switching frequency of 500 kHz and 28 kHz indicated higher efficiency in removing silica acid compared to single frequency.

Perspective for future work

With the difference on generation mechanisms of cavitation threshold, threshold of chemical effect, and threshold of mechanical effect, those values were well determined in this study. To be more effective in non-damage cleaning, the sound pressure should be used in the range between cavitation threshold and mechanical effect threshold in the ultrasonic cleaner.

Researches on optimization of distribution of sound pressure and bubbles will be continuously carried out to enhance the sonochemical reactions fields.

The combination of different ultrasonic frequencies at different switching conditions of frequency and time should be conducted to get the highest efficiency of removing silicic acid in geothermal water.

Researches on application of ultrasound on various industries will be conducted. Ultrasound will be used to treat artificial sweeteners such as Saccharin and Sucralose. Applications of ultrasound on ultrasonic cleaner, metal nano particles synthesis, polymer synthesis, polymer synthesis and therapeutic medical will be practically studied.

List of publications

1. Tam Thanh Nguyen, Yoshiyuki Asakura, Shinobu Koda, Keiji Yasuda, Dependence of cavitation, chemical effect, and mechanical effect thresholds on ultrasonic frequency, Ultrasonics Sonochemistry, Vol.39, pp.301-306 (2017)
2. Tam Thanh Nguyen, Yoshiyuki Asakura, Nagaya Okada, Shinobu Koda, Keiji Yasuda, Effect of ultrasonic cavitation on measurement of sound pressure using hydrophone, Japanese Journal of Applied Physics, Vol.56, No.7S1, pp.07JE061-07JE065 (2017)
3. Tam Thanh Nguyen, Yuta Takahashi, Yoshiyuki Asakura, Keiji Yasuda, Removal of silicic acid in geothermal water by a combination of ultrasonication and silica gel seed, Journal of Chemical Engineering of Japan, Vol.50, No.7, pp.542-547 (2017)
4. Keiji Yasuda, Tam Thanh Nguyen, Yoshiyuki Asakusa, Measurement of distribution of broadband noise and sound pressures in sonochemical reactor, Ultrasonics Sonochemistry, Vol.43, pp.23-28 (2018)

Acknowledgement

I would like to express my sincere gratitude to my academic supervisor Associate Professor Keiji Yasuda, Department of Chemical Engineering, Graduate School of Engineering, Nagoya University for the continuous support, instruction, and encouragement of my Ph.D study for his patience, motivation, and immense knowledge. I would also like to send my deep thankfulness to Dr. Yoshiyuki Asakura (Honda Electrics Co.) for detailed instruction and precious advices for my research. Their guidance helped me in all the time of research and writing of this Ph.D thesis. I appreciated the kind instruction and support of Professor Shinobu Koda (Nagoya University) for my research and study. My sincere thanks also goes to Professor Goto Motonobu, Professor Norinaga Koyo, and Associate Professor Yoshiie Ryo in Nagoya University for their agreement in revising this work. I am grateful to my teachers and colleagues in University of Science, Vietnam National University, Ho Chi Minh City for the warm care and encouragement for my life and study.

I acknowledged the support of Ministry of Education, Culture, Sports, Science and Technology, Japan (MOBUKAGAKUSHO) which enabled me to pursue my Ph. D study in Nagoya University.

At the end I would like to express appreciation to my family for supporting me spiritually throughout my study and my life in general.